



Hollandse Kust (noord) Field Measurement Campaign

Campaign Report - April 2017 to April 2019



Hollandse Kust (noord) Field Measurement Campaign

Campaign Report - April 2017 to April 2019

Sofia Caires (Deltares) and Irene Pathirana (Fugro)

1230377.001

©Deltares, 2019

Title

Hollandse Kust (noord) Field Measurement Campaign

Client

RvO.nl

Project

1230377.001

Reference

1230377-001-HYE-0004

Pages

99

Classification

None

Keywords

North Sea, wind farm, metocean data, validation, offshore wind

Summary

Two Carbon Trust pre-commercial Stage 2 classified *SEAWATCH Wind LiDAR Buoys*, HKNA and HKNB, and associated bottom mounted sensors were deployed by Fugro at the Hollandse Kust (noord) Wind Farm Zone on the 10th of April 2017 with the intention of measuring wind, waves, temperature, air pressure and currents for a period of one year. The two SWLBs provide a redundant arrangement of instrumentation for the measurement campaign in particular in order to safeguard against data loss. After the completion of one year of observations on the 9th of April 2018, another year was commissioned. The HKNA station was kept operational whilst the HKNB station was not kept operational during the transition of approximately 1 month. The second campaign year was completed on the 10th of April 2019. The buoys were kept operational to complete the in-situ validation of the HKNB buoy until June 2019.

In this report the HKN field measurement campaign is described and the full two-year campaign dataset are validated and presented.

During the measurement campaign, the available data (mostly satellite transmitted) were validated and made available on a monthly basis. The basis of this full campaign report and dataset is the data downloaded from each station over the course of the project. Consequently, the signal availability of the full two-year dataset differs from that of the monthly reported datasets.

Given the further application of quality control procedures in the generation of the final dataset and on the basis of the validation results, we assess the quality of the full campaign dataset to be higher or equal to that of the compilation of all monthly datasets. With in general higher availability, this final campaign dataset should, therefore, be the preferred dataset for further studies.

Assessing the final 2-year data return of the individual stations, the availability of

- the wind data is acceptable to high (~80-90%),
- the wave data is high from HKNA and good from HKNB,
- current data is at all levels acceptable from HKNA and limited from HKNB,
- the air and water temperature is good and of the air pressure is high from HKNA.

Missing data return (i.e less than 100% availability) is due to circumstances such as contractual deployment (e.g contractual transition with HKNB not deployed for ~1 month accounting for approximately 5% missing data return), regular service and maintenance as well as some unscheduled instrument specific outages with duration depending on workable weather for offshore operations as summarized in the report.

In more detail, the following conclusions ensue from the validation of the data.

- The comparisons between the HKNA and HKNB wind velocities show at all levels and in terms of both wind speed and direction low biases and correlations and slopes close to 1. The agreement between the wind observations from HKN and from the reference stations is relatively high, especially when considering the differences in the location of the stations.
- The agreement between the wave data from the two buoys is excellent for all parameters except for the peak wave period and the mean wave period of swell which is good and the mean wave direction of swell which is poor. These poorer agreements are as expected, given that these parameters depend more strongly on the sampling variability (randomness of the sea surface elevation) and discreteness of the wave spectra. The agreement between the wave observations from HKN and from the reference stations is relatively high, especially when considering the distances between the stations.
- The validation of the temperature data shows that there is a general agreement between HKN temperature observations and those from the fixed stations.
- The validation of the air pressure data shows, as expected given their proximity in terms of macro-atmospheric forcings, an excellent agreement between the HKN observations and those from the fixed stations.
- The HKN inferred water levels had to be bias corrected given uncertainties in the depths at which the WLRs were located. The resulting processed water levels show a high agreement between stations and with the model data.
- The agreement between the current speed observations and model results is high. There are mismatches between the current directions, which are partly due to the nature and variability of the current direction signal.


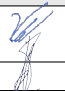

The overall results validate the assumption that the distance between the two stations is negligible and the datasets are interchangeable. Therefore, the station datasets can be combined into a single dataset with the highest possible availability. For illustration, if the gaps in the data collected at one of the stations are filled with the data collected at other station in order to compile a complete HKN dataset, the availabilities are then high for wind and waves (above 98.3%), good for currents (up to 94%), high for pressure and water temperature, good for air temperature and limited for water level.

The overall conclusion of the validation is that the quality of the HKNA and HKNB data is high and the dataset trustworthy. This makes this comprehensive dataset—including vertical wind and current profiles and directional wave spectra—a sound basis for site study analysis, for instance, for wind assessment studies, morphodynamics and metocean desk studies and in particular for the Hollandse Kust (noord) Wind Farm Zone.

References

Revised according to

HKN 20190805 RVO DRF full campaign report v1.2 RVO F.xlsx

Version	Date	Author	Initials	Review	Initials	Approval	Initials
3.0	Aug. 20, 2019	S. Caires I. Pathirana	and 	V. Neshaug J.-J. Schouten	and 	A. Berg M. van Gent	

Status

Final

Contents

1	Introduction	1
1.1	Description of the campaign	2
1.1.1	Monthly data reports	5
1.1.2	Monthly validation reports	5
1.2	QHSE	5
1.3	Definitions and abbreviations	5
1.4	Outline of the report	6
2	Instrumentation and measurement configuration	7
2.1	Wind data collection	10
2.2	Wave data collection	11
2.3	Temperature data collection	11
2.4	Air pressure data collection	11
2.5	Water level data collection	11
2.6	Current data collection	12
3	Post processing, quality control and file descriptions	13
3.1	Post processing and quality control	13
3.2	File descriptions	16
3.3	Data Files	18
4	Data Validation	21
4.1	Measurement uncertainties	21
4.2	Validation procedure	21
5	Data Availability	25
5.1	Introduction	25
5.2	Validated parameters	26
5.3	Non-validated parameters	32
6	Wind	33
6.1	Introduction	33
6.2	Intercomparison of the HKN data	33
6.3	Comparison with data from the fixed stations	36
6.3.1	Validation of HKNA	37
6.3.2	Validation of HKNB	43
6.4	Quality Statement	48
6.5	Climate description	48
7	Waves	55
7.1	Introduction	55
7.2	Intercomparison of the HKN data	55
7.3	Validation of the HKN data	57
7.4	Quality Statement	68
7.5	Climate description	68
8	Temperature	73
8.1	Introduction	73
8.2	Intercomparison of the HKN data	73
8.3	Validation of the HKN data	74
8.3.1	Water Temperature	74

8.3.2	Air Temperature	75
8.4	Quality Statement	76
8.5	Climate description	77
9	Air Pressure	79
9.1	Introduction	79
9.2	Validation of the HKN data	79
9.3	Quality Statement	80
9.4	Climate description	80
10	Water Level	81
10.1	Introduction	81
10.2	Model description	81
10.3	Intercomparison of the HKN data	82
10.4	Model Validation	82
10.5	Quality Statement	82
10.6	Climate description	83
11	Currents	85
11.1	Introduction	85
11.2	Intercomparison of the HKN data	85
11.3	Validation of the HKN data	89
11.4	Quality Statement	90
11.5	Climate description	90
12	Final remarks	93

List of Figures

1.1	Map of the HKN Wind Farm Zone	1
1.2	Buoy locations	4
2.1	Mooring design for the SWLB at Hollandse Kust (noord)	8
2.2	Illustration of the wind and current profile measurements from the LiDAR buoy. Heights ref. sea surface	10
3.1	Dataset generation from transmitted and downloaded (recovered and raw) data	14
4.1	Location of buoys and fixed measurement stations (via Google Earth).	22
5.1	Data availability HKNA (red), HKNB (blue) and HKNA WLR and HKNB WLR (grey) for the full campaign period from April 10, 2017 00:00 until April 10, 2019 23:50.	27
5.2	Comparison of the HKNA data availability in the monthly reports (red) and for the full campaign dataset (black).	29
5.3	Comparison of the HKNB data availability in the monthly reports (red) and for the full campaign dataset (black).	30
5.4	Data availability HKN for the full campaign period from April 10, 2017 00:00 until April 10, 2019 23:50. The red (blue) indicates data from HKNA (HKNB). . .	31
6.1	Time evolution of the vertical wind speed (top panel) and direction (bottom panel) profiles at HKNA.	33
6.2	Time evolution of the vertical wind speed (top panel) and direction (bottom panel) profiles at HKNB.	33
6.3	Wind speeds (by elevation) at each buoy.	34
6.4	Wind directions (by elevation) at each buoy.	34
6.5	Direct scatter comparison between buoy wind at elevations of 100 and 160 m. . .	35
6.6	Wind roses for all locations.	37
6.7	Validation of HKNA wind with Q1. Left panels: Timeseries. Right panels: Density scatter, with the darker colours indicating more data density.	38
6.8	Roses of the simultaneously available HKNA and Q1 wind data.	39
6.9	Validation of HKNA wind with LEG. Left panels: Timeseries. Right panels: Density scatter, with the darker colours indicating more data density.	39
6.10	Roses of the simultaneously available HKNA and LEG wind data.	40
6.11	Validation of HKNA wind with EPL. Left panels: Timeseries. Right panels: Density scatter, with the darker colours indicating more data density.	40
6.12	Roses of the simultaneously available HKNA and EPL wind data.	41
6.13	Validation of HKNA wind with K13. Left panels: Timeseries. Right panels: Density scatter, with the darker colours indicating more data density.	41
6.14	Roses of the simultaneously available HKNA and K13 wind data.	42
6.15	Validation of HKNB wind with Q1. Left panels: Timeseries. Right panels: Density scatter, with the darker colours indicating more data density.	43
6.16	Roses of the simultaneously available HKNB and Q1 wind data.	44
6.17	Validation of HKNB wind with LEG. Left panels: Timeseries. Right panels: Density scatter, with the darker colours indicating more data density.	44
6.18	Roses of the simultaneously available HKNB and LEG wind data.	45
6.19	Validation of HKNB wind with EPL. Left panels: Timeseries. Right panels: Density scatter, with the darker colours indicating more data density.	45
6.20	Roses of the simultaneously available HKNB and EPL wind data.	46

6.21	Validation of HKNB wind with K13. Left panels: Timeseries. Right panels: Density scatter, with the darker colours indicating more data density.	46
6.22	Roses of the simultaneously available HKNB and K13 wind data.	47
6.23	Wind roses at levels 100, 140 and 200 m.	49
6.24	Wind speed and direction joint occurrence table at levels 100 m.	50
6.25	Wind speed and direction joint occurrence table at levels 140 m.	50
6.26	Wind speed and direction joint occurrence table at levels 200 m.	51
6.27	Left: Observed wind profiles. Right: Histogram of the alpha estimates.	52
6.28	Observed wind profiles with $U_4 > 10.8$ m/s (top), $U_4 > 13.9$ m/s (middle) and $U_4 > 17.2$ m/s (bottom).	53
6.29	Observed wind profiles under approximately neutral (top left), unstable (top right), stable (bottom left) atmospheric stability and observed wind profiles in which $U_{180} < U_{160} < U_{140} < U_{100}$ (bottom right)	53
6.30	Rose of the 100m wind of the observed data falling under approximately neutral (top left), unstable (top right), stable (bottom left) atmospheric stability and in which $U_{180} < U_{160} < U_{140} < U_{100}$ (bottom right)	54
6.31	Mean observed wind profiles at HKNA under different conditions.	54
7.1	Normalized spectral density at each buoy.	55
7.2	Wave parameters at each buoy.	56
7.3	Validation of HKNA waves with Q1.	58
7.4	Validation of HKNA waves with IJmuiden.	59
7.5	Roses of the simultaneously available HKNA (left) and IJmuiden (right) wave data.	59
7.6	Validation of HKNA waves with EPL.	60
7.7	Roses of the simultaneously available HKNA (left) and EPL (right) wave data.	61
7.8	Validation of HKNA waves with K13.	62
7.9	Roses of the simultaneously available HKNA (left) and K13 (right) wave data.	62
7.10	Validation of HKNB waves with Q1.	63
7.11	Validation of HKNB waves with IJmuiden.	64
7.12	Roses of the simultaneously available HKNB (left) and IJmuiden (right) wave data.	64
7.13	Validation of HKNB waves with EPL.	65
7.14	Roses of the simultaneously available HKNB (left) and EPL (right) wave data.	66
7.15	Validation of HKNB waves with K13.	67
7.16	Roses of the simultaneously available HKNB (left) and K13 (right) wave data.	67
7.17	HKNA significant wave height and peak wave period roses.	68
7.18	HKNA significant wave height and peak wave period joint occurrence table.	69
7.19	HKNA swell (left) and sea (right) significant wave height roses.	69
7.20	Distribution of H_{sswell} percentage of H_{ssea} . Top panel: Frequency plot. Bottom panel: Rose of H_{sswell}/H_{ssea} percentage versus the MWD.	70
7.21	Directional wave spectrum of 03-Jan-2018 13:10:00, $H_s=7.15$ m, $H_{sswell}=5.02$ m, $H_{ssea}=5.10$ m and MWD= $286^\circ N$	71
7.22	Directional wave spectrum of 08-Jan-2019 09:00:00, $H_s=7.03$ m, $H_{sswell}=5.74$ m, $H_{ssea}=4.08$ m and MWD= $337^\circ N$	71
7.23	Directional wave spectrum of 03-Jan-2018 12:10:00, $H_s=6.88$ m, $H_{sswell}=3.98$ m, $H_{ssea}=5.61$ m and MWD= $255^\circ N$	72
8.1	Temperature and temperature difference measured at HKN.	73
8.2	Timeseries (left) and scatter plot (right) comparisons between the measured at HKN air (top) and surface water (bottom) temperatures.	74
8.3	Water temperature measurements from all locations.	74
8.4	Surface water temperature comparison at HKNA.	75
8.5	Surface water temperature comparison at HKNB.	75

8.6	Air temperature measurements from all locations.	75
8.7	Air temperature comparison at HKNA.	76
8.8	Air temperature comparison at HKNB.	76
8.9	Distribution of temperature and temperature differences measured at HKNA.	78
9.1	Air pressure measurements from all locations.	79
9.2	Air pressure comparison at HKNA.	79
9.3	Air pressure comparison at HKNB.	80
9.4	Distribution of air pressure measured at HKNA.	80
10.1	DCSMv6-ZUNOV4 model bathymetry (via Google Earth).	81
10.2	HKNA and HKNB water level.	82
10.3	Validation of HKNA and HKNB water levels with DCSMv6-ZUNOV4 model output.	82
11.1	Time evolution of the vertical current speed (top panel) and direction (bottom panel) profiles at HKNA.	85
11.2	Time evolution of the vertical current speed (top panel) and direction (bottom panel) profiles at HKNB.	86
11.3	Timeseries of surface currents at each buoy. The oceanographic convention is used for the current directions, so all current directions are <i>going to</i> , clockwise from North.	86
11.4	Timeseries of 10 m depth currents at each buoy. The oceanographic convention is used for the current directions, so all current directions are <i>going to</i> , clockwise from North.	87
11.5	Timeseries of 20 m depth currents. The oceanographic convention is used for the current directions, so all current directions are <i>going to</i> , clockwise from North.	87
11.6	Timeseries of HKNA (top) and HKNB (bottom) current speeds (by depth) at each buoy.	88
11.7	Timeseries of HKNA (top) and HKNB (bottom) current directions (by depth). The oceanographic convention is used for the current directions, so all current directions are going to clockwise from North.	88
11.8	Depth-averaged current comparison at HKNA.	89
11.9	Depth-averaged current comparison at HKNB.	90
11.10	Normalized current speed vertical profiles.	91
11.11	Roses of the surface (top), 10 m (middle) and 20 m (bottom) currents at HKNA. The current direction is the direction the piles point to away from the centre of the rose.	92

List of Tables

1.1	Hollandse Kust (noord) LiDAR buoy locations and measurement intervals. Spherical coordinates are given in ETRS89 and the cartesian coordinates in UTM 31N.	3
1.2	Hollandse Kust (noord) buoy swaps.	4
2.1	Measurement configurations for the SWLB at Hollandse Kust (noord)	9
3.1	List of variables. All parameters are presented as averages over 10 minutes. . .	15
3.2	QA/QC filter ranges for each parameter	16
3.3	Data files that make up the complete set of data presented in this report. . . .	19
6.1	Statistical comparison between the winds from the LiDAR buoys with elevation. .	36
6.2	Direction statistical comparison between HKNA (z = 30.0 m) and Q1.	39
6.3	Direction statistical comparison between HKNA (z = 40.0 m) and LEG.	40
6.4	Direction statistical comparison between HKNA (z = 30.0 m) and EPL.	41
6.5	Direction statistical comparison between HKNA (z = 80.0 m) and K13.	42
6.6	Statistical comparison between HKNA and LEG LiDARs at different heights. . .	42
6.7	Statistical comparison between HKNA and EPL LiDARs at different heights. . .	43
6.8	Direction statistical comparison between HKNB (z = 30.0 m) and Q1.	44
6.9	Direction statistical comparison between HKNB (z = 40.0 m) and LEG.	45
6.10	Direction statistical comparison between HKNB (z = 30.0 m) and EPL.	46
6.11	Direction statistical comparison between HKNB (z = 80.0 m) and K13.	47
6.12	Statistical comparison between HKNB and LEG LiDARs at different heights. . .	47
6.13	Statistical comparison between HKNB and EPL LiDARs at different heights. . .	48
7.1	Statistical comparison between HKNA and HKNB wave parameters.	57
7.2	Direction statistical comparison between HKNA and IJmuiden.	60
7.3	Direction statistical comparison between HKNA and EPL.	61
7.4	Direction statistical comparison between HKNA and K13.	63
7.5	Direction statistical comparison between HKNB and IJmuiden.	65
7.6	Direction statistical comparison between HKNB and EPL.	66
7.7	Direction statistical comparison between HKNB and K13.	68
11.1	Statistical comparison between LiDAR buoy current measurements with depth. .	89

1 Introduction

Fugro was contracted by RVO.nl to supply meteorological and oceanographic measurement data at the Hollandse Kust (noord) (HKN) Wind Farm Zone (WFZ) in the Dutch sector of the southern North Sea, located 26 km from the Dutch Coast. The goal of the measurement campaign is to provide a 24-month continuous wind and metocean dataset. The starting point assumptions given to Fugro by RVO.nl detail the extent of the HKN Wind Farm Zone given in [Figure 1.1](#). In addition, two recommended areas for positioning the systems approximately in the middle of the wind farm zone were provided by RVO.nl.

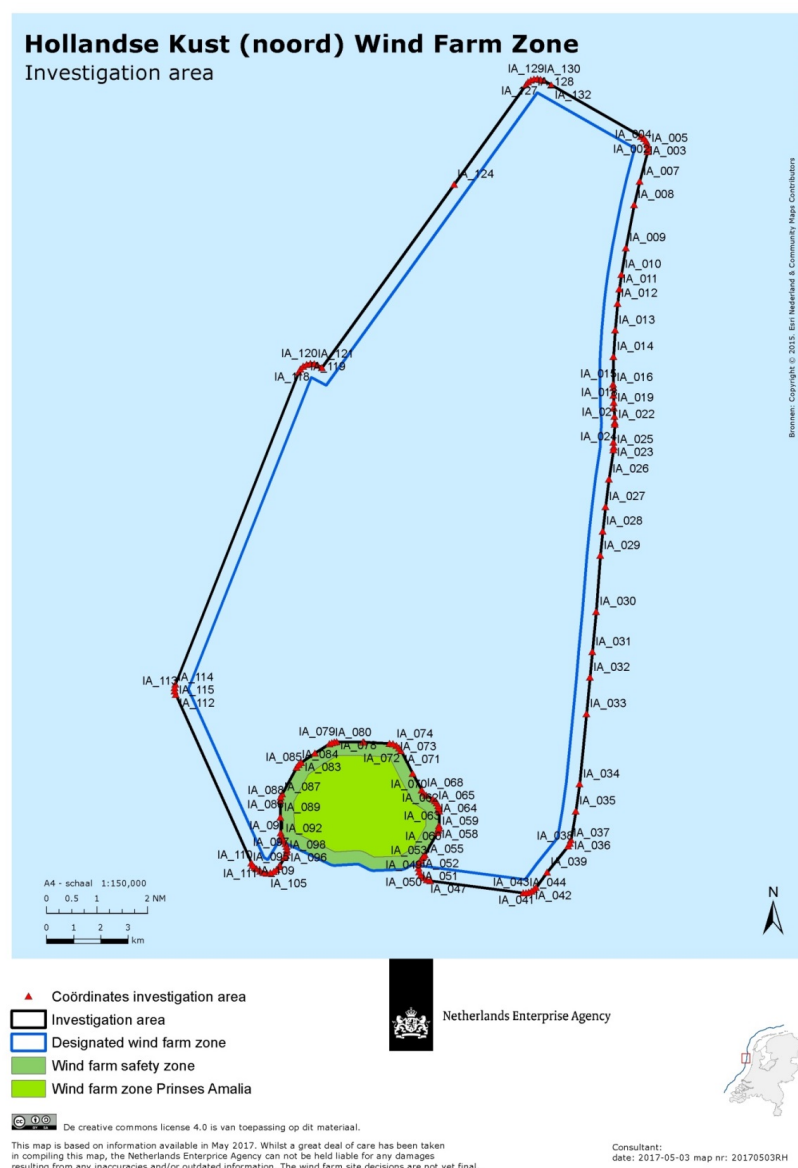


Figure 1.1: Map of the HKN Wind Farm Zone

In this report the HKN field measurement campaign is described and the data are validated

and presented. Furthermore, this is a joint Fugro and Deltares report, with the presented data validation and analysis having been carried out and reported by Deltares and the data processing and campaign instrumentation description having been reported by Fugro.

1.1 Description of the campaign

Two Carbon Trust pre-commercial Stage 2 classified SEAWATCH Wind LiDAR buoys (SWLBs) were deployed at HKN on 8th April 2017 at 13:50, and 9th April 2017 at 12:00, respectively. The two buoys are referred to as Station A and Station B but are abbreviated in this report as HKNA and HKNB, respectively. After the completion of one year of observations on the 9th of April 2018, another year was commissioned. The HKNA station was kept operational whilst the HKNB station was not kept operational during the transition of approximately 1 month. The second campaign year was completed on the 10th of April 2019. The buoys were kept operational to complete the in-situ validation of the HKNB buoy until June 2019.

The full dataset for this campaign spans two years from 10th April 2017, 00:00 UTC, until 10th April 2019, 23:50 UTC.

The buoys were equipped with a directional wave sensor, a motion sensor, a wind sensor (measuring winds at 4 m above water level), an air pressure sensor, an air temperature and humidity sensor, a current profiler, a water level sensor and a LiDAR (measuring winds at 30 to 200 m above water level). The two SWLBs provide a redundant arrangement of instrumentation for the measurement campaign in particular in order to safeguard against data loss. The SWLBs transmit data in near real-time to Fugro for continuous monitoring of the performance as well as monthly reporting. 10-minute average data from the sensors on the buoys and buoy monitoring data are packed atomically at the same time into binary messages and are both stored locally onboard and transmitted via satellite at the same time. During buoy maintenance stored data were downloaded and referred to as recovered data. Monthly data reports were based on either transmitted data only or on recovered data when available. The final dataset consists of the full recovered dataset.

The location of the water level sensor mooring is approximately the same as that of the corresponding buoy and the depth is at both locations ≈ 23 m. The water depths relative to Mean Sea Level (MSL) for this region are based on data from a detailed bathymetric survey by Fugro commissioned by RVO.nl. As the buoys are free to float around the mooring point within a radius of about 110 m, the actual water depth at the actual position of the buoy at any time would vary by approximately ± 0.1 m.

Information on the locations, serial numbers and recording intervals of the two SEAWATCH Wind LiDAR buoys used during the measurement campaign is given in [Table 1.1](#). The positions are given on the map in [Figure 1.2](#). Station HKNB was initially 593 m south of HKNA with a nominal distance between the HKNA and HKNB of 500 m. Buoy 156 at station HKNA was dragged out of position 430 m to southeast by 3rd party (4b in [Figure 1.2](#)). Station HKNB was moved 1000 m to the north due to work on telecommunications cables in the area in July 2018. Buoy WS140 was placed 2500 m to the east of its intended position in June 2018 and stayed for the duration of its deployment.

Table 1.1: *Hollandse Kust (noord) LiDAR buoy locations and measurement intervals. Spherical coordinates are given in ETRS89 and the cartesian coordinates in UTM 31N.*

Deployment	Buoy	LiDAR unit	Interval (UTC)		Nominal Positions		
Number			First measurement	Last measurement	Easting (m)	Northing (m)	DM
Station HKNA							
1	WS149	Z428	2017-04-10 00:00	2017-06-10 14:00	583949	5838365	52°41.3217' 4°14.5212'
3	WS155	Z505	2017-06-11 11:00	2017-09-07 00:00	583949	5838365	52°41.3217' 4°14.5212'
4	WS156	Z501	2017-09-07 12:10	2018-01-26 00:00	584043	5838345	52°41.3100' 4°14.6043'
6	WS158	Z513	2018-01-26 17:50	2018-06-08 13:30	583952	5838366	52°41.3220' 4°14.5260'
7	WS140	Z417	2018-06-08 13:40	2018-10-13 11:50	586354	5838212	52°41.2140' 4°16.6560'
11	WS156	Z501	2018-10-13 12:00	2019-02-25 15:50	583943	5838265	52°41.2680' 4°14.5140'
13	WS156	Z501	2019-03-01 13:00	2019-04-10 23:50	583943	5838265	52°41.2680' 4°14.5140'
Station HKNB							
2	WS170	Z585	2017-04-10 00:00	2017-12-02 00:00	583952	5837767	52°40.9992' 4°14.5147'
5	WS140	Z417	2017-12-02 09:20	2018-04-09 09:40	583958	5837731	52°40.9797' 4°14.5195'
8	WS170	Z585	2018-05-15 15:00	2018-07-17 10:40	583954	5837773	52°41.0040' 4°14.5140'
9	WS170	Z585	2018-07-17 13:30	2018-10-13 13:00	583954	5838773	52°41.5440' 4°14.5320'
10	WS170	Z585	2018-10-16 10:00	2018-11-25 08:00	583954	5838773	52°41.5440' 4°14.5320'
12	WS158	Z417	2018-11-25 08:10	2019-02-27 10:00	583907	5838773	52°41.5421' 4°14.4903'
12b	WS158	Z417	2019-02-27 14:30	2019-03-21 11:50	583957	5838577	52°41.4360' 4°14.5320'
14	WS158	Z513	2019-03-24 12:20	2019-04-10 23:50	583957	5838577	52°41.4360' 4°14.5320'

Some circumstances have caused partially missing campaign data per station. Missing data return (i.e. less than 100% availability) is due to circumstances such as contractual deployment (e.g. contractual transition with HKNB not deployed for ~1 month accounting for approximately 5% missing data return), regular service and maintenance as well as some unscheduled instrument specific outages with duration depending on workable weather for offshore operations as summarized in [Table 1.2](#) below. The nature of these circumstances demonstrates that the strategy of implementing two stations for redundancy was sensible.

Table 1.2: Hollandse Kust (noord) buoy swaps.

Deployment	Buoy	LiDAR unit	Issues
HKNA			
1	WS149	Z428	LiDAR stopped working on 2017-05-27, defective met station, buoy recovered for LiDAR servicing & swapped for WS155 on 2017-06-11.
3	WS155	Z505	No WLR deployed. No Aquadopp data. Buoy stopped on 2017-08-28, swapped for WS156 on 2017-09-07.
4	WS156	Z501	WLR data for December 2017 only. Buoy dragged out of position by 3 rd party 2017-11-22 until recovery (4b in Figure 1.2). Buoy and data verified ok. LiDAR stopped on 2018-01-16 due to low power supply from empty fuel canisters, defective met station on LiDAR. WS156 swapped for WS158 on 2018-01-26.
6	WS158	Z513	LiDAR defective met station. WS158 swapped with WS140 on 2018-06-08.
7	WS140	Z417	No Aquadopp data, swap with WS156 due to scheduled maintenance on 2018-10-13.
11	WS156	Z501	Transmission stop on 2018-10-29, manual reboot on 2018-11-05. Scheduled maintenance 2019-02-25 - 2019-03-01.
13	WS156	Z501	Resumed operations after scheduled maintenance on 2019-03-01 until end of campaign.
HKNB			
2	WS170	Z585	No WLR data from June 2017, no Aquadopp data August - November 2017, WS170 swapped with WS140 due to scheduled maintenance on 2017-12-02.
5	WS140	Z417	WS140 removed at end of 1 st campaign year. LiDAR defective met station.
8	WS170	Z585	Planned deployment on 2018-05-15.
9	WS170	Z585	WS170 moved 1 km north on 2018-07-17 due to telecommunications cable work in the area, no Aquadopp data August - October 2018.
10	WS170	Z585	Scheduled maintenance 2018-10-13 - 2018-10-16, transmission stop 2018-11-22. WS170 swapped with WS158 on 2018-11-25.
12	WS158	Z417	LiDAR Z513 not usable. WS158 deployed with Z417 (defective met station) on 2018-11-25. Transmission stop on 2019-02-21. Buoy stuck in re-boot sequence. No Aquadopp data February-March 2019.
12b	WS158	Z417	WS158 re-booted on 2019-02-27. Transmission stop on 2019-03-12, buoy stuck in re-boot sequence. Recovered on 2019-03-21.
14	WS158	Z513	WS158 re-deployed on 2019-03-24 with original LiDAR Z513 placed back on buoy until end of campaign.

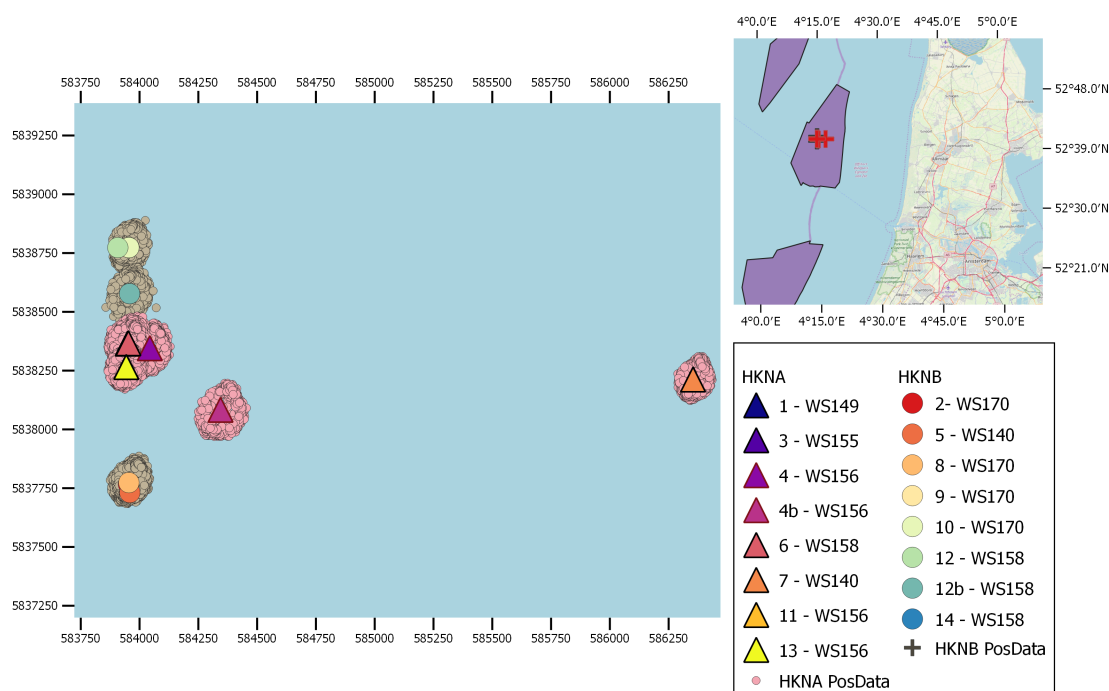


Figure 1.2: Buoy locations

1.1.1 Monthly data reports

During the measurements campaign the data was reported on a monthly basis, see [Fugro \(2017b, 2018i, 2018g, 2018b, 2018p, 2018n, 2018m, 2018d, 2018f, 2018e, 2018k, 2018a, 2018l, 2018j, 2018h, 2018c, 2018q, 2018o, 2019e, 2019a, 2019c, 2019b, 2019d\)](#). In these reports information on instrumentation, serial numbers, and post-processing can be found in more detail than in this summary report. Monthly data reports are published on <https://offshorewind.rvo.nl/windwaternh>.

1.1.2 Monthly validation reports

During the measurement campaign the data has been validated on a monthly basis using the same statistics, reference stations and model data as used to validate the full campaign data, see [Deltares \(2017a, 2017b, 2018i, 2018g, 2018b, 2018p, 2018n, 2018m, 2018d, 2018f, 2018e, 2018k, 2018a, 2018l, 2018j, 2018h, 2018c, 2018q, 2018o, 2019e, 2019a, 2019c, 2019b, 2019d\)](#). In those reports the ECN LiDAR data and the model data are also validated against observations from the reference stations, those validations are not repeated in this report. Monthly validation reports are published on <https://offshorewind.rvo.nl/windwaternh>.

1.2 QHSE

There were no personnel accidents or injuries during this campaign.

There were no other HSE related issues during any other field operations or other work related to this project.

1.3 Definitions and abbreviations

Time: All times refer to UTC.

Convention of directions:

Directions are given in degrees (°) increasing clockwise from North.

- Wind and wave direction is defined as "coming from" and rotating clockwise from North, i.e. 0° means wind/waves from the North, 90° from the East etc.
- Current direction is defined as "flowing towards", i.e. 0° means current flowing towards the North, 90° towards the East etc.

Abbreviations:

- SWLB: Seawatch Wind LiDAR Buoy
- UTC: Universal Time Coordinated
- MSL: Mean Sea Level
- LAT: Lowest Astronomical Tide
- NaN: Not-a-number
- TI: Turbulence Intensity

1.4 Outline of the report

The next 3 chapters describe the campaign instrumentation, the post-processing and quality control of the data, the files in which the data are made available, and the data validation routine. In Chapter 5 the full campaign data availability is given. The subsequent chapters present for each variable group, namely wind, waves, temperature, air pressure, water level and currents, the validation of the data and description of some of the HKN climate characteristics according to the campaign data. The report ends with a concluding chapter.

2 Instrumentation and measurement configuration

Each buoy is a SEAWATCH Wind LiDAR Buoy based on the original SEAWATCH Wavescan buoy design with the following sensors:

- Wavesense 3: 3-directional wave sensor
- Gill Windsonic M ultrasonic wind sensor
- Vaisala PTB330A air pressure sensor
- Vaisala HMP155 air temperature and humidity sensor
- Nortek Aquadopp 600kHz current profiler
- ZephIR 300S LiDAR

The LiDARs used in this project received marine upgrades by ZephIR and are equivalent to the 300M marine version.

An independent Thelma water pressure sensor was located on the bottom. The pressure sensor transmits data to the buoy via an acoustic link.

The core datalogging facility of all instrumentation on a SWLB is the Wavesense 3 providing time-synchronized logging and onboard real-time processing of all parameters. The Wavesense 3 datalogging unit converts all measurements to physical quantities in SI units. The data are packed atomically for transmission and storage using a proprietary compression algorithm, giving sufficient resolution while using minimal storage space. Both transmitted data and buoy stored downloaded data are unpacked to physical values in real numbers using the reverse conversion method. This also means that the downloaded data and transmitted data are exact copies and data in transmission are encrypted.

The mooring for the buoys is shown in [Figure 2.1](#).

The final report is a summary of the full campaign, more information detailing the instrumentation configuration for each buoy/station can be found in the monthly reports. [Table 2.1](#) shows the measurement configurations used throughout the campaign.

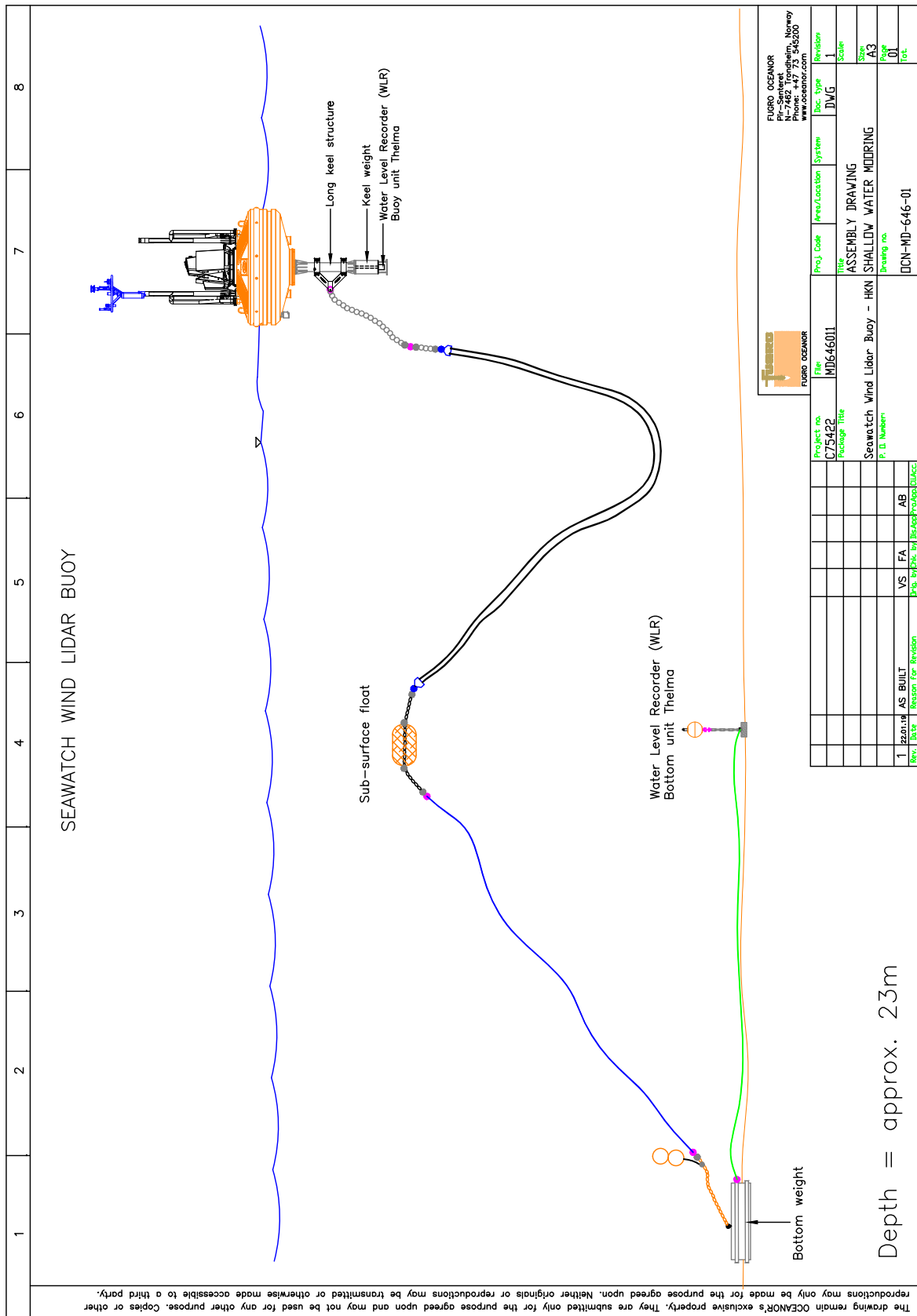


Figure 2.1: Mooring design for the SWLB at Hollandse Kust (noord)

Instrument type	Sensor height ¹ (m)	Parameter measured	Sample height ¹ (m)	Sampling interval (s)	Averaging period (s)	Burst interval ² (s)	Transmitted?
Vaisala PTB330A	0.5	Air pressure	0.5	30	60	600	Yes
Vaisala HMP155	4.1	Air temperature Air humidity	4.1	5	60	600	Yes
Wavesense 3	0	Heave, pitch, roll, heading	0	0.5	Time series duration: 1024 s	600	No
		Sea state parameters (See Table 3.2)	0	600	1024	600	Yes
Gill Windsonic M	4	Wind speed, wind direction	4	1	600	600	Yes
ZephIR 300M LiDAR	2	Wind speed and direction at 10 heights (The 11 th level, the so-called reference level which is not configurable, is also located at 40 m and referred to as 40.0 Ref.)	30	17.4 s ³	600	600	Yes
			40				
			40.0 ref				
			60				
			80				
			100				
			120				
			140				
Nortek Aquadopp	-1	Current speed and direction profile, water temperature (at 1 m depth)	160	N/A	600	600	Yes
			180				
			200				
			-4				
Thelma WLR	-23	Water pressure Temperature	-6			600	Yes
			...				
			-30 (14 levels)				

¹ Height relative to actual sea surface. The depth of the WLR is an approximate number.

² A burst of measurements is the raw data time series used to calculate the average parameters. The burst interval is the time from the beginning of one burst to the beginning of the next burst, and equal to the interval between writing of raw data to disk and transmissions. Note that wave bursts overlap by 424 s.

³ This is the approximate time between the beginning of one sweep of the profile and the next one; the interval may vary slightly. The ZephIR sweeps one level at a time beginning at the lowest one. After the top level has been swept, it uses some time for calculations and re-focusing back to the lowest level for a new sweep. Minimum 18 samples per height must be measured in the 10-minute interval in order to produce wind speed and direction, and derived parameters thereof.

Table 2.1: Measurement configurations for the SWLB at Hollandse Kust (noord)

2.1 Wind data collection

There are two types of wind sensors on the LiDAR buoy: *Gill Windsonic* and *ZephIR 300 LiDAR*. The drawing in [Figure 2.2](#) shows the location of these sensors and the current profiler, and illustrates the LiDAR and current profiler beams. Heights indicate the levels of the LiDAR optical window (2 m), the height of the Gill sensor (4 m), and the lowest and highest possible LiDAR profile levels, all relative to the sea surface. The buoys used in this campaign are set-up to measure the wind at the levels 4 m (Gill) and at 30, 40, 60, 80, 100, 120, 140 160, 180 and 200 m (LiDAR) above the sea surface.

The *Gill Windsonic* is an ultrasonic wind sensor measuring the wind along the two horizontal axes defined by the sensor transmitting and receiving elements. The travel time difference of ultrasound emitted in opposite directions along the two perpendicular axes is used to calculate the wind speed components along those axes. From the components the wind speed and direction relative to the instruments x-axis is computed. Then the wind direction relative to magnetic North is calculated using the measurement of buoy heading from the internal compass.

The *ZephIR LiDAR* is a Continuous Wave (CW) LiDAR system. The continuous beam emitted from the window at the top of the LiDAR is slanted at an angle from the vertical and rotates with a period of 1 second around the central axis to continually scan a cone in the air. The return is focused to a particular elevation using an optical focus stage and samples individual line of sight points around the circle. The magnitude of the Doppler shift of the backscattered individual line of sight samples is used to reconstruct the 1 second wind field at a particular elevation.

The LiDAR focuses each of the 10 selected elevations in sequence sampling the wind profile. Before going back to another profile, the LiDAR spends some time doing other tasks, such as looking for precipitation, fog and cloud base, and measuring at the reference height of 38 m above the laser. The effective interval between each profile is about 17 s.

The profiles collected at 17 s intervals are averaged to give a time series of 10-minute average horizontal and vertical wind. In the SWLB Wavesense 3 processing unit, each 1 s sample is processed by an algorithm which fuses data from other sensors (compass, Gill) to produce the 10-minute averages. From the components, the wind speed and direction relative to the instrument's x-axis are computed. Then the wind direction is calculated using the measurement of buoy heading from the compass. Wind directions are also checked in real-time against the data from the Gill wind sensor to resolve the 180° ambiguity in the results due to the ambiguity in the magnitude of the Doppler shift.

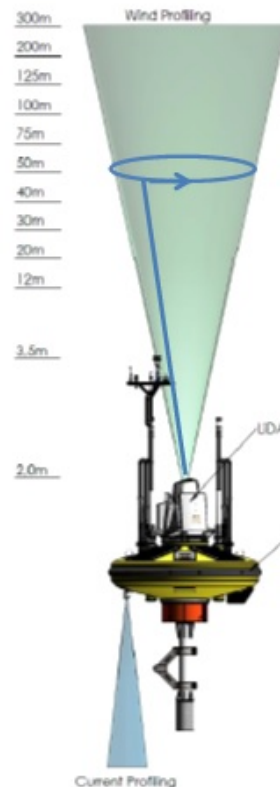


Figure 2.2: Illustration of the wind and current profile measurements from the LiDAR buoy. Heights ref. sea surface

2.2 Wave data collection

The wave measurements are based on the fact that the discus shaped buoy will respond to the waves by following the height and slope of the waves, so that the wave motion can be interpreted as the motion of the sea surface. The Wavesense 3 wave sensor employs accelerometers, rotation sensors and a compass to calculate the position, velocities and rotations of the buoy in all directions in space. From these data the spectra of wave height and direction are calculated, and the parameters of wave height, period and direction listed in [Table 3.1](#) are calculated. The wave parameters are based on a time series of 1024 1Hz values, i.e. 17 minutes ($1024 \text{ s} \approx 17 \text{ min}$). When the acquisition is complete, the analysis phase starts using FFT (Fast Fourier Transform) algorithms. Wave bursts overlap by 424 s, i.e. data is collected for 1024 s, but data is analyzed and written to file every 600 s. The measurements are taken continuously and the processing windows overlap.

2.3 Temperature data collection

The Vaisala HMP155 measures air temperature and humidity using a state of the art HUMICAP[®]180R humidity sensor element and a fast temperature probe. The mounting of the sensor in a protective housing on the mast top sensor carrier ensures that the sensor is exposed to the free air and yet shielded from cooling and heating due to solar and diffuse radiation. The surface temperature (1 m below sea surface) is sampled by the Nortek Aquadopp current meter. The bottom temperature is measured by the bottom mounted pressure sensors.

2.4 Air pressure data collection

The air pressure is measured by the Vaisala pressure sensor PTB330A located inside the buoy and includes Vaisala's top class BAROCAP[®] pressure sensing technology. The sensor is exposed to the pressure of the open air through a diffusor head on the top of the mast which removes the pressure reducing effect of the wind from the air pressure measurement.

2.5 Water level data collection

Water level is not measured directly, but inferred from measurements of pressure at the seabed. The bottom mounted pressure sensor gives out an approximate value of water level as the actual pressure in dbar minus 10 dbar which is then approximate equal to the depth in meters. However, to get the proper height of the water column above the sensor, the air pressure measurement from the buoy must be subtracted from the total measured water pressure as follows:

$$h_w = (P_w - P_a) / \rho g \quad (2.1)$$

where h_w is the height of the water column, P_w is the measured total water pressure, P_a is the measured total air pressure, ρ is the average density of the water (1025.7 kg/m^3) according to average temperature and salinity data from this area stored by ICES (International Council for the Exploration of the Sea), and g is the normal acceleration of gravity. Note that the pressure sensor head is located approximately 1.00 m above the seabed. The vertical position of the sensor relative to mean sea level can be obtained from bathymetry data at the deployed coordinates given in [Table 1.1](#), or by the difference in bias with an already MSL referenced tide gauge or the DCSMv6-ZUNOV4 model as shown in [Figure 10.1](#) in [Section 10.4](#). During the campaign an operational correction was used based on bathymetry. In the final dataset a bias between the observations and the model was determined and applied to the water level data.

2.6 Current data collection

The AquaDopp current profiler is mounted in the buoy hull with the acoustic head immediately below the hull. The three slanted transducers emit sound pulses forming 3 acoustic beams at an angle from the vertical. The Doppler shift of sound echoed from particles such as plankton in the water is used to calculate the current velocity component along the beam. The vertical and horizontal velocity components are then calculated, and a large number of pulses are used to calculate the 10-minute average current velocity

3 Post processing, quality control and file descriptions

3.1 Post processing and quality control

Quality control is an integral part of each stage of a measurement campaign from manufacturing and assembly (factory acceptance tests, instrument documentation), validation of the full set up (and Site Acceptance Tests if applicable), deployment records, internal system checks and data integrity through the Wavesense data logging unit and throughout post processing and data delivery.

A live test site at the island of Frøya, Norway, with various references is maintained by Fugro. The site has been used by the Norwegian University of Technology and Science (NTNU) for wind research for many years. In particular for the SEAWATCH Wind LiDAR buoy this site is routinely used for validation prior to delivery of an SWLB to a project, using a land reference LiDAR to verify the SWLB is in accordance with Carbon Trust OWA criteria ([OWA, 2013, 2018](#)).

This section outlines the processing steps applied to the data before they are delivered to RVO.nl. In post processing the system integrity is maintained. No tampering or modifications have been applied to increase the post processed availability. Not all data from all instruments are transmitted via satellite due to package size and cost restraints. Monthly post processing and quality control was done mainly on transmitted data.

[Figure 3.1](#) shows the data reception and post processing flow. The buoy converts all measurements to physical quantities in SI units. The data are packed simultaneously for transmission and storage in binary integer numbers using a proprietary compression algorithm (binary pff-telegrams), giving sufficient resolution while using minimal storage space. At the receiving end the data are unpacked to physical values in real numbers using the reverse conversion method (pffx to pff csv). This also means that the data in transmission are encrypted. The data are then imported into the in-house measurements database (live import) for post-processing and quality control. Once all quality criteria are met, the dataset is shared for validation and issued to the client together with the monthly data and validation reports.

Incoming transmitted data are first checked for gaps, instrument and buoy operation issues and timestamp and compass alignment. Any data during downtimes are removed. Then a set of filters according to agreed ranges for each parameter are applied as detailed below in [Table 3.2](#) and [Section 3.2](#). The data are inspected for any outliers and, if related to instrument or transmission issues, removed.

During buoy maintenance all stored data are downloaded and used to check any issues (data availability and missing data, error messages, potential bias in data from a sensor, etc.) identified during quality-control and validation for the respective monthly reports. If data packages were not received during transmission and resulted in gaps in the data record, the corresponding stored packages are then used to fill these gaps.

The same processing and quality control criteria are applied to all downloaded data for the full range of measurements for the full 2-year campaign period. Consequently the downloaded dataset is more complete and of the same or higher quality as in the monthly reports.

Raw data are data stored on the respective instrument in instrument native format (ZephIR,

Aquadopp, Wavesense) and are downloaded during buoy maintenance and at the end of the campaign.

Each SWLB is set up with unique telemetry message identifiers. Together with deployment records, timestamps and position data, the datasets for each of the two stations (HKNA, HKNB) in this campaign are kept separate and unique.

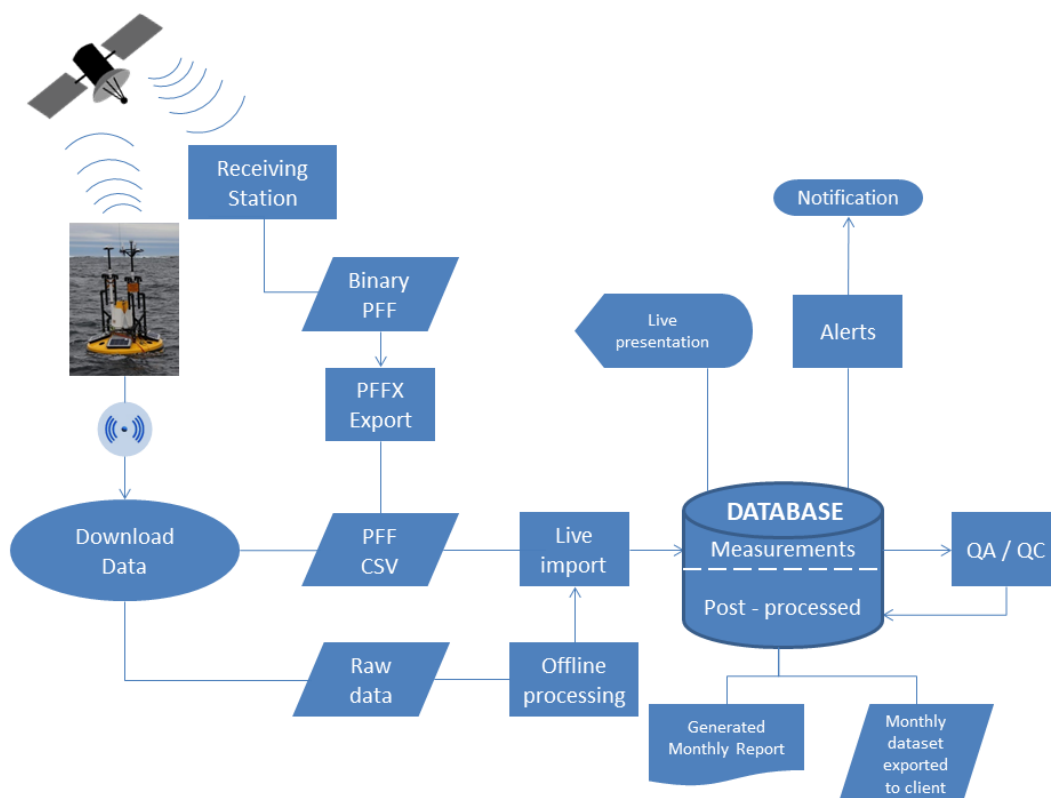


Figure 3.1: Dataset generation from transmitted and downloaded (recovered and raw) data

Table 3.1 gives a brief explanation of what the variable names mean, their units and, if applicable, the symbols used in the data validation to refer to them.

Table 3.1: List of variables. All parameters are presented as averages over 10 minutes.

Name	Description	Units	Symbol
WindSpeed z mh	Wind speed at an elevation of z m above the sea surface	m/s	U_z
WindGust z mh	3-second wind gust speed at an elevation of z m above the sea surface	m/s	
WindDir z m	Wind direction at an elevation of z m above the sea surface	°N	$U_{z\theta}$
hm0	Spectral significant wave height	m	H_s
hm0a	Spectral significant swell wave height. Frequency band between 0.04 and 0.10 Hz.	m	H_{sswell}
hm0b	Spectral significant sea wave height. Frequency band between 0.10 and 0.50 Hz.	m	H_{ssea}
hmax	Spectral maximal individual wave height	m	H_{max}
mdir	Mean wave direction	°N	MWD
mdira	Mean wave direction of swell	°N	MWD_{swell}
mdirb	Mean wave direction of sea	°N	MWD_{sea}
sprtp	Wave spreading at spectral peak period	°	$DSPR$
thhf	High frequency mean wave direction. Frequency band between 0.4 and 0.44 Hz.	°N	
thmax	Period of highest wave.	s	
thtp	Wave direction at spectral peak period.	°N	
tm0x	Spectral mean absolute wave period (1 based on the 1 st spectral moment, 2 based on the 2 nd spectral moment, a swell, b sea)	s	T_{m0x}
tp	Spectral peak wave period	s	T_p
AqSpd d	Current speed at a depth of d m below the sea surface	m/s	u_d
AqDir d	Current direction at a depth of d m below the sea surface	°N	
airTemperature	Air temperature	°C	T_{air}
airPressure	Air pressure	hPa	
airHumidity	Air humidity	%	
WaterTemp0001	Water temperature (surface)	°C	T_{water}
WaterLevel	Sea surface elevation	m	WL
BottomTemp	Water temperature (bottom)	°C	T_{water}

Table 3.2: QA/QC filter ranges for each parameter

Parameter	min	max	Unit
Wind speed LiDAR	0.0001	58	m/s
Wind speed Gill	0.001	35	m/s
Direction (all)	0	360	°
Inflow Angle	-15	15	°
Current speed	0	135	cm/s
Hm0	0	18	m
Hmax	0	18	m
TP	0.1	23	s
Thmax	0.01	23	s
Air humidity	0	100	%
Air pressure	905	1100	hPa
Air temperature	-4	30	°C
Water temperature	2.9	25	°C
Water pressure (HKNA)	20	26	dbar
Water pressure (HKNB)	20	26	dbar

3.2 File descriptions

Definitions:

- NaN (Not a Number): Label indicating data as invalid/missing
- All filenames have prefixes 'HKN_YYYYMMDD_Fugro_MetOcean Buoys HKNX'
- YYYY = year 4 digits
- MM = month 2 digit
- DD = day of month 2 digits
- X = A or B to separate HKNA and HKNB

File: *WindResourceSpeedDirectionTISat*

LiDAR data:

The file contains 10-minute averaged wind measurements calculated on the buoy. The signals are all timestamped with the end of the averaging period. All timestamps must have wind speed values between 0.0001 and 58.0 m/s. The directional, turbulence and inflow angles are set to NaN for the same timestamps and heights where the wind speeds are set to NaN. To correct for 180 degrees ambiguities in the LiDAR wind directions an additional correction with 10 minute average directions from the Gill wind sensor as ground truth has been used. The correction is done automatically using an algorithm checking each height for ambiguous wind directions and flipping it 180 degrees if necessary.

File: *WaveCurrentData*

The file contains 10-minute average data calculated on the buoy from the current meter, wave and meteorological sensors. All timestamps are set at the end of the averaging period.

Current data: For all current speed signals AqSpd(d), where d = 4, 6, ..., 22 m, it is checked that $0.0 < \text{AqSpd}(d) \leq 200.0$ cm/s. For timestamps and depths where the speed is outside this range, the speed and direction are set to NaN.

Water temperature: All data with temperature outside a reasonable range (Table 3.2) are marked as NaN.

Water level and bottom temperature: Bottom Temperature measurements are filtered as *Water temperature* above.

Water level data or Bottom Temperature sequences of 10 or more identical values are replaced by NaN. The data is then linearly interpolated across sequences of up to 4 NaNs, and the Water level data is corrected with the air pressure data as described in [Equation 2.1](#). A MSL referenced water level at the position is subtracted to give the water level relative to the mean sea level. Finally the Water level data is interpolated again as before to fill some potential gaps where the air pressure measurements are missing.

Wave data: The following signals derived from the wave spectra are checked: ['hm0 m', 'hm0a m', 'hm0b m', 'hmax m', 'mdir deg', 'mdir a deg', 'mdir b deg', 'sprtp deg', 'thhf deg', 'thmax s', 'thtp deg', 'tm01 s', 'tm02 s', 'tm02a s', 'tm02b s', 'tp s'].

Wave height signal 'hm0 m' is checked for values above 18 m. If found, all wave parameters (as indicated above) are set to NaN.

Wave period signal 'tp s' is checked for values above 23 s. If found all wave parameters (as indicated above) are set to NaN.

File: *WaveSpectraComponents*

The wave spectra parameters [hspec, a1, a2, b1, b2] are all set to NaN if any of the above wave parameters values are set to NaN.

File: *WaterLevelNonInterpolated*

The file contains the original temperature measurements in degrees Celsius and pressure measurements in dbar - which is approximately the height of the water column in metres - from the seabed pressure sensor. Water level data sequences of 10 or more identical values have been replaced by NaN. The pressure and temperature data have not been modified. No interpolation or other corrections have been performed on these data.

File: *WindResourceInflowAnglesStat*

This file contains the inflow angles in degrees, calculated on the buoy using data from the ZephIR unit. The angles are calculated as the angle between the 10-minute average horizontal and vertical components. The inflow angles are checked after the signals in the file *WindResourceSpeedDirectionTISat* are checked and timestamps where wind speed measurements are invalid there are also set as invalid in this file. All measurements where the inflow angle is larger than 40 degrees or less than -40 degrees are set to NaN.

File: *WindResourceVeerShearStat*

This file veer and shear statistics calculated from the already processed LiDAR wind directions and speeds in the *WindResourceSpeedDirectionTISat* file using the same timestamps to store data. Wind shear is calculated as the difference in wind speed per meter between the height levels indicated by the parameter name. Positive values indicate wind speed increasing with height. Wind veer is the difference in direction between the two levels divided by the height difference, positive if direction rotates counter-clockwise going upward. No further processing is done on the signals here. These signals are stored in a separate file because they depend on other data and are calculated as part of the data post processing.

File: *PosData*

Geographical Latitude and Longitude in Degrees with 6 decimals. This file contains hourly values of buoy position according to GPS.

Raw data

Raw wave data

Raw wave data is provided in *chpr* files. These files contain the Wavesens raw motion compass, heave, pitch and roll data. All angles (compass, pitch and roll) are given in degrees, heave elevations are in m. Sensor sampling rate is at 1 Hz. For each row the timestamp in the first column given represents the start of the sampling of the time series in that row.

The index in the parameter name, given by [0],[1],...[1023], is the sample number for the parameter. So heave[0] would be the first sample starting at the timestamp in the first column and heave[1023] would be the last sample for the measurement period with start time given by the first column.

Raw wind data:

Raw 1 Hz LiDAR data directly from the ZephIR units (unprocessed) is delivered in *zph* files addition to the processed and quality checked products. The filename convention for this file is: "Wind_*unit*Y_M_D.ZPH", where *unit* refers to the ZephIR unit identifier.

The same buoys and thus the respective LiDAR units were used several times during this campaign (downtime for maintenance, details in the deployment log in [Table 1.1](#)). Recurring identifiers for both the *chpr* and the *zephir* data files are possible but can be resolved using timestamps. [Table 1.1](#) gives the respective start and stop times. The raw data files are grouped by deployment number to minimize ambiguities (e.g. Deployment 1 contains *chpr_WS149.csv* and all corresponding *Wind_428@Y_M_D.ZPH* files).

3.3 Data Files

The delivered data files are listed in [Table 3.3](#). The dataset is based on complete downloaded data from April 2017 to April 2019, both from the respective buoy and corresponding ZephIR unit.

Table 3.3: Data files that make up the complete set of data presented in this report.

HKNA_20190815_Fugro MetOcean Buoys HKNA	PosData_F.csv
HKNA_20190815_Fugro MetOcean Buoys HKNA	WaterLevelNonInterpolated_F.csv
HKNA_20190815_Fugro MetOcean Buoys HKNA	WaveCurrentDataStat_F.csv
HKNA_20190815_Fugro MetOcean Buoys HKNA	WaveSpectraComponents_F.csv
HKNA_20190815_Fugro MetOcean Buoys HKNA	WindResourceInflowAnglesStat_F.csv
HKNA_20190815_Fugro MetOcean Buoys HKNA	WindResourceSpeedDirectionT1Stat_F.csv
HKNA_20190815_Fugro MetOcean Buoys HKNA	WindResourceVeerShearStat_F.csv
Deployment 1	1_chpr_WS149.csv
Deployment 3	3_chpr_WS155.csv
Deployment 4	4_hpr_WS156.csv
Deployment 6	6_chpr_WS158.csv
Deployment 7	7_chpr_WS140.csv
Deployment 11	11_chpr_WS156.csv
Deployment 13	13_chpr_WS156.csv
ZephIR	"Wind_unitY_M_D.ZPH"
HKNB_20190815_Fugro MetOcean Buoys HKNB	PosData_F.csv
HKNB_20190815_Fugro MetOcean Buoys HKNB	WaterLevelNonInterpolated_F.csv
HKNB_20190815_Fugro MetOcean Buoys HKNB	WaveCurrentDataStat_F.csv
HKNB_20190815_Fugro MetOcean Buoys HKNB	WaveSpectraComponents_F.csv
HKNB_20190815_Fugro MetOcean Buoys HKNB	WindResourceInflowAnglesStat_F.csv
HKNB_20190815_Fugro MetOcean Buoys HKNB	WindResourceSpeedDirectionT1Stat_F.csv
HKNB_20190815_Fugro MetOcean Buoys HKNB	WindResourceVeerShearStat_F.csv
Deployment 2	2_chpr_WS170.csv
Deployment 5	5_chpr_WS140.csv
Deployment 8	8_chpr_WS170.csv
Deployment 9	9_chpr_WS170.csv
Deployment 10	10_chpr_WS170.csv
Deployment 12 & 12b	12_chpr_WS158.csv
Deployment 14	14_chpr_WS158.csv
ZephIR	"Wind_unitY_M_D.ZPH"

4 Data Validation

4.1 Measurement uncertainties

The Seawatch Wind LiDAR Buoy is 3rd party type validated by the accredited institution DNVGL to be in the pre-commercial stage according to Carbon Trust's requirements (OWA, 2013) over a six-month trial (DNVGL, 2015b). That trial took place in 2014 at the now decommissioned RWE met mast in Dutch waters. A similar six-month trial was conducted at the East Anglia One met mast in 2015 as part of the Carbon Trust programme, with the performance independently verified by Natural Power (2015). In addition, the specific systems used in the HKN campaign were validated in a pre-deployment validation campaign before the start of the HKN measurement campaign. The performance of the systems was independently verified by DNVGL (2015b,a) to reproduce accurate wind speed and direction across a range of wind and sea states against a reference. The pre-deployment validation campaign took place at the Fugro validation site at the island of Frøya, Norway. The validation site has also been 3rd party evaluated by DNVGL (2015a) as suitable for the purpose of validating systems like the SWLB.

An uncertainty assessment for the SEAWATCH Wind LiDAR Buoy based on the RWE Meteomast IJmuiden was conducted by Ecofys (2016). According to this assessment, wind profile measurements from the Seawatch wind LiDAR buoys in this region can be used with a measurement uncertainty of 3.3-3.4%. The Carbon Trust OWA roadmap version 2.0 (issued Oct 2018), OWA (2018), outlines a procedure to quantify uncertainties pertaining to LiDAR wind measurements in accordance with RP18 (IEAwind, 2016) and IEC 61400-12-1 Annex L. (IEC 61400-12-1, 2017).

All buoys were pre-deployment validated and two in-situ validations comparing buoys in operation were performed (DNVGL (2019a), DNVGL (2019b), DNVGL (2017), DNVGL (2017), DNVGL (2016c), DNVGL (2016b), DNVGL (2016d), DNVGL (2016a)). All pre-deployment and in-situ validation reports are published on <https://offshorewind.rvo.nl/windwaternh>.

4.2 Validation procedure

The validation is carried out by quantifying the agreement between the HKNA and HKNB data and data from other reliable sources (anemometer, LiDAR, hydrodynamic model, etc) in the North Sea. Furthermore, for some variables their general characteristics are also qualitatively assessed, such as for current and wind measurements their respective vertical profiles. Per variable the most suitable available data validation sources have been sought, leading to the following combinations:

- The reference stations for validating the buoy wind data against anemometer observations are platform K13a, referred to as K13, Lichteiland Goeree, referred to as LEG, platform Q1, referred to as Q1 or Q11 (Q11 being the name used to identify archived observations from platform Q1) and EuroPlatform, referred to as EPL. Note that K13, LEG and EPL are at a considerable distance from both HKNA and HKNB, thus comparisons between these datasets are expected to lack precision. These stations are, nevertheless, considered since the anemometers in these platforms are at a higher height than at Q1, 73.8 m, 38.3 m, and 29.1 m in the case of respectively K13, LEG and EPL, whereas measurements are carried out at 23.1 m at Q1. The considered anemometer observations, as most other observations considered in this study, have been collected by the Dutch Government. LiDAR wind velocity observations at vertical levels 63 m, 91 m, 116 m, 141 m, 166 m and

191 m at LEG and EPL from the Energy research Centre of the Netherlands (ECN) part of the Dutch organization for applied research (TNO) have also been made available and are also considered in the validation of the wind data.

- The wave heights, periods and directions are validated against Dutch Government observations. The locations for validating the buoy wave data are Q1, EPL, K13, and IJmuiden munitiestortplaats, referred to as IJmuiden. Again, it is expected that the correspondence between HKNA and HKNB observations and those from K13 and EPL is lower than with those from the nearer stations, but the K13 and EPL data are considered to also provide a more spatial view of the waves in the North Sea.
- The Dutch Government observations at IJmuiden, EPL, LEG and K13 are used for validating the water temperature.
- Available online data from weather stations located at Q1 and P11-b are used for validating the air temperature.
- Dutch Government observations at EPL, LEG, K13 and Q1 are used for validating air pressure.
- Lastly, the WLR water levels are compared with observations from the considered North Sea reference stations and validated against hydrodynamic model predictions at their exact locations, which are also used to validate the buoy's currents.

Figure 4.1 shows an overview of all measurement locations. The present report provides the validation results for the full campaign period - extended from April 10, 2017 00:00 until April 10, 2019 23:50.

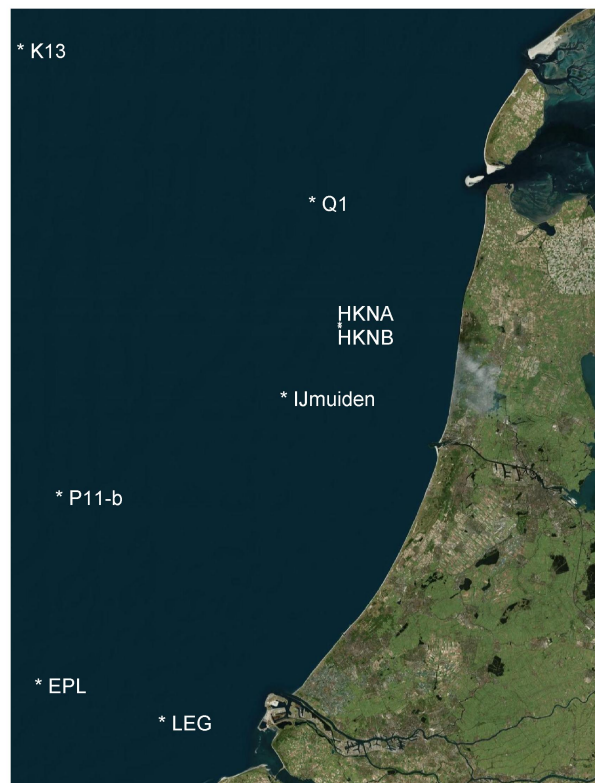


Figure 4.1: Location of buoys and fixed measurement stations (via Google Earth).

All comparisons are presented as a timeseries and further validated via direct scatter plots for quantifying statistical correspondence between the datasets.

The error statistics are computed differently whether a linear or circular (directional) variable is considered. For linear variables we have:

- the bias: $\bar{y} - \bar{x}$;
- the root-mean-square error: $\text{rmse} = \sqrt{n^{-1} \sum (y_i - x_i)^2}$;
- the symmetric slope: $s = \sqrt{\sum x_i^2 / \sum y_i^2}$; and
- the correlation coefficient:

$$r = \sum [(x_i - \bar{x})(y_i - \bar{y})] / \sqrt{\sum (x_i - \bar{x})^2 \sum (y_i - \bar{y})^2}.$$

In all these formulae x_i usually represents observations (or the dataset which is considered less uncertain or baseline) and in this study we use it to represent the fixed observations, y_i usually represents the model results (or the dataset which is considered more uncertain or with a certain deviation from the baseline results) and in this study we use it to represent the HKNA and HKNB data and n the number of observations.

When dealing with circular data, each observation is considered as unit vector, and it requires vector addition rather than ordinary (or scalar) addition to compute the average of angles, the so-called mean direction.

Writing

$$C_n = \sum_{i=1}^n \cos x_i \quad \text{and} \quad S_n = \sum_{i=1}^n \sin x_i, \quad (4.1)$$

the sample resultant vector R_n of a sample $\mathbf{x} = x_i, i = 1, \dots, n$ is defined as $R_n = \sqrt{C_n^2 + S_n^2}$, and its sample mean direction $\bar{x} \equiv \bar{x}_n$ as the direction of R_n :

$$\bar{x} = \text{TAN}^{-1}(S_n/C_n)$$

where

$$\text{TAN}^{-1}(S_n/C_n)$$

is the inverse of the tangent of

$$(S_n/C_n)$$

in the range $[0, 2\pi]$, i.e.,

$$\text{TAN}^{-1}(S_n/C_n) := \begin{cases} \tan^{-1}(S_n/C_n), & S_n > 0, C_n > 0 \\ \tan^{-1}(S_n/C_n) + \pi, & C_n < 0 \\ \tan^{-1}(S_n/C_n) + 2\pi, & S_n < 0, C_n > 0. \end{cases} \quad (4.2)$$

The sample mean resultant length of $\mathbf{x} = x_i, i = 1, \dots, n$ is defined by $\bar{R}_n = R_n/n$, $0 \leq \bar{R} \leq 1$. If $\bar{R}_n = 1$, then all angles coincide.

Equation 4.2 can be used to compute the bias between two circular variables by substituting x_i by $y_i - x_i$ in Equation 4.1. In a similar way, the root-mean-square error between two circular variables can be computed.

There are several circular analogues of the correlation coefficient, but the most widely used is the so-called T-linear correlation coefficient ([Fisher and Lee \(1983\)](#) and [Fisher \(1993\)](#)). Given two sets $\mathbf{x} = x_i, i = 1, \dots, n$, $\mathbf{y} = y_i, i = 1, \dots, n$ of circular data, the T-linear correlation coefficient between x and y is defined by

$$r = \frac{\sum_{1 \leq i < j \leq n} \sin(x_i - x_j) \sin(y_i - y_j)}{\sqrt{\sum_{1 \leq i < j \leq n} \sin^2(x_i - x_j) \sum_{1 \leq i < j \leq n} \sin^2(y_i - y_j)}}.$$

In the following we shall refer to comparisons in which r is higher than 0.9 as excellent, between 0.8 and 0.9 as good, between 0.7 and 0.8 as reasonable and lower than 0.7 as poor. Note that this is no absolute quality statement given that there are uncertainties in both observations and, due to the distance between the instruments, the spatial variability is expected to affect the comparisons.

Note that all reported dates are in UTC.

5 Data Availability

5.1 Introduction

Although in measuring campaigns the aim is always to have a full (gap free) timeseries of all measured parameters, this is typically hampered by severe metocean conditions and loss of signal between instruments. The redundant deployment of two SWLBs aimed to mitigate loss of data due to these circumstances. Signal and dataset availability are calculated and reported monthly, calculated for the full 2-year dataset and for each month separately in the 2-year dataset.

The Floating LiDAR System is ready to function according to specifications and to deliver data, taking into account all time stamped data entries in the output data files including flagged data (e.g. by NaNs or 9999s) for the given month. Note that for the system to be considered "ready", at least one valid data point must be recorded (at any height). The Monthly Overall System Availability is the number of those time stamped data entries relative to the maximum possible number of (here 10-minute) data entries including periods of maintenance within the respective calendar month.

The *Monthly Post-processed Data Availability* is the number of those data entries remaining after subtraction of all non-valid entries caused by including but not limited to:

- downtime (due to equipment failure, maintenance, weather, damage, malfunction, theft, or any other events)
- system internal (unseen) filtering
- application of quality filters based on system own parameters, as defined in [Section 3.2](#)

divided by the maximum possible number of 10-minute data entries within the respective calendar month based on the given time interval of 10-minutes.

Notes:

- 1 The Monthly Post-processed Data Availability is calculated and presented per system and for each system per main data set:
 - a. Wind: Direction and speed availability at 10 levels, turbulence intensity, inflow angle, wind shear and wind veer averaged to a single availability value.
 - b. Wave: Significant wave height, peak wave period, mean wave period, mean wave direction, wave spectra.
 - c. Current: Current speed and direction at 10 levels.
 - d. Water level
 - e. Atmospheric pressure
 - f. Temperature: Air temperature, Sea temperature.
- 2 The Monthly Post-processed Data Availability per system is the average of the Monthly post processed data availabilities per main data set per system.
- 3 In the case of multiple (redundant) measurement instruments determining one parameter value, the availability of at least one parameter value is the determining base for the data availability.

In this study we do not look at the monthly availability but at the overall campaign availability.

Furthermore, we use the following qualification of data availability:

- >95% referred to as high availability,
- 90 - 95% referred to as good availability,
- 80 - 90% referred to as acceptable availability,
- 60 - 80% referred to as limited availability, and
- <60% referred to as poor availability.

5.2 Validated parameters

Figure 5.1 shows a detailed breakdown of the amount of missing data throughout the temporal record for each measured parameter for each buoy. Table 3.1 gives a brief explanation of what the variable names mean, their units and, if applicable, the symbols used in the data validation to refer to them.

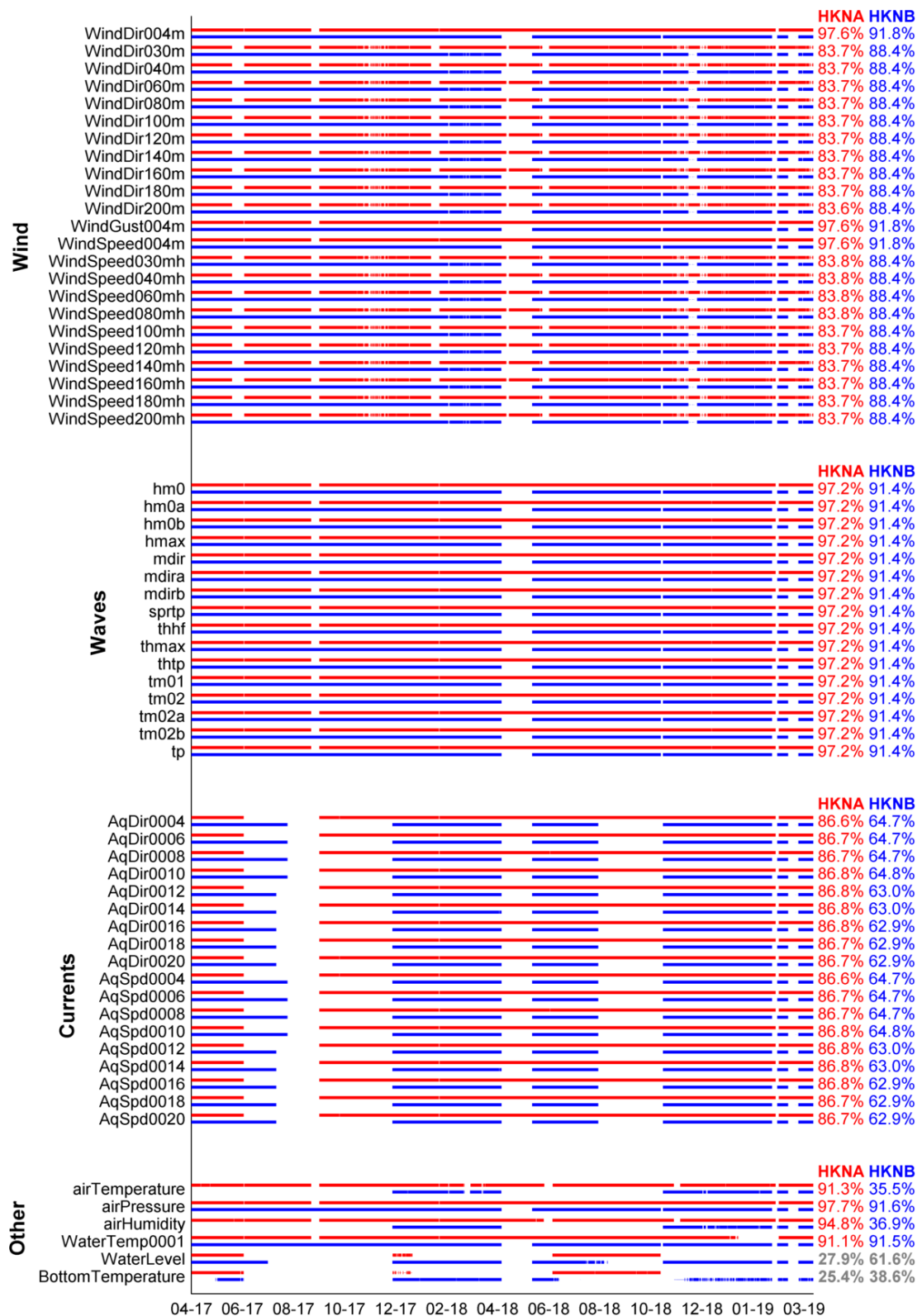


Figure 5.1: Data availability HKNA (red), HKNB (blue) and HKNA WLR and HKNB WLR (grey) for the full campaign period from April 10, 2017 00:00 until April 10, 2019 23:50.

As can be seen in Figure 5.1, the collected data include wind speed and direction at different heights, a number of wave height, period and direction parameters, current speed and

direction at different depths, water levels, water and air temperature, pressure and humidity. Complementing the wave parameters of which availability is shown in [Figure 5.1](#), the Fourier coefficients and the heave spectra, from which the 2D-wave spectra can be computed, are also collected.

The availability of the

- wind data is acceptable to high, of the
- wave data is high from HKNA and good from HKNB, of the
- current data is at all levels acceptable from HKNA and limited from HKNB, of the
- air and water temperature is good and of the air pressure is high from HKNA, of the
- water level data from the WLR at HKNB is limited and only of the
- other WLR data is poor.

Note that the overall data availability at HKNB is reduced by approximately 5% since HKNB was not operational during the contractual transition period in April-May 2018.

[Figure 5.2](#) and [Figure 5.3](#) show the comparison between the availability of the released monthly data and the full campaign data for HKNA and HKNB, respectively. The downloading of the data has the potential of increasing availability of data points which were not available in the monthly operational reports due to transmission errors. [Figure 5.2](#) and [Figure 5.3](#) show that this is generally the case. However, and in particular, the current profile data from HKNA have lower availability in the recovered dataset due to re-evaluating the decision of the monthly operational reporting of including suspicious current profile data. The current meter data from June to September 2017 at HKNA was flagged in the monthly reports as “bias in current direction, more noise, spikes, data to be used with caution”. Given that unfortunately the raw current meter data from that deployment are not available to double check what went wrong, it has been decided to err on the side of caution and take these data out completely.

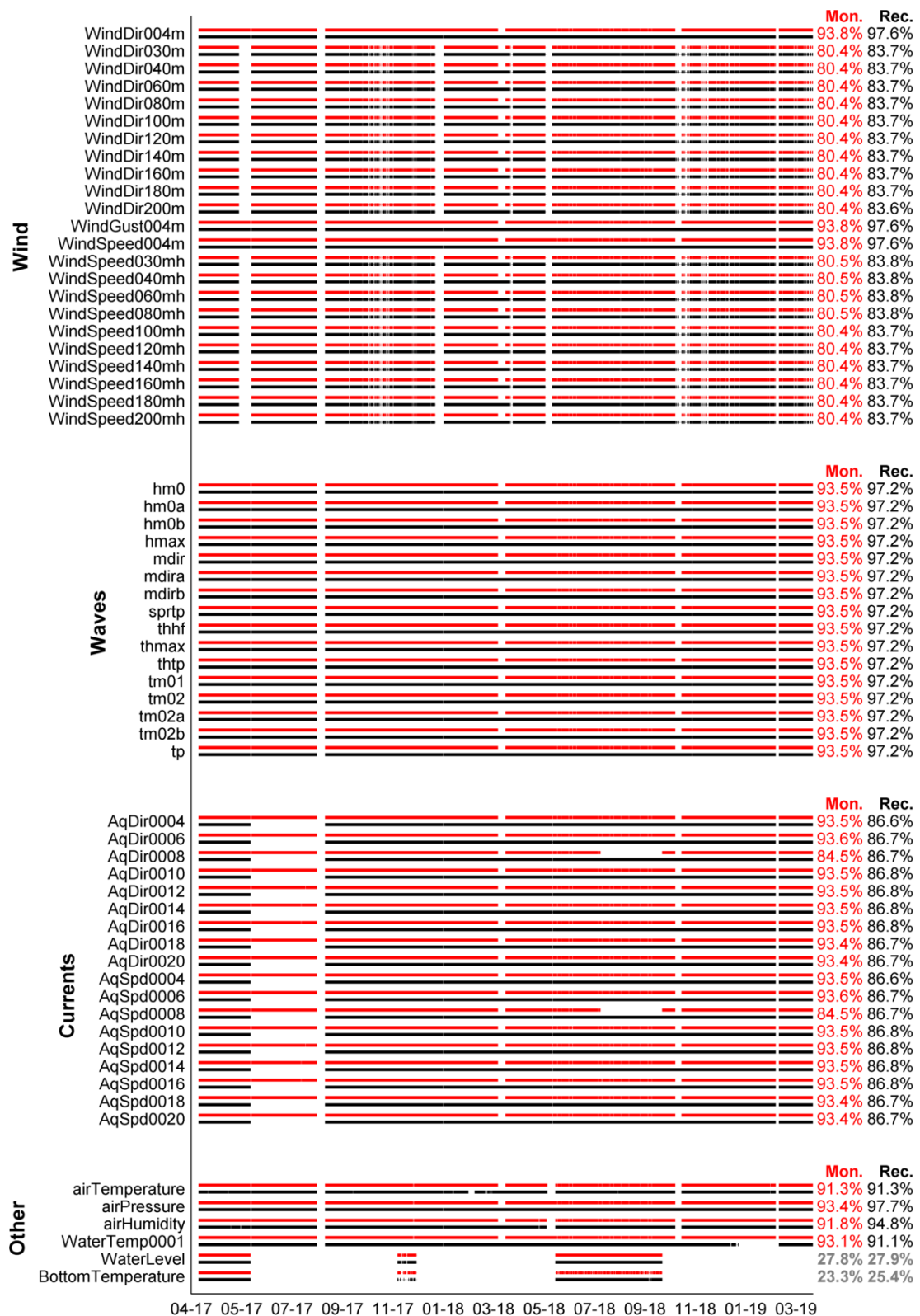


Figure 5.2: Comparison of the HKNA data availability in the monthly reports (red) and for the full campaign dataset (black).

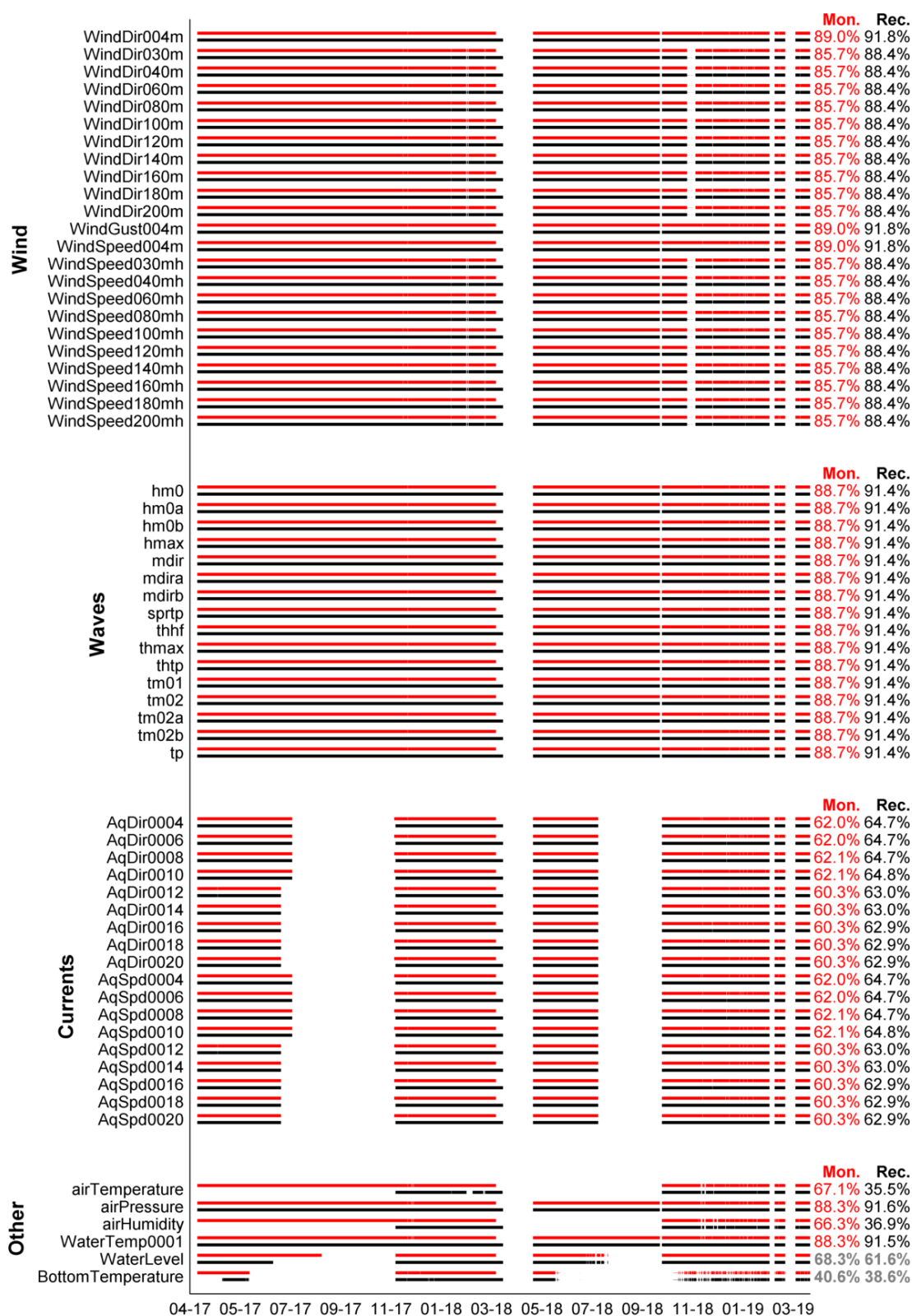


Figure 5.3: Comparison of the HKNB data availability in the monthly reports (red) and for the full campaign dataset (black).

For illustration, if the gaps in the data collected from the location with the highest data return per variable are filled with the data collected from the other station in order to compile a complete HKN dataset, the resulting data return is as given in [Figure 5.4](#). As can be seen

in the figure, the availabilities are then high for wind and waves, good for currents, high for pressure and water temperature, good for air temperature and limited for water level.

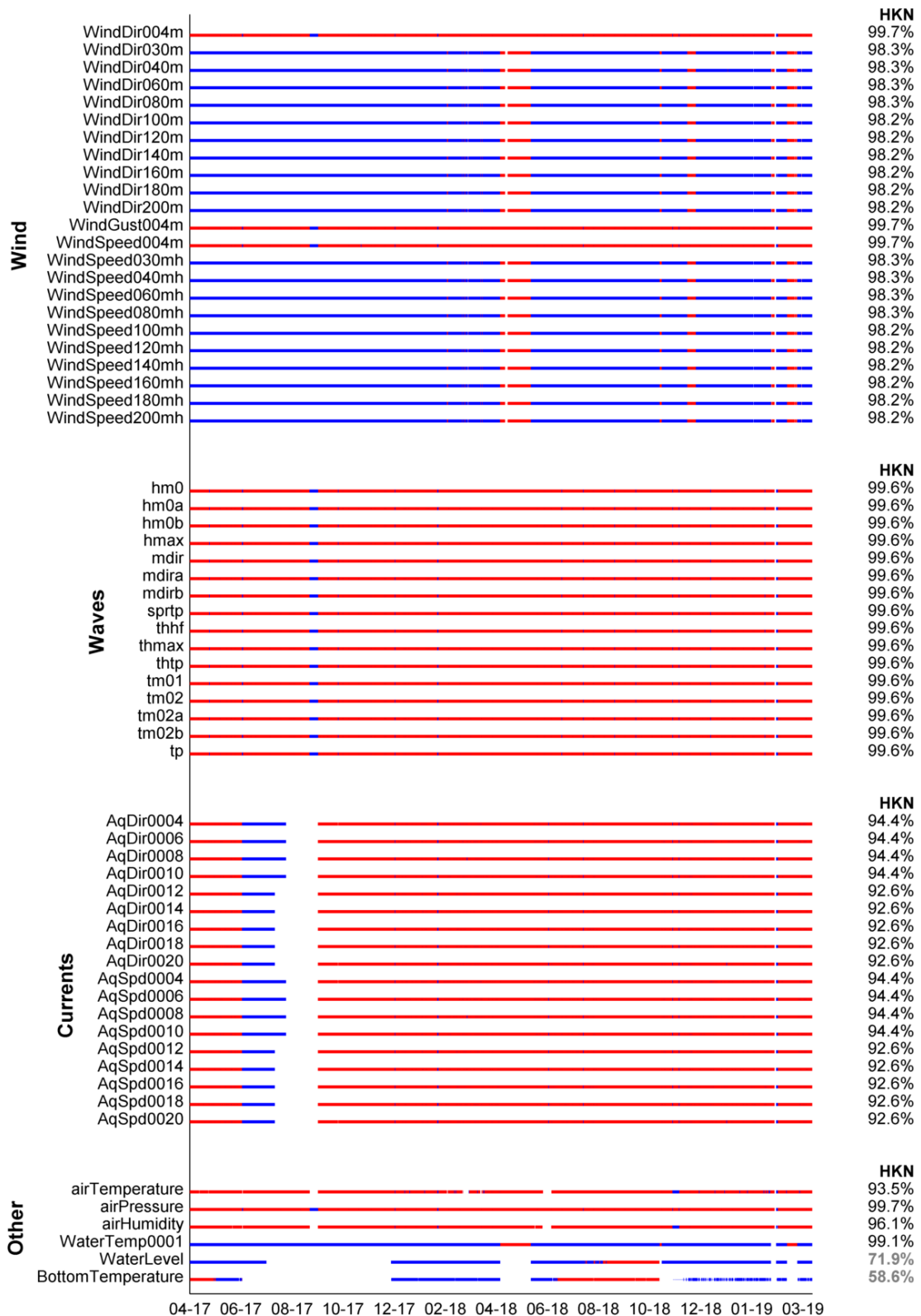


Figure 5.4: Data availability HKN for the full campaign period from April 10, 2017 00:00 until April 10, 2019 23:50. The red (blue) indicates data from HKNA (HKNB).

5.3 Non-validated parameters

Humidity data are not considered further in this report.

The additional wind parameters turbulence intensity, wind shear, wind veer and inflow angle are also provided but are not validated in this report.

Turbulence Intensity (TI) is defined as $TI = (\sigma/\bar{u})C$, where σ is the standard deviation and \bar{u} is the mean of the wind speed for a 10-min period. $C = 0.95$ is a constant needed to convert the scan-averaged LiDAR measurements to the point-measurements of a cup anemometer (ZephIR, 2013). Note that this definition frequently gives relatively high values in situations with low but variable wind speed. Note also that TI is not compensated for the motion of the buoy, which is a source of increased standard deviation in the measurements, and TI is therefore over-estimated compared to what would be obtained from a LiDAR on a fixed platform. This definition of TI was deemed an acceptable approximation for this campaign. However, users of this data are advised to apply further scrutiny to ensure full applicability to the desired analysis.

Wind veer and *wind shear* statistics are calculated from the already processed LiDAR wind directions and speeds. *Wind shear* is calculated as the difference in wind speed per meter between the height levels indicated by the parameter name. Positive values indicate wind speed increasing with height. *Wind veer* is the difference in direction between the two levels divided by the height difference, positive if direction rotates counter-clockwise going upward. No further processing is done on the signals here.

Inflow Angle (IA) is the angle of the 3-dimensional wind vector (in °) based on the 10-min averaged values of the horizontal and vertical wind velocity components. A positive *IA* means that the wind vector has an upward directed vertical component.

6 Wind

6.1 Introduction

This chapter focuses on validating and analyzing processed wind speeds (by elevation) from the *SEAWATCH LiDAR Buoys*. The wind speed and direction is measured at levels 4, 30, 40, 60, 80, 100, 120, 140, 160, 180 and 200 m above water level. The measurements at 4 m are carried out with an acoustic wind sensor and those at 30 to 200 m with a LiDAR.

6.2 Intercomparison of the HKN data

To get a full overview of the data, [Figure 6.1](#) and [Figure 6.2](#) show the time evolution of vertical wind profiles at HKNA and at HKNB, respectively. In order to further present the data, [Figure 6.3](#) and [Figure 6.4](#) show timeseries of wind speed and direction, respectively, at the observation levels.

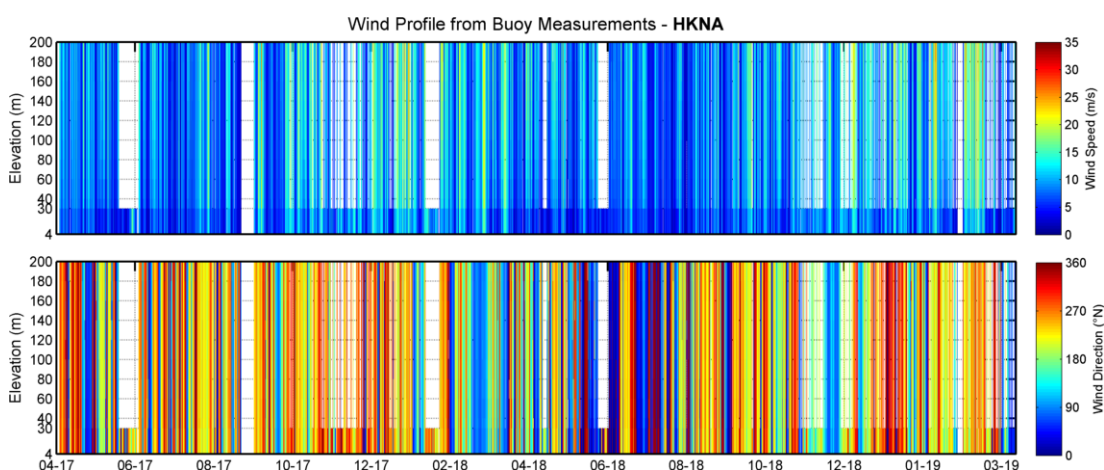


Figure 6.1: Time evolution of the vertical wind speed (top panel) and direction (bottom panel) profiles at HKNA.

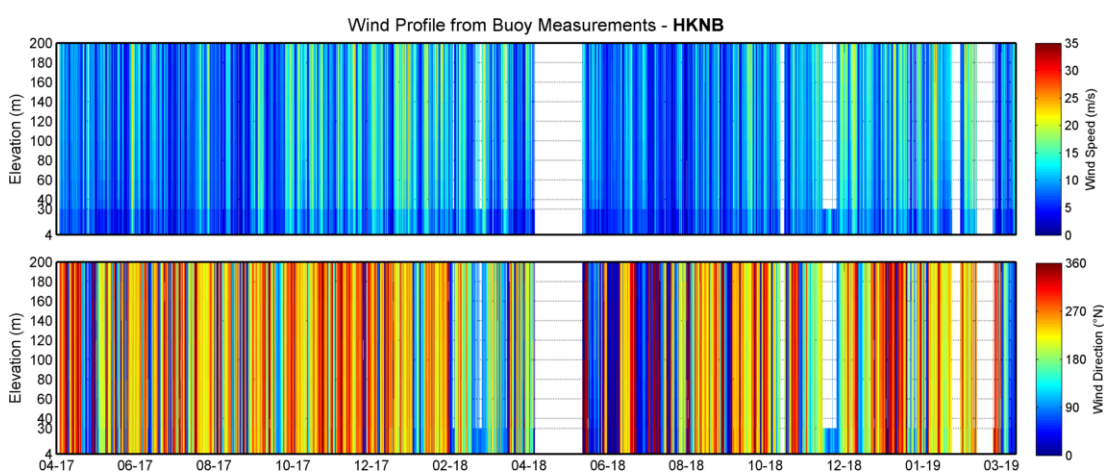


Figure 6.2: Time evolution of the vertical wind speed (top panel) and direction (bottom panel) profiles at HKNB.

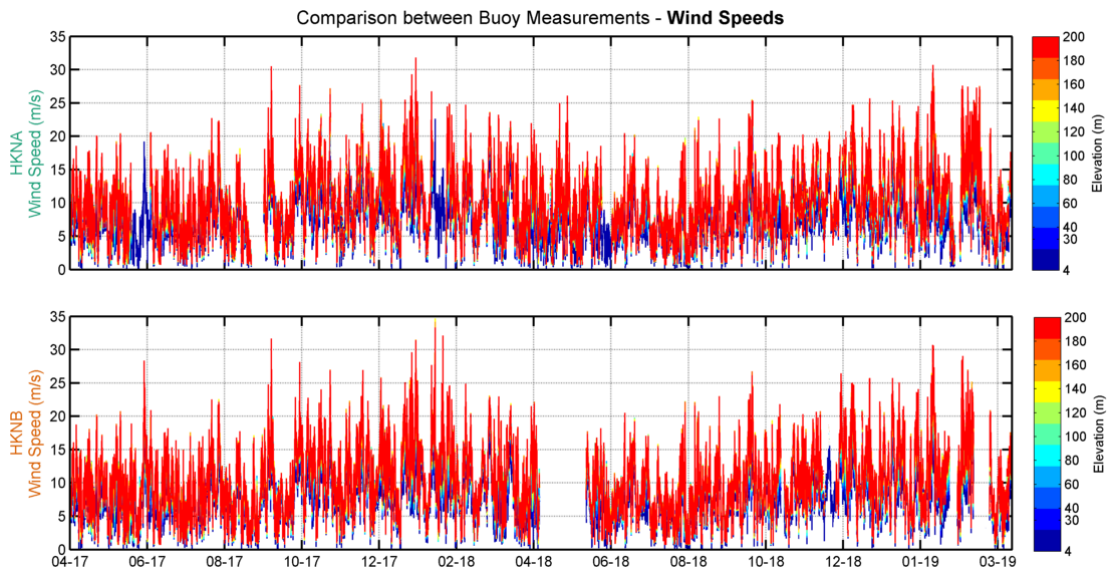


Figure 6.3: Wind speeds (by elevation) at each buoy.

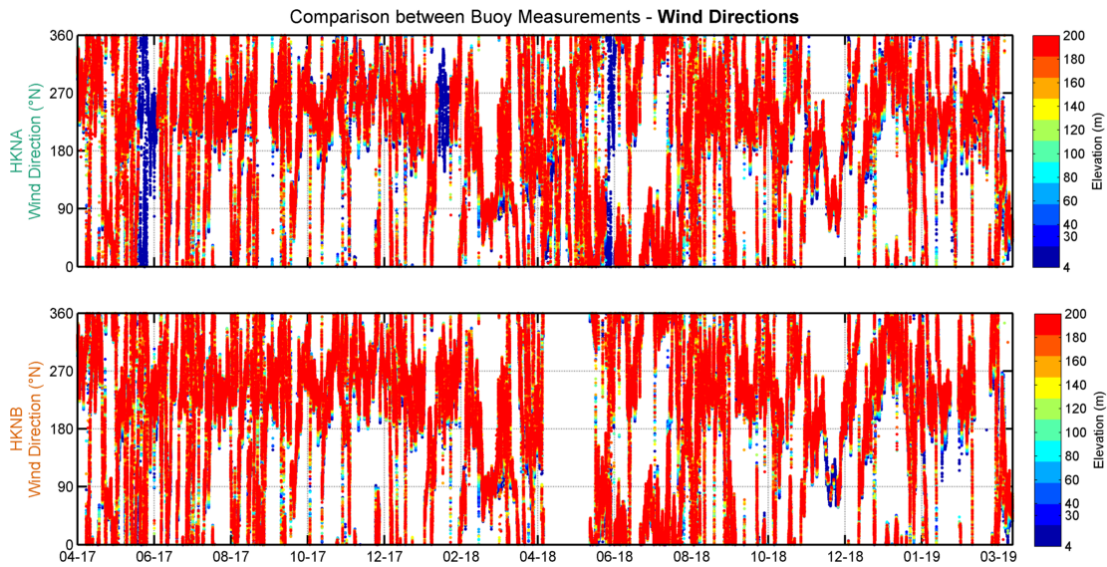


Figure 6.4: Wind directions (by elevation) at each buoy.

Figure 6.5 shows density scatter comparisons between wind speed and direction measured by HKNA and HKNB at levels 100m and 160m. The figure shows a general agreement between the observations at HKNA and HKNB, as could already be seen in Figure 6.3 and Figure 6.4.

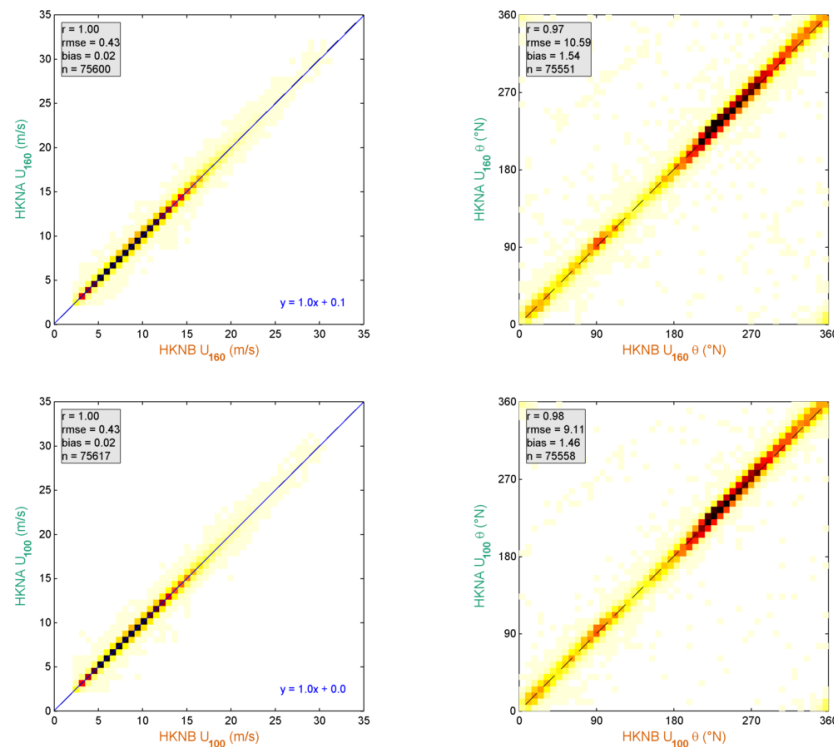


Figure 6.5: Direct scatter comparison between buoy wind at elevations of 100 and 160 m.

The differences between the HKNA and HKNB wind speed and direction observations are further quantified by means of the slope, bias, correlations and square correlations between the HKNA and HKNB wind speed observations at all levels and the bias, correlations and square correlations between the HKNA and HKNB wind direction observations at all levels have been computed considering all wind speeds above 2 m/s. These are given in [Table 6.1](#) and can be compared against the criteria given in [IEC 61400-12-1 \(2017\)](#) and [IEA Wind \(2017\)](#). Note that the statistic we use to determine the correlation between the wind directions differs from the one applied in [IEA Wind \(2017\)](#). We apply a T-linear correlation coefficient which leads to correlations that are slightly lower than those of the standard correlation coefficient. Nevertheless, as can be seen in [Table 6.1](#), the comparisons are at all levels excellent in terms of both wind speed and direction, which substantiate that the instruments were working correctly and the high accuracy of the data.

Table 6.1: Statistical comparison between the winds from the LiDAR buoys with elevation.

Elev. (m)	Wind Speed					Wind Direction			
	r^2 (-)	r (-)	Bias (m/s)	Sym. Slope (-)	n (-)	r^2 (-)	r (-)	Bias ($^{\circ}$ N)	n (-)
4	0.98	0.99	0.01	1.00	89929	0.98	0.99	2.2	89922
30	0.99	0.99	0.02	1.00	75447	0.96	0.98	1.5	75371
40	0.99	0.99	0.02	1.00	75532	0.96	0.98	1.5	75461
60	0.99	0.99	0.02	1.00	75626	0.96	0.98	1.5	75562
80	0.99	0.99	0.02	1.00	75643	0.96	0.98	1.5	75573
100	0.99	1.00	0.02	1.00	75617	0.96	0.98	1.5	75558
120	0.99	1.00	0.02	1.00	75612	0.96	0.98	1.5	75552
140	0.99	1.00	0.02	1.00	75609	0.95	0.98	1.5	75552
160	0.99	1.00	0.02	1.00	75600	0.95	0.97	1.5	75551
180	0.99	1.00	0.02	1.00	75622	0.95	0.97	1.6	75568
200	0.99	1.00	0.03	1.00	75628	0.94	0.97	1.5	75556

6.3 Comparison with data from the fixed stations

In this section the buoy data are validated against the observations from the fixed stations.

Before comparing the data, the Q1 (z=23.1m), EPL (z=29.1m), LEG (z=38.3m) and K13 (z=73.8m) anemometer wind observations were quality controlled in terms of outliers in wind speed looking at deviation from the monthly mean and deviation from one timestamps to the next using as criteria 6 times the standard deviation of the monthly data and no outliers were found.

An overview of the data from the buoy and the anemometers at the platform locations is given by means of wind roses in [Figure 6.6](#). The figure shows the roses of the Q1, LEG, EPL and K13 observations and the HKNA and HKNB LiDAR observations at the levels closer to those of the LEG, EPL and K13 anemometers for the campaign period. The roses show a general agreement across the locations, that the prevailing winds are from the Southwest and with a more southern direction at EPL and a larger directional spreading at Q1 and K13.

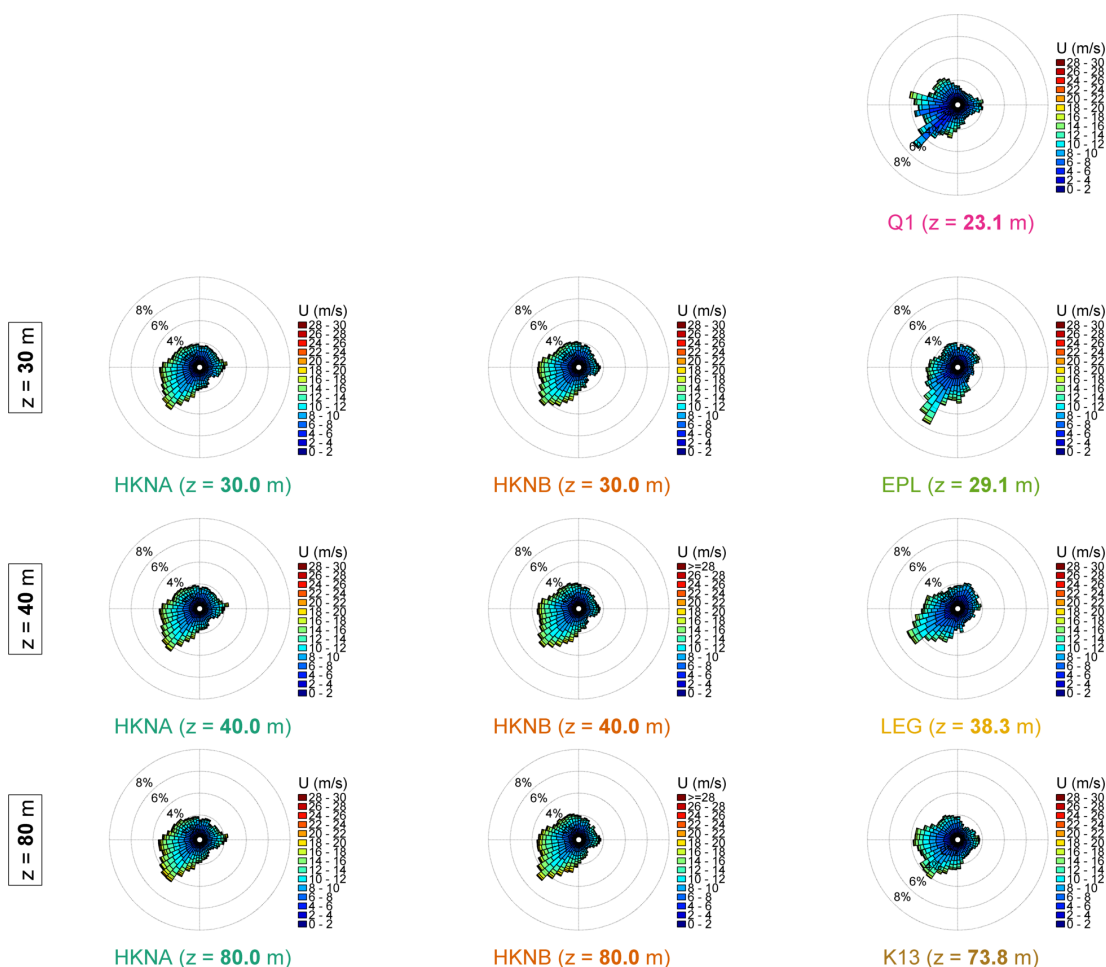


Figure 6.6: Wind roses for all locations.

In the following sections the HKNA and HKNB winds are directly compared to the fixed observations data, first considering the anemometer data and then the ECN LiDAR observations at LEG and EPL ($z=63, 91, 116, 141, 166$ and 191m). In the comparisons with the anemometer data, directional statistics (for different wind direction sectors) are given and in the comparisons with the ECN LiDAR data height dependent statistics are given. Given that for low wind speeds there is much scatter in the data and that these data are not relevant in the data validation, all observations for which the observed wind speeds are below 5 m/s are excluded in the determination of error statistics. This threshold was chosen pragmatically, being in line with the work of [Wieringa and Rijkoort \(1983\)](#) and in line with other wind climate assessments of the Dutch meteorological institute and close to the 4 m/s threshold prescribed for the calibration of cup anemometers in the IEC 61400-12-1 standard.

6.3.1 Validation of HKNA

In order to further validate the HKNA data, the data was compared with the Q1, LEG, EPL and K13 simultaneous observations.

[Figure 6.7](#), [Figure 6.9](#), [Figure 6.11](#) and [Figure 6.13](#) show timeseries and density scatter comparisons between HKNA observations and those from the anemometers at LEG, EPL and K13, respectively. The correlation, root-mean-square error and bias statistics are printed in the figures. [Figure 6.8](#), [Figure 6.10](#), [Figure 6.12](#) and [Figure 6.14](#) compare the wind roses of the simultaneous observations. Note that these roses may differ from those in [Figure 6.6](#)

because the roses in Figure 6.6 show all available observations at each station in the campaign period. Table 6.2, Table 6.3, Table 6.4 and Table 6.5 show the error statistics between the HKNA and the fixed platform data per directional sector, i.e. when the HKNA wind direction at the considered level falls within the direction range given in the left column of the tables. Note that lower correlations in terms of wind direction are to be expected from this data binning.

The following conclusions are taken from the assessment of these figures and tables:

- At Q1 the omni-directional comparisons with HKNA are good in terms of wind speed and excellent in terms of wind direction. The roses show comparable conditions, with a larger predominance of West and Southwest winds at Q1. The directional comparisons are good to excellent in terms of wind speed and reasonable to good in terms of wind direction. The larger biases in the Q1 observations from the Southwest have already been observed in the monthly validations (see e.g. Deltares, 2019c) and are maybe due to a local obstruction.
- At LEG the omni-directional comparisons with HKNA are also good in terms of wind speed and excellent in terms of wind direction. The roses show comparable conditions, with a lower directional spread for the predominant Southwest wind at LEG. The directional comparisons are reasonable to good in terms of wind speed, whereas poor in terms of wind direction as expected from the rose comparisons.
- At EPL the omni-directional comparisons with HKNA are again good in terms of wind speed and excellent in terms of wind direction. The roses show that the predominant winds from the Southwest have a more southern direction at EPL. The directional comparisons are also reasonable to good in terms of wind speed, whereas again poor in terms of wind direction as expected from the rose comparisons.
- At K13 the omni-directional comparisons with HKNA are good both in terms of wind speed and direction. The roses show a lower predominance of Southwest wind conditions at K13. The directional comparisons are reasonable to excellent in terms of wind speed and poor to reasonable in terms of wind direction.

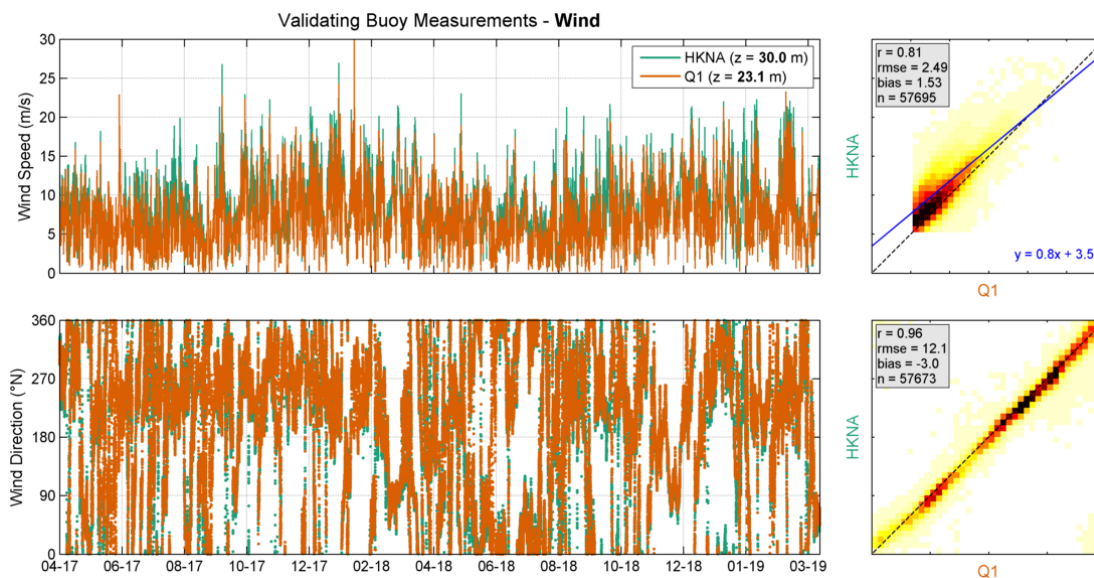


Figure 6.7: Validation of HKNA wind with Q1. Left panels: Timeseries. Right panels: Density scatter, with the darker colours indicating more data density.

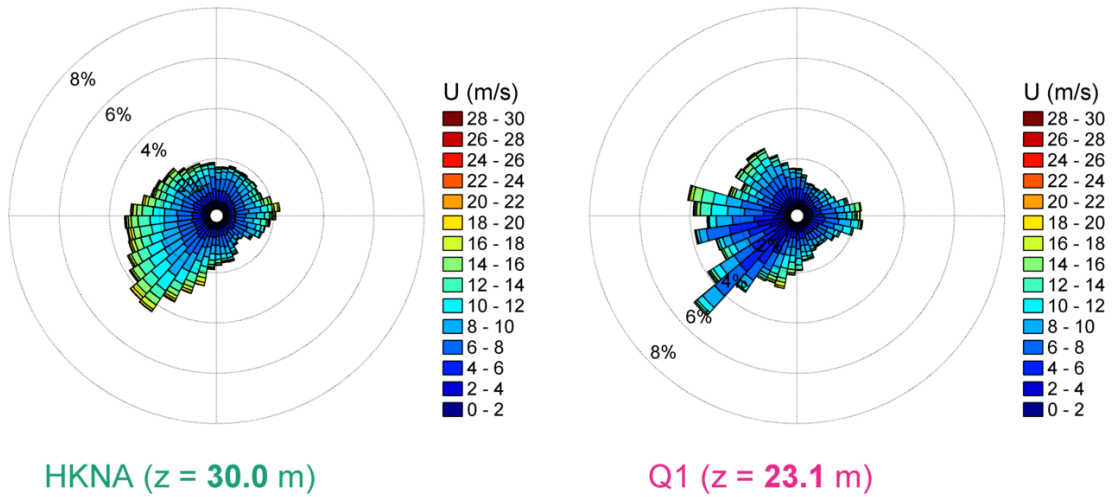


Figure 6.8: Roses of the simultaneously available HKNA and Q1 wind data.

Table 6.2: Direction statistical comparison between HKNA (z = 30.0 m) and Q1.

Sector	n (-)	Wind Speed			Wind Direction		
		r (-)	RMSE (m/s)	Bias (m/s)	r (-)	RMSE (°N)	Bias (°N)
337.5 °N : 22.5 °N	5086	0.86	1.58	0.98	0.76	14.01	7.45
22.5 °N : 67.5 °N	4832	0.82	1.81	1.14	0.76	15.36	-3.12
67.5 °N : 112.5 °N	7052	0.92	1.73	1.14	0.80	10.50	-5.59
112.5 °N : 157.5 °N	3752	0.86	1.19	0.19	0.82	10.96	-5.28
157.5 °N : 202.5 °N	6925	0.89	1.67	0.43	0.80	10.17	-3.21
202.5 °N : 247.5 °N	12026	0.81	3.84	3.36	0.79	12.21	-4.73
247.5 °N : 292.5 °N	10575	0.80	2.94	1.92	0.71	12.52	-5.32
292.5 °N : 337.5 °N	7475	0.92	1.46	0.73	0.73	10.69	-0.01

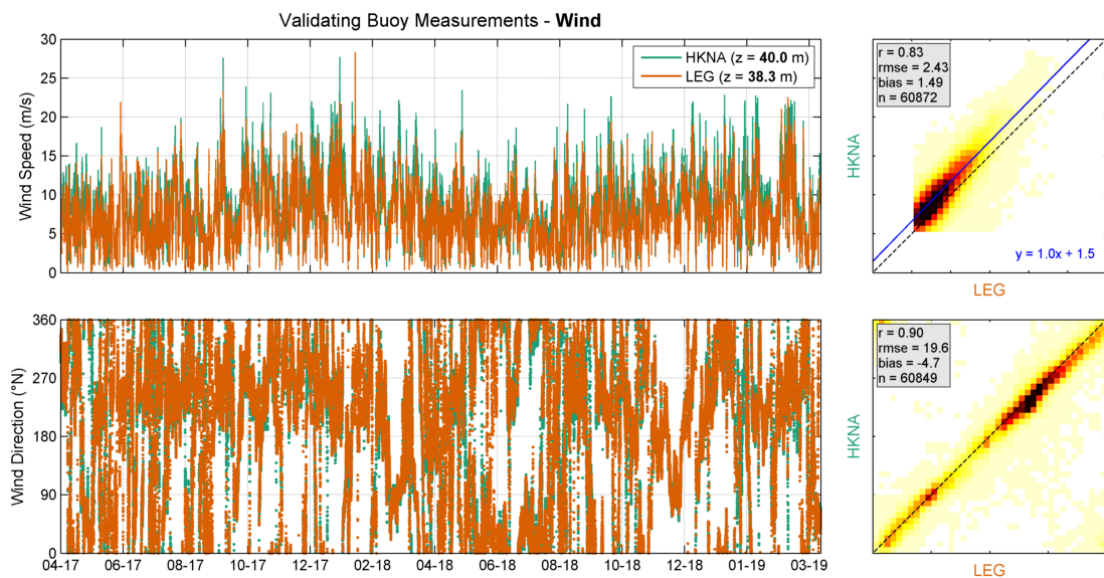
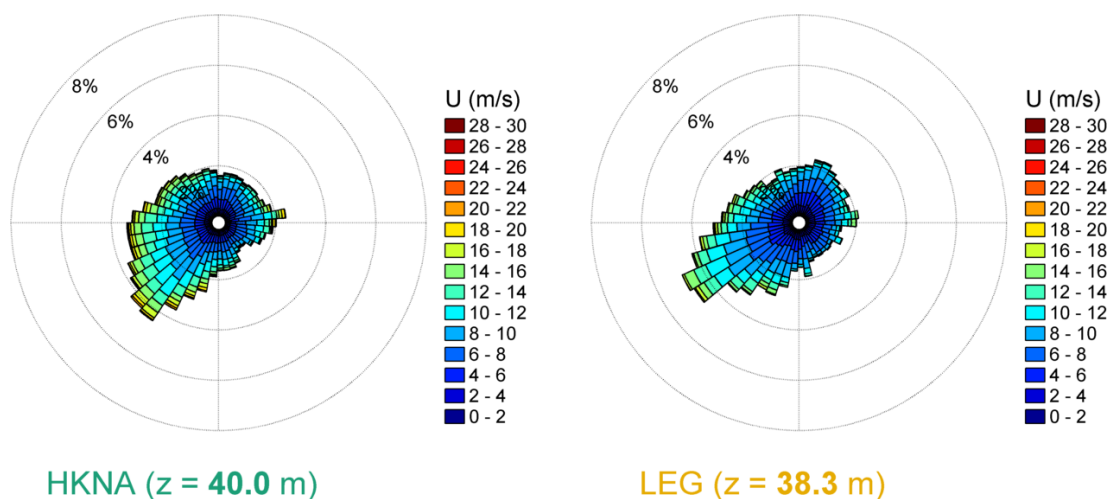


Figure 6.9: Validation of HKNA wind with LEG. Left panels: Timeseries. Right panels: Density scatter, with the darker colours indicating more data density.



HKNA (z = 40.0 m)

LEG (z = 38.3 m)

Figure 6.10: Roses of the simultaneously available HKNA and LEG wind data.

Table 6.3: Direction statistical comparison between HKNA (z = 40.0 m) and LEG.

Sector	n (-)	Wind Speed			Wind Direction		
		r (-)	RMSE (m/s)	Bias (m/s)	r (-)	RMSE (°N)	Bias (°N)
337.5 °N : 22.5 °N	5537	0.78	1.81	0.67	0.55	19.60	-5.64
22.5 °N : 67.5 °N	5171	0.74	1.98	0.79	0.58	20.30	1.80
67.5 °N : 112.5 °N	6553	0.85	2.64	1.87	0.67	23.70	-1.95
112.5 °N : 157.5 °N	3665	0.79	1.94	1.23	0.52	27.41	-8.99
157.5 °N : 202.5 °N	6752	0.84	2.75	2.01	0.60	21.33	-6.83
202.5 °N : 247.5 °N	14930	0.84	2.44	1.56	0.61	16.16	-6.48
247.5 °N : 292.5 °N	11368	0.85	2.50	1.55	0.64	16.43	-2.65
292.5 °N : 337.5 °N	6918	0.79	2.67	1.66	0.63	19.42	-6.84

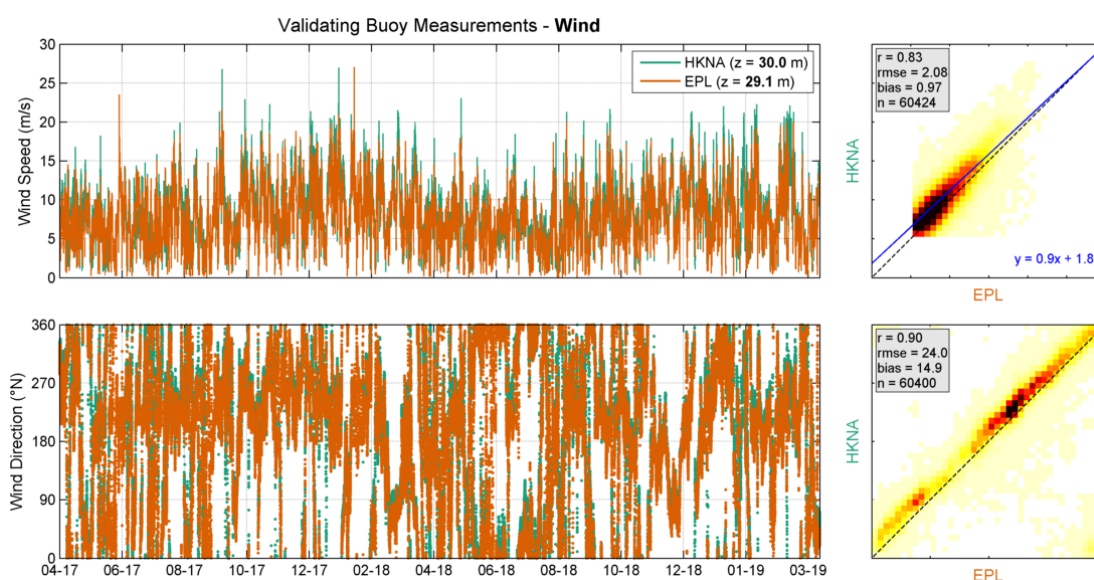


Figure 6.11: Validation of HKNA wind with EPL. Left panels: Timeseries. Right panels: Density scatter, with the darker colours indicating more data density.

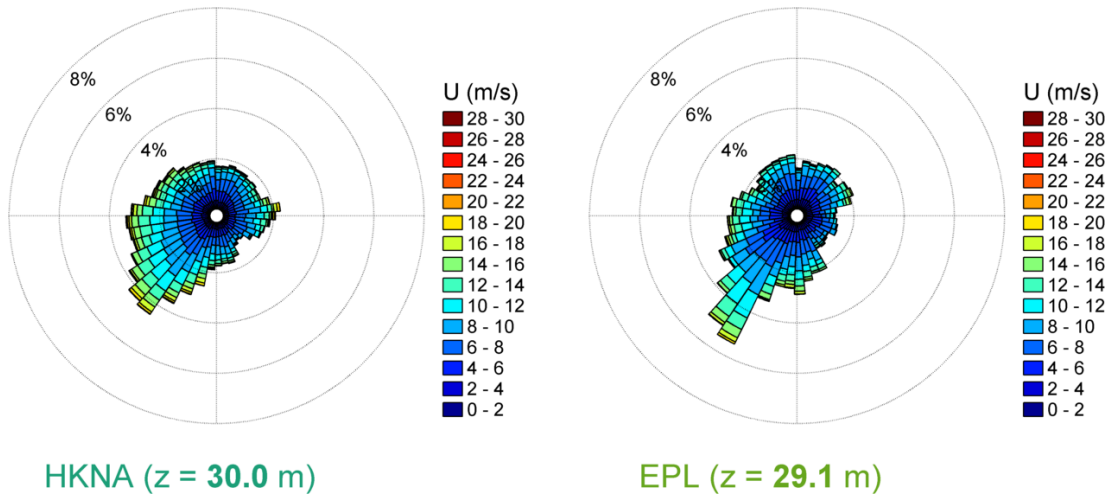


Figure 6.12: Roses of the simultaneously available HKNA and EPL wind data.

Table 6.4: Direction statistical comparison between HKNA (z = 30.0 m) and EPL.

Sector	n (-)	Wind Speed			Wind Direction		
		r (-)	RMSE (m/s)	Bias (m/s)	r (-)	RMSE (°N)	Bias (°N)
337.5 °N : 22.5 °N	5519	0.77	1.71	0.31	0.53	23.86	15.84
22.5 °N : 67.5 °N	5303	0.78	1.69	0.46	0.59	28.68	21.74
67.5 °N : 112.5 °N	6772	0.86	2.12	1.18	0.66	28.63	17.79
112.5 °N : 157.5 °N	3599	0.79	1.58	0.59	0.55	26.56	7.55
157.5 °N : 202.5 °N	7190	0.88	1.69	0.53	0.54	24.07	11.49
202.5 °N : 247.5 °N	14945	0.85	1.93	0.90	0.62	21.26	14.91
247.5 °N : 292.5 °N	10474	0.83	2.60	1.65	0.64	22.42	15.16
292.5 °N : 337.5 °N	6642	0.76	2.60	1.47	0.64	21.30	12.71

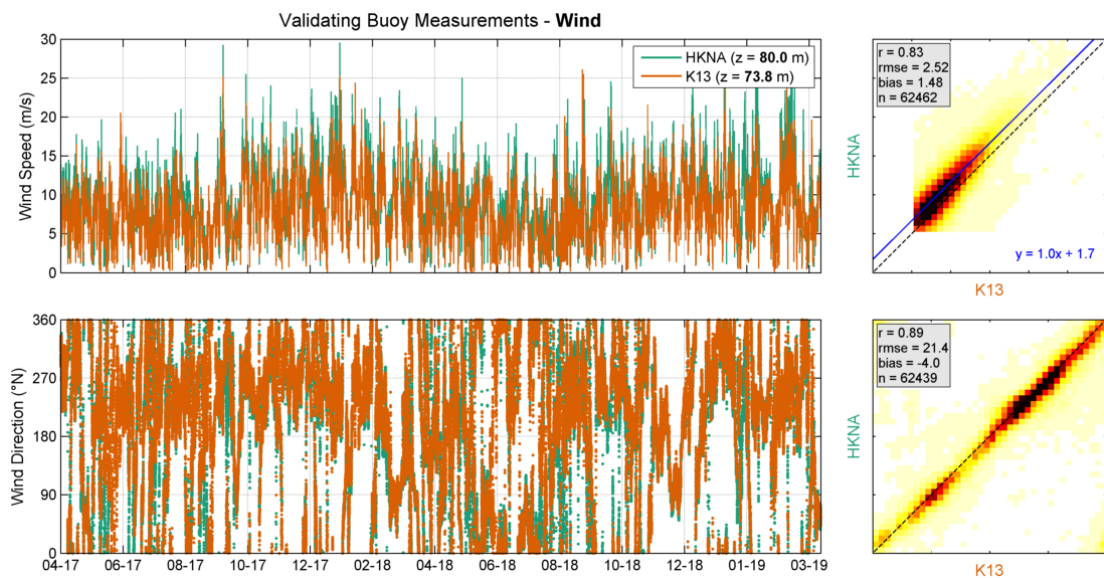


Figure 6.13: Validation of HKNA wind with K13. Left panels: Timeseries. Right panels: Density scatter, with the darker colours indicating more data density.

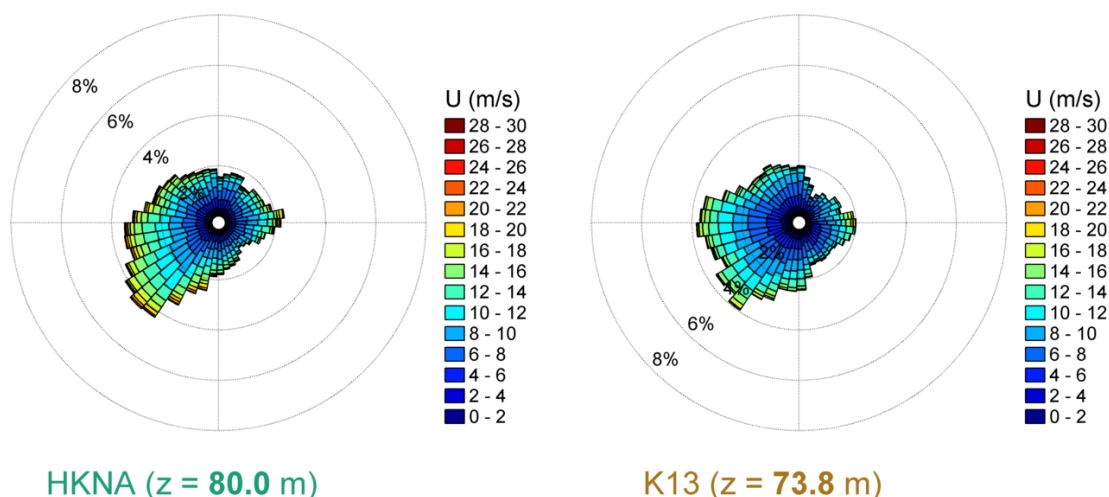


Figure 6.14: Roses of the simultaneously available HKNA and K13 wind data.

Table 6.5: Direction statistical comparison between HKNA (z = 80.0 m) and K13.

Sector	n (-)	Wind Speed			Wind Direction		
		r (-)	RMSE (m/s)	Bias (m/s)	r (-)	RMSE (°N)	Bias (°N)
337.5 °N : 22.5 °N	4693	0.72	2.52	1.54	0.62	15.91	2.83
22.5 °N : 67.5 °N	4342	0.69	2.63	1.71	0.71	18.57	-2.14
67.5 °N : 112.5 °N	7442	0.90	1.87	1.01	0.58	18.06	-4.81
112.5 °N : 157.5 °N	3918	0.80	1.72	0.52	0.68	20.14	-5.83
157.5 °N : 202.5 °N	7093	0.82	2.34	0.79	0.59	26.09	-5.34
202.5 °N : 247.5 °N	15339	0.81	3.00	1.95	0.52	26.91	-4.39
247.5 °N : 292.5 °N	12127	0.89	2.42	1.57	0.57	18.09	-5.93
292.5 °N : 337.5 °N	7537	0.86	2.60	1.83	0.63	16.50	-2.50

Table 6.6 and Table 6.7 show the error statistics between the HKNA observations and those of the closer vertical levels by the LiDAR at LEG and EPL, respectively. The comparisons are at all levels good in terms of wind speed and good (EPL) to excellent (LEG) in terms of wind direction.

Table 6.6: Statistical comparison between HKNA and LEG LiDARs at different heights.

Elevation		Wind Speed				Wind Direction		
HKNA (m)	LEG (m)	r (-)	Bias (m/s)	Symmetrical Slope (-)	n (-)	r (-)	Bias (°N)	n (-)
60	63	0.85	-0.29	0.97	55205	0.90	-2.1	55188
100	91	0.85	-0.38	0.97	55587	0.89	-2.1	55567
120	116	0.85	-0.30	0.97	55643	0.90	-1.7	55624
140	141	0.86	-0.25	0.98	55454	0.90	-1.3	55433
160	166	0.86	-0.19	0.98	55067	0.90	-0.8	55056
200	191	0.86	-0.22	0.98	54263	0.90	-1.0	54247

Table 6.7: Statistical comparison between HKNA and EPL LiDARs at different heights.

Elevation		Wind Speed				Wind Direction		
HKNA (m)	EPL (m)	r (-)	Bias (m/s)	Symmetrical Slope (-)	n (-)	r (-)	Bias ($^{\circ}$ N)	n (-)
60	63	0.85	0.01	1.00	37950	0.89	-10.6	37942
100	91	0.85	-0.11	0.99	38365	0.89	-10.9	38356
120	116	0.85	-0.07	0.99	38562	0.88	-10.6	38554
140	141	0.86	-0.06	0.99	38693	0.88	-10.3	38682
160	166	0.86	-0.06	0.99	38756	0.88	-10.1	38750
200	191	0.87	-0.13	0.99	38832	0.88	-10.5	38821

6.3.2 Validation of HKNB

The same comparisons just presented between the data from HKNA and the fixed stations are presented in the following for the HKNB data.

Figure 6.15, Figure 6.17, Figure 6.19 and Figure 6.21 show timeseries and density scatter comparisons between HKNB observations and those at Q1, LEG, EPL and K13, respectively. Figure 6.18, Figure 6.16, Figure 6.20 and Figure 6.22 compare the wind roses of the simultaneous observations. Table 6.8, Table 6.9, Table 6.10 and Table 6.11 show the error statistics between the HKNB data and the fixed platform data per directional sector.

Although the sample sizes of the comparisons between the HKNB data and the fixed platform data are slightly larger than those of the comparisons between HKNA data, the comparisons between the HKNB and the fixed station data are in line with those between the HKNA and the fixed station data.

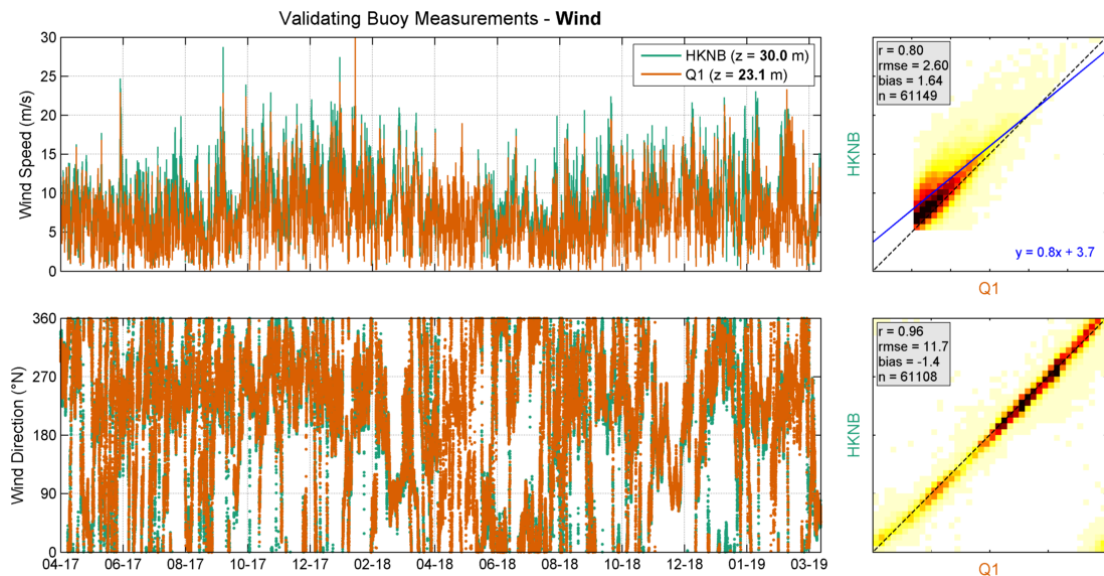


Figure 6.15: Validation of HKNB wind with Q1. Left panels: Timeseries. Right panels: Density scatter, with the darker colours indicating more data density.

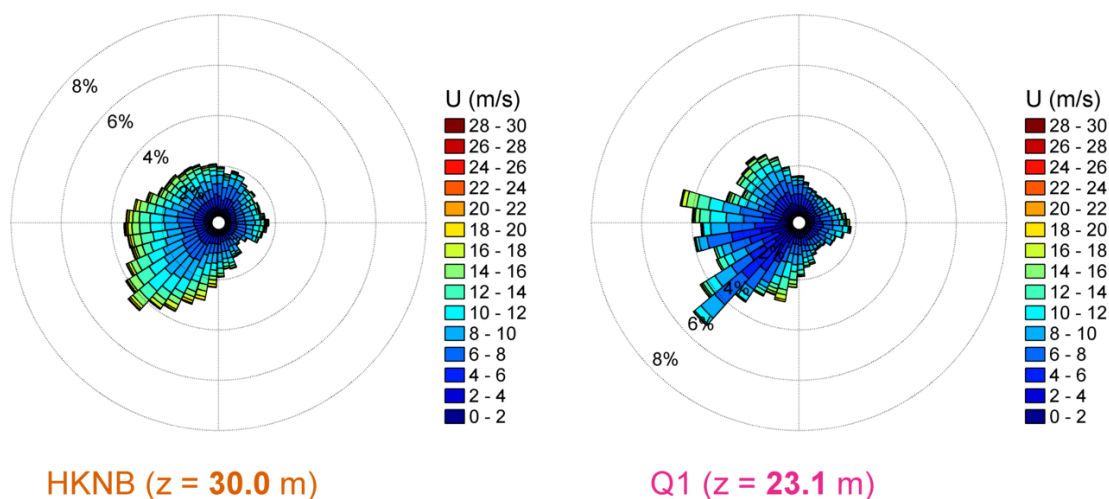


Figure 6.16: Roses of the simultaneously available HKNB and Q1 wind data.

Table 6.8: Direction statistical comparison between HKNB ($z = 30.0$ m) and Q1.

Sector	n (-)	Wind Speed			Wind Direction		
		r (-)	RMSE (m/s)	Bias (m/s)	r (-)	RMSE ($^{\circ}$ N)	Bias ($^{\circ}$ N)
337.5 $^{\circ}$ N : 22.5 $^{\circ}$ N	5993	0.89	1.66	1.03	0.79	14.38	9.46
22.5 $^{\circ}$ N : 67.5 $^{\circ}$ N	4362	0.77	1.76	1.04	0.76	14.24	-1.40
67.5 $^{\circ}$ N : 112.5 $^{\circ}$ N	5744	0.91	1.71	1.12	0.79	11.30	-3.93
112.5 $^{\circ}$ N : 157.5 $^{\circ}$ N	3409	0.86	1.21	0.26	0.83	11.41	-5.36
157.5 $^{\circ}$ N : 202.5 $^{\circ}$ N	8262	0.87	1.93	0.70	0.82	10.52	-4.92
202.5 $^{\circ}$ N : 247.5 $^{\circ}$ N	13092	0.80	3.86	3.37	0.76	11.70	-4.02
247.5 $^{\circ}$ N : 292.5 $^{\circ}$ N	11884	0.78	3.14	2.15	0.73	10.78	-2.70
292.5 $^{\circ}$ N : 337.5 $^{\circ}$ N	8417	0.92	1.51	0.80	0.76	11.05	3.53

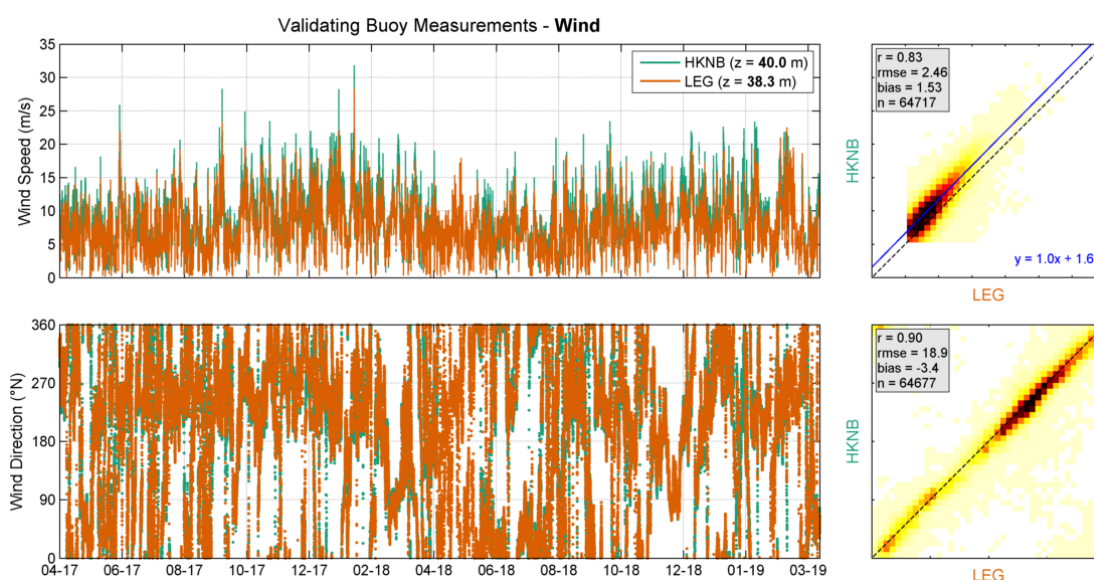


Figure 6.17: Validation of HKNB wind with LEG. Left panels: Timeseries. Right panels: Density scatter, with the darker colours indicating more data density.

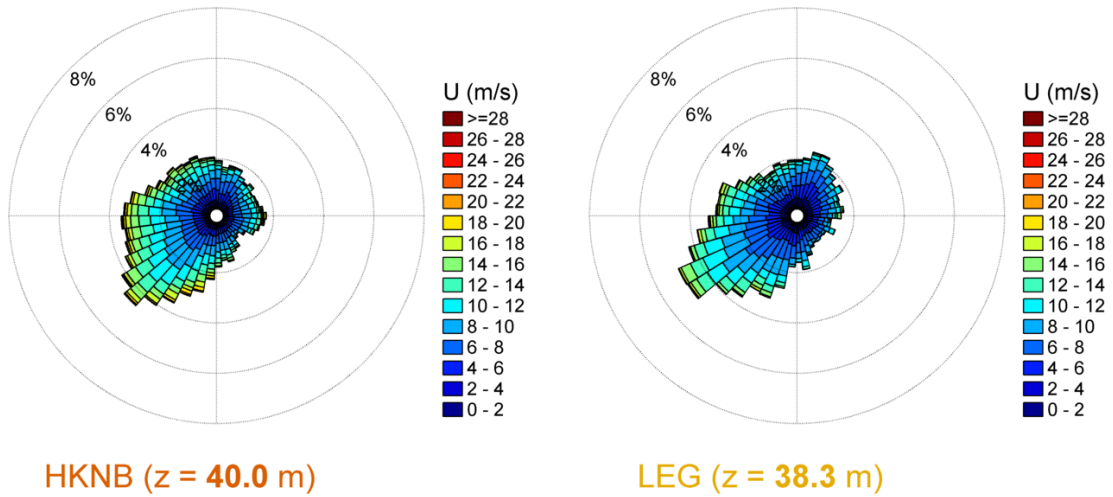


Figure 6.18: Roses of the simultaneously available HKNB and LEG wind data.

Table 6.9: Direction statistical comparison between HKNB (z = 40.0 m) and LEG.

Sector	n (-)	Wind Speed			Wind Direction		
		r (-)	RMSE (m/s)	Bias (m/s)	r (-)	RMSE (°N)	Bias (°N)
337.5 °N : 22.5 °N	6453	0.81	1.99	0.90	0.58	19.46	-3.87
22.5 °N : 67.5 °N	4677	0.67	2.03	0.78	0.55	20.29	2.04
67.5 °N : 112.5 °N	5367	0.82	2.59	1.75	0.67	25.12	-0.33
112.5 °N : 157.5 °N	3374	0.78	1.98	1.24	0.55	27.16	-10.76
157.5 °N : 202.5 °N	7993	0.85	2.95	2.25	0.57	21.28	-8.44
202.5 °N : 247.5 °N	16038	0.83	2.45	1.55	0.61	14.88	-4.85
247.5 °N : 292.5 °N	13022	0.86	2.43	1.52	0.64	15.79	-0.16
292.5 °N : 337.5 °N	7821	0.81	2.67	1.75	0.67	17.58	-2.08

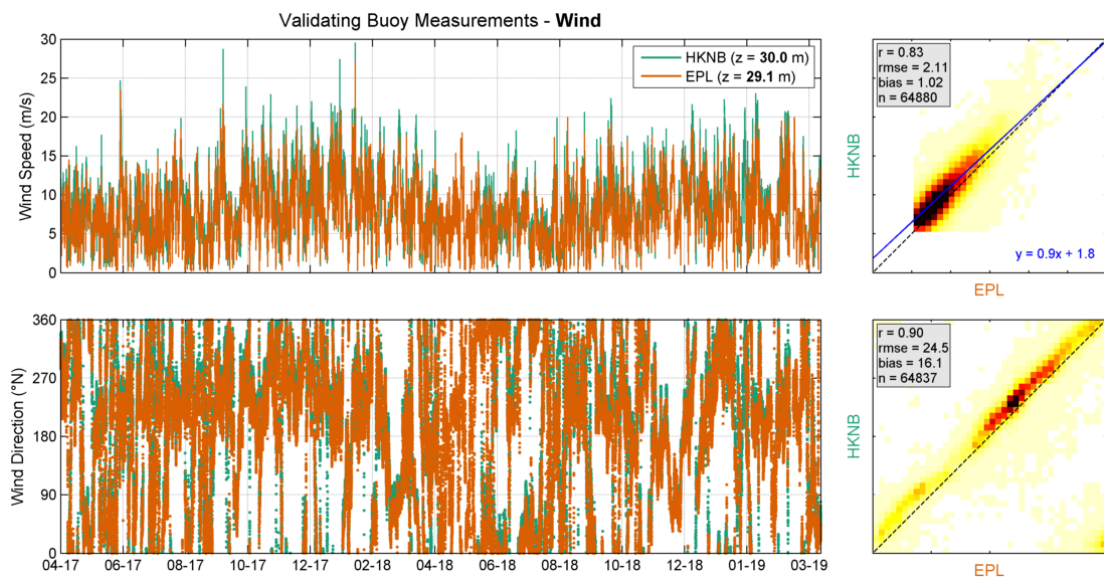


Figure 6.19: Validation of HKNB wind with EPL. Left panels: Timeseries. Right panels: Density scatter, with the darker colours indicating more data density.

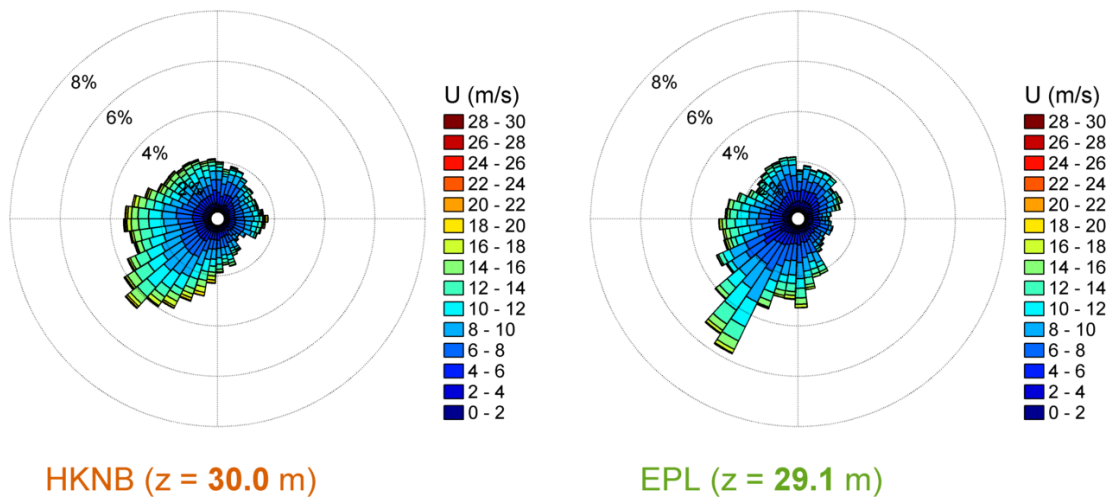


Figure 6.20: Roses of the simultaneously available HKNB and EPL wind data.

Table 6.10: Direction statistical comparison between HKNB ($z = 30.0$ m) and EPL.

Sector	n (-)	Wind Speed			Wind Direction		
		r (-)	RMSE (m/s)	Bias (m/s)	r (-)	RMSE ($^{\circ}$ N)	Bias ($^{\circ}$ N)
337.5 $^{\circ}$ N : 22.5 $^{\circ}$ N	6501	0.81	1.83	0.58	0.58	24.95	17.72
22.5 $^{\circ}$ N : 67.5 $^{\circ}$ N	4809	0.73	1.71	0.45	0.55	29.28	22.31
67.5 $^{\circ}$ N : 112.5 $^{\circ}$ N	5563	0.84	2.10	1.09	0.70	30.29	19.87
112.5 $^{\circ}$ N : 157.5 $^{\circ}$ N	3359	0.80	1.58	0.52	0.58	25.58	5.13
157.5 $^{\circ}$ N : 202.5 $^{\circ}$ N	8578	0.89	1.79	0.69	0.51	22.41	10.03
202.5 $^{\circ}$ N : 247.5 $^{\circ}$ N	16318	0.84	1.97	0.89	0.60	21.95	15.92
247.5 $^{\circ}$ N : 292.5 $^{\circ}$ N	12230	0.84	2.52	1.62	0.66	23.87	17.88
292.5 $^{\circ}$ N : 337.5 $^{\circ}$ N	7537	0.78	2.62	1.58	0.66	24.05	17.15

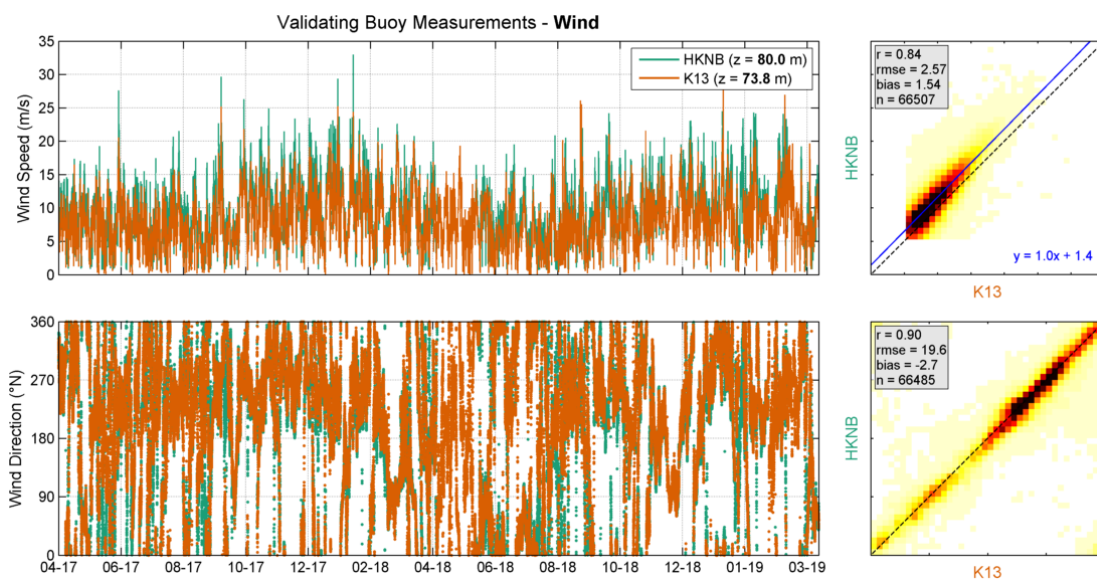


Figure 6.21: Validation of HKNB wind with K13. Left panels: Timeseries. Right panels: Density scatter, with the darker colours indicating more data density.

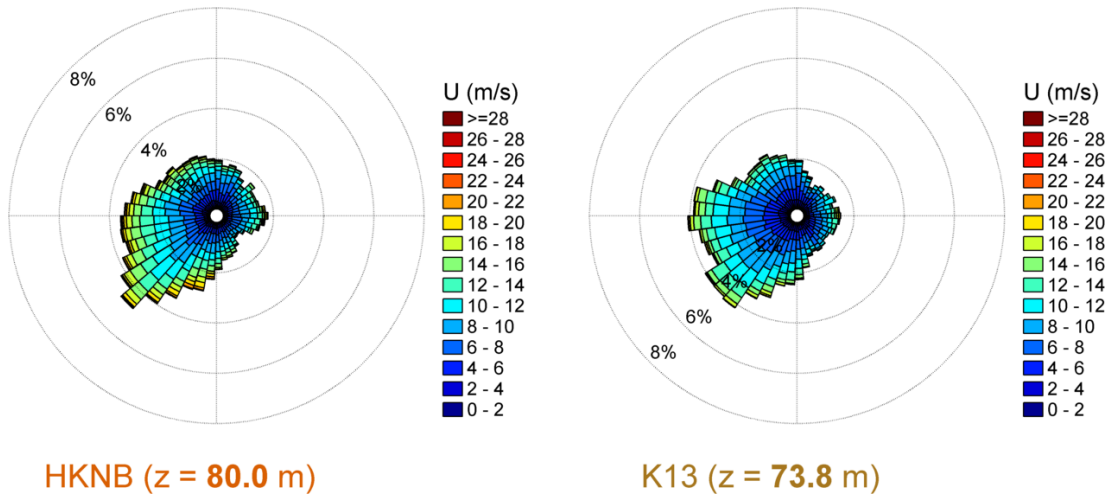


Figure 6.22: Roses of the simultaneously available HKNB and K13 wind data.

Table 6.11: Direction statistical comparison between HKNB (z = 80.0 m) and K13.

Sector	n (-)	Wind Speed			Wind Direction		
		r (-)	RMSE (m/s)	Bias (m/s)	r (-)	RMSE (°N)	Bias (°N)
337.5 °N : 22.5 °N	5761	0.79	2.65	1.79	0.64	15.77	4.34
22.5 °N : 67.5 °N	3988	0.65	2.60	1.67	0.68	17.61	-0.13
67.5 °N : 112.5 °N	6094	0.88	1.90	0.97	0.61	19.31	-1.84
112.5 °N : 157.5 °N	3625	0.81	1.72	0.51	0.65	21.19	-6.47
157.5 °N : 202.5 °N	8319	0.82	2.58	1.07	0.60	24.75	-8.56
202.5 °N : 247.5 °N	16395	0.80	2.96	1.89	0.49	21.32	-4.10
247.5 °N : 292.5 °N	13951	0.90	2.38	1.60	0.59	17.59	-2.92
292.5 °N : 337.5 °N	8415	0.86	2.67	1.87	0.65	16.00	1.14

Table 6.12 and Table 6.13 show the error statistics between the HKNB observations and those of the closer vertical levels by the LiDARs at LEG and EPL. As was the case for the comparisons with the HKNA data, at LEG the comparisons are at all levels excellent both in terms of wind speed and direction. As was also the case for the comparisons with the HKNA data, the comparisons are at all levels good in terms of wind speed and good (EPL) to excellent (LEG) in terms of wind direction.

Table 6.12: Statistical comparison between HKNB and LEG LiDARs at different heights.

Elevation		Wind Speed				Wind Direction		
HKNB (m)	LEG (m)	r (-)	Bias (m/s)	Symmetrical Slope (-)	n (-)	r (-)	Bias (°N)	n (-)
60	63	0.85	-0.32	0.97	58119	0.90	-3.6	58095
100	91	0.85	-0.40	0.96	58467	0.90	-3.7	58450
120	116	0.86	-0.31	0.97	58450	0.90	-3.3	58427
140	141	0.86	-0.25	0.98	58262	0.90	-2.9	58247
160	166	0.86	-0.19	0.98	57889	0.90	-2.6	57871
200	191	0.87	-0.24	0.98	56987	0.90	-2.8	56964

Table 6.13: Statistical comparison between HKNB and EPL LiDARs at different heights.

Elevation		Wind Speed				Wind Direction		
HKNB (m)	EPL (m)	r (-)	Bias (m/s)	Symmetrical Slope (-)	n (-)	r (-)	Bias ($^{\circ}$ N)	n (-)
60	63	0.85	-0.01	1.00	42976	0.88	-12.1	42968
100	91	0.85	-0.13	0.99	43442	0.88	-12.4	43432
120	116	0.85	-0.08	0.99	43639	0.88	-12.2	43632
140	141	0.86	-0.06	0.99	43801	0.88	-11.8	43790
160	166	0.86	-0.05	0.99	43848	0.88	-11.6	43837
200	191	0.87	-0.13	0.99	43909	0.88	-12.2	43893

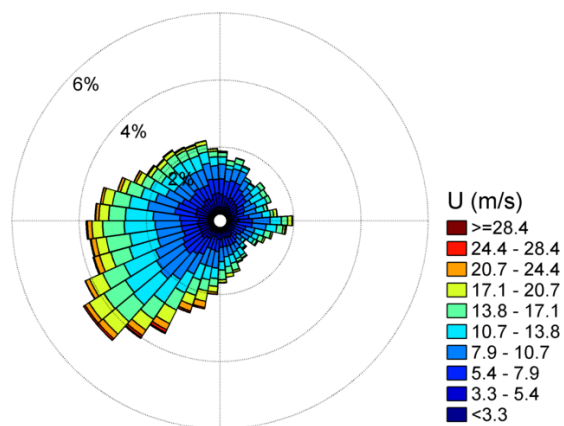
6.4 Quality Statement

Based on the comparisons between the data from the buoys, which are excellent at all levels and within the best practice range, the validation of the data against observations in which mismatches can be explained by local effects and spatial and vertical variations, it can be concluded that the accuracy of the LiDAR and ultrasonic meter wind speeds and directions is high. Furthermore, as can also be verified in the monthly validation reports, this is true over the whole campaign period.

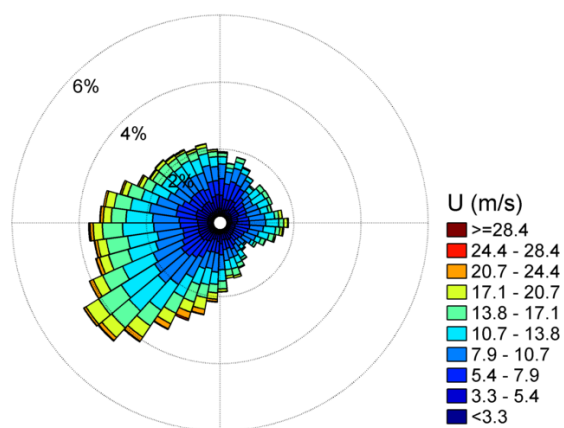
6.5 Climate description

Given that the observations at HKNA do not differ much from those at HKNB and the availability of the HKNB LiDAR data is generally larger than that of the HKNA LiDAR data and above 88% during the 2-year campaign, the HKNB data is used to determine some of the wind climate characteristics at HKN.

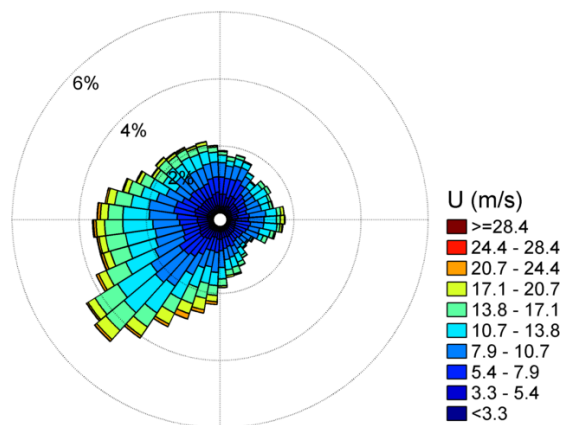
Figure 6.23 shows the roses of the wind velocity at 100 m, 140 m and 200 m. The respective joint occurrences tables are given in Figure 6.24, Figure 6.25 and Figure 6.26. The figure and tables show that the wind climate at HKN is characterized by prevailing southwestern winds with velocities between 5 and 17 m/s. The wind can attain speeds above 28 m/s from the Southwest to Northwest; high wind speeds from North and Northeast are less frequent and the maximums are lower in magnitude. As expected, the variability of wind direction with height is low and the wind speeds generally increase with height.



HKNB (z = 200.0 m)



HKNB (z = 140.0 m)



HKNB (z = 100.0 m)

Figure 6.23: Wind roses at levels 100, 140 and 200 m.

	338-23	23-68	68-113	113-158	158-203	203-248	248-293	293-338	
>32.6								0.00	0.00
28.4-32.6						0.00	0.03	0.01	0.04
24.4-28.4					0.02	0.05	0.07	0.01	0.14
20.7-24.4	0.03		0.06	0.00	0.29	0.44	0.35	0.16	1.33
17.1-20.7	0.25	0.01	0.35	0.04	0.87	1.71	1.22	0.49	4.94
13.8-17.1	0.78	0.38	0.60	0.36	1.65	3.41	2.84	1.59	11.62
10.7-13.8	1.53	1.46	1.83	0.77	2.21	5.55	4.14	2.51	20.00
7.9-10.7	2.46	1.73	2.43	1.48	2.55	5.23	4.40	2.87	23.16
5.4-7.9	2.78	2.03	2.06	1.51	2.03	3.34	3.16	2.42	19.32
3.3-5.4	2.03	1.45	0.94	1.07	1.20	1.72	1.85	1.89	12.15
1.5-3.3	0.98	0.96	0.59	0.57	0.67	0.80	0.80	0.81	6.18
0.0-1.5	0.16	0.17	0.12	0.09	0.12	0.14	0.13	0.19	1.12
	11.01	8.19	8.97	5.91	11.61	22.39	18.97	12.95	100.00
HKN Dir (° N) versus U ₁₀₀ (m/s)									Total

Figure 6.24: Wind speed and direction joint occurrence table at levels 100 m.

	338-23	23-68	68-113	113-158	158-203	203-248	248-293	293-338	
>32.6								0.00	0.00
28.4-32.6						0.01	0.04	0.01	0.05
24.4-28.4					0.07	0.13	0.06	0.01	0.27
20.7-24.4	0.04		0.07	0.00	0.34	0.75	0.44	0.19	1.84
17.1-20.7	0.27	0.01	0.37	0.08	0.94	2.10	1.39	0.55	5.71
13.8-17.1	0.83	0.46	0.72	0.40	1.61	3.58	3.01	1.67	12.29
10.7-13.8	1.46	1.41	1.78	0.79	2.09	5.26	4.23	2.56	19.58
7.9-10.7	2.45	1.66	2.37	1.43	2.43	5.01	4.35	2.86	22.55
5.4-7.9	2.70	1.93	2.01	1.43	1.88	3.29	3.01	2.45	18.69
3.3-5.4	2.04	1.38	0.93	0.95	1.19	1.69	1.79	1.85	11.82
1.5-3.3	0.97	0.93	0.62	0.57	0.57	0.81	0.81	0.80	6.08
0.0-1.5	0.18	0.20	0.11	0.10	0.10	0.11	0.12	0.18	1.11
	10.95	7.98	8.99	5.76	11.22	22.73	19.25	13.13	100.00
HKN Dir (° N) versus U ₁₄₀ (m/s)									Total

Figure 6.25: Wind speed and direction joint occurrence table at levels 140 m.

	338-23	23-68	68-113	113-158	158-203	203-248	248-293	293-338	
>32.6								0.00	0.00
28.4-32.6					0.00	0.09	0.05	0.00	0.15
24.4-28.4	0.00				0.08	0.31	0.09	0.04	0.53
20.7-24.4	0.04		0.08	0.00	0.37	0.99	0.64	0.22	2.34
17.1-20.7	0.29	0.02	0.38	0.17	0.91	2.50	1.62	0.70	6.59
13.8-17.1	0.97	0.46	0.89	0.39	1.53	3.64	3.17	1.70	12.75
10.7-13.8	1.38	1.28	1.60	0.94	1.80	5.01	4.16	2.53	18.69
7.9-10.7	2.38	1.63	2.23	1.27	2.30	4.81	4.35	2.89	21.87
5.4-7.9	2.65	1.86	2.02	1.26	1.75	3.25	3.03	2.44	18.27
3.3-5.4	1.96	1.42	0.94	0.99	1.16	1.61	1.81	1.89	11.80
1.5-3.3	1.02	0.92	0.58	0.57	0.53	0.77	0.77	0.80	5.96
0.0-1.5	0.21	0.20	0.12	0.09	0.08	0.09	0.10	0.15	1.05
	10.90	7.80	8.84	5.69	10.52	23.09	19.80	13.36	100.00
HKN Dir (° N) versus U_{200} (m/s)									Total

Figure 6.26: Wind speed and direction joint occurrence table at levels 200 m.

In order to look in more detail into the wind speed variations with height, for each observed profile for which the wind speed is above 5 m/s, a power profile of the form

$$U(z) = U_{30} \left(\frac{z}{4} \right)^\alpha$$

has been fitted, where U_4 is the wind speed at 30m above the surface and α is the power-law constant.

In the following we analyse the observed profiles, looking also into the dependence of the profile on the atmospheric circumstances (vertical temperature differences). In this case, given that the availability of the air temperature data from HKNB is 35.5% whereas that of the data from HKNA data is 91.3%, we consider the HKNA data.

Figure 6.27 presents the results of the analysis of the HKNA data and shows that the mean observed wind profile is close to the mean power profile, but there is a very large spread in the profiles (with U_{200}/U_4 ranging from 0.4 to 3.4) and estimates of alpha (ranging from -0.05 to 0.4).

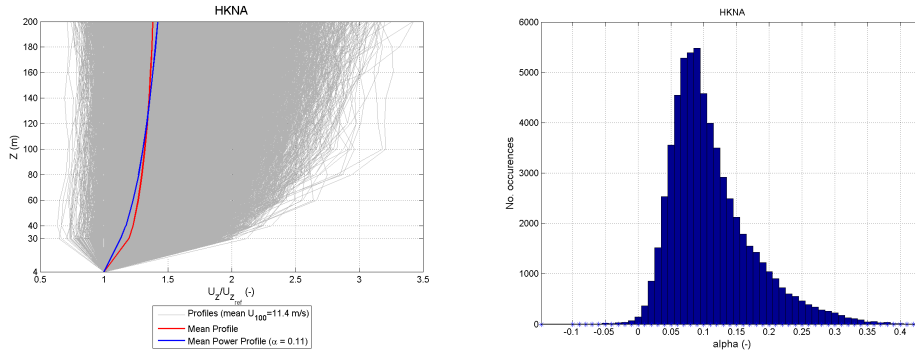


Figure 6.27: Left: Observed wind profiles. Right: Histogram of the alpha estimates.

To illustrate the uncertainties in the form of the vertical wind profile the observed profiles are classified under different circumstances. Furthermore, the mean values of the fitted power profiles are compared with the mean values of the observed profiles under the considered circumstances. Figure 6.28 presents the observed profiles applying surface wind speed thresholds of Beaufort 6, 7 and 8. Figure 6.29 presents the observed profiles considering differences between the observed air and water temperatures between -1.5°C and 1.5°C , of more than 1.5°C and of less than -1.5°C . A temperature induced meteorological feature (or anomalous events [Kalverla et al., 2017](#)) in the North Sea are low-level jets, in which the wind speed at 100 m is generally higher than above, where it falls off, i.e. there is a higher wind speed jet around the 100 m level. We roughly identify such events with a simple algorithm and the results are also given in Figure 6.29. The 100 m wind velocity roses of the data falling under the classes for which the vertical profiles are grouped in Figure 6.29 are given in Figure 6.30.

Figure 6.28 shows an increase of alpha with the threshold and that the power profile generally underestimates the increase of wind speed with height up to about 120 m and overestimates above that level. Figure 6.29 and Figure 6.30 show that the large vertical gradients in wind velocity occur under stable conditions, i.e. when the air temperature is at least 1.5°C higher than the water temperature and that under such circumstances the mean power profile deviates quite much from the mean observed profile. Such conditions are less frequent than the neutral and unstable conditions, but do correspond to on average higher and generally southwestern wind speeds at 100 m. Furthermore, the figures also show that the low-level jets generally occur under stable conditions ($T_a > T_w$, cf. bottom left and right panels of Figure 6.29). In general the unstable conditions are those occurring more frequently (53.5% of the time) and predominantly in the winter (cf. Figure 8.1).

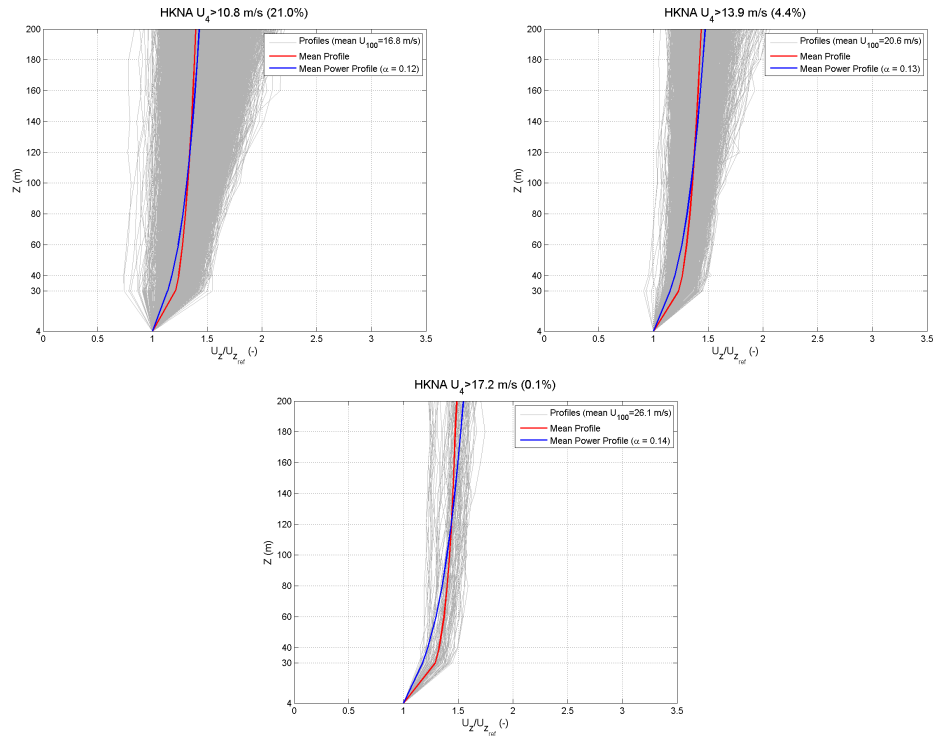


Figure 6.28: Observed wind profiles with $U_4 > 10.8$ m/s (top), $U_4 > 13.9$ m/s (middle) and $U_4 > 17.2$ m/s (bottom).

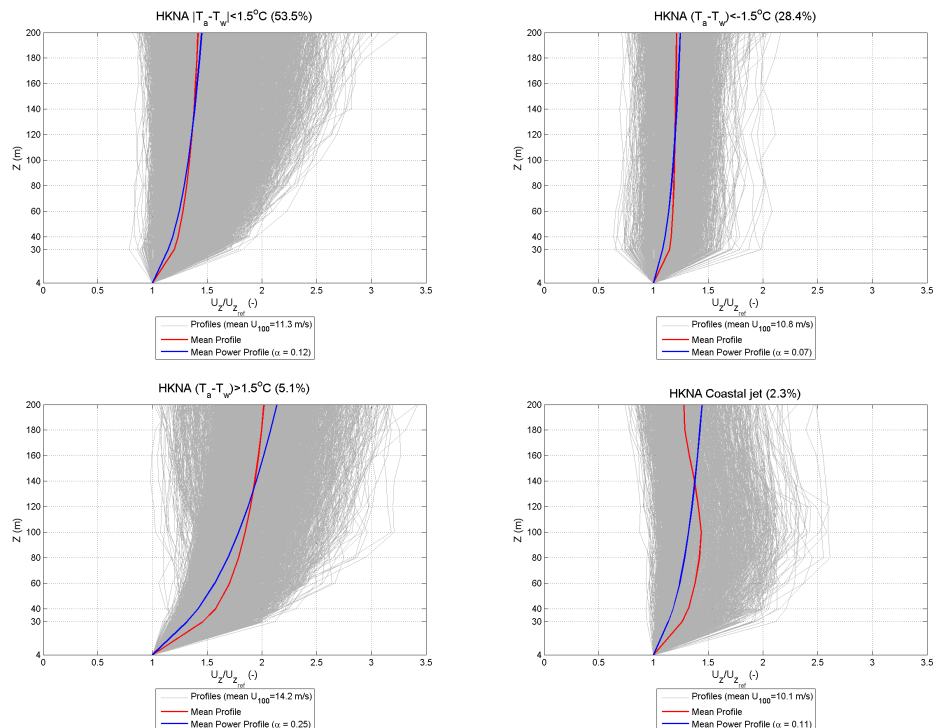


Figure 6.29: Observed wind profiles under approximately neutral (top left), unstable (top right), stable (bottom left) atmospheric stability and observed wind profiles in which $U_{180} < U_{160} < U_{140} < U_{100}$ (bottom right)

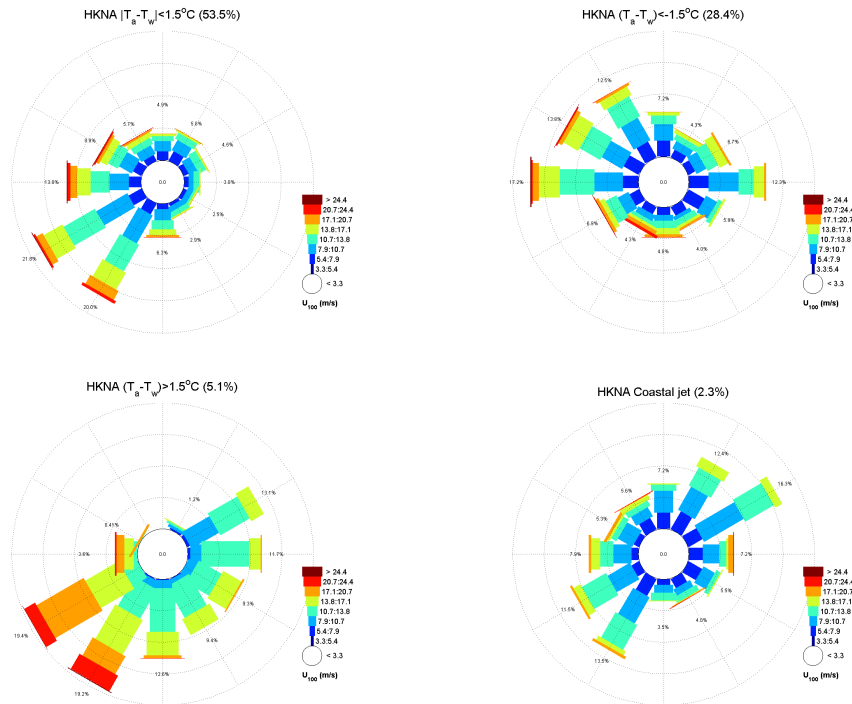


Figure 6.30: Rose of the 100m wind of the observed data falling under approximately neutral (top left), unstable (top right), stable (bottom left) atmospheric stability and in which $U_{180} < U_{160} < U_{140} < U_{100}$ (bottom right)

Figure 6.31 shows a summary of the mean vertical wind profiles for the circumstances analysed.

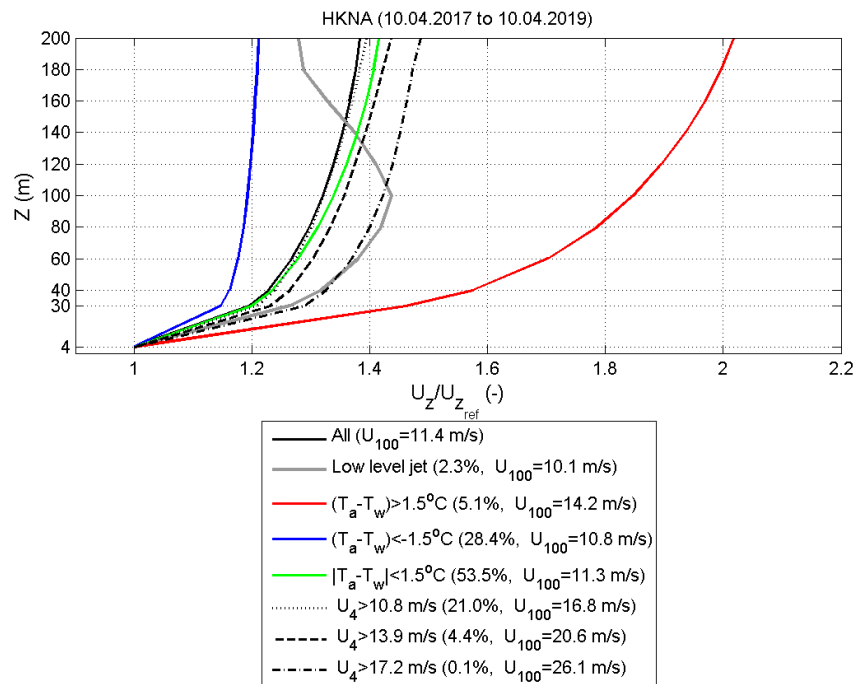


Figure 6.31: Mean observed wind profiles at HKNA under different conditions.

7 Waves

7.1 Introduction

The measured waves from both buoys are presented and analyzed within this chapter. The goal is to assess the reliability and accuracy of the retrieved wave data from both HKNA and HKNB. This is completed by first intercomparing the HKN data, followed by a statistical validation against fixed wave measurements in the area.

7.2 Intercomparison of the HKN data

To get an overview of the data, the frequency spectra timeseries are shown in [Figure 7.1](#).

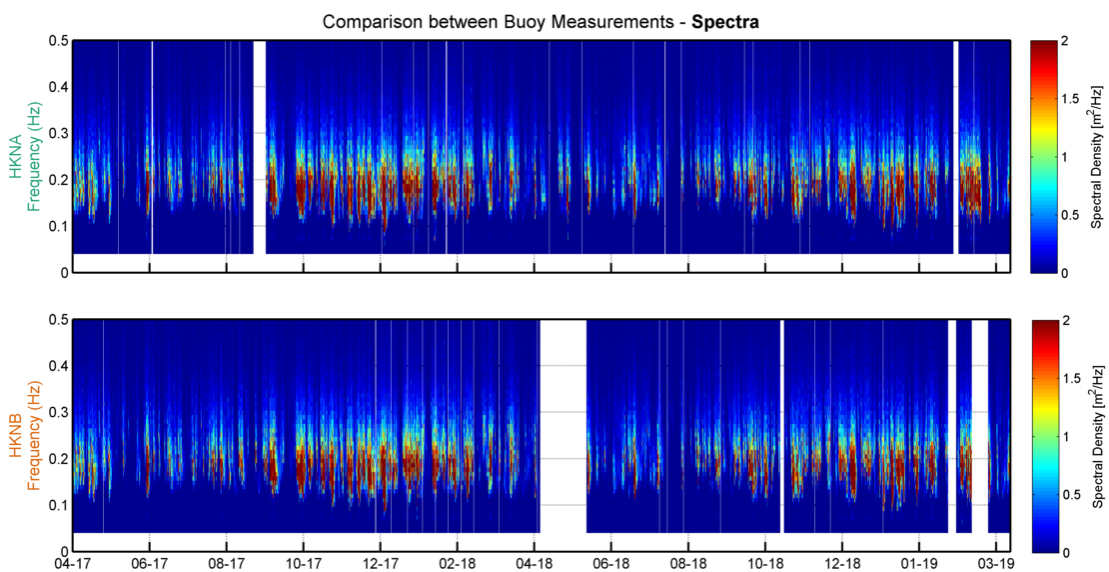


Figure 7.1: Normalized spectral density at each buoy.

Timeseries of the main wave parameters for both HKNA and HKNB is shown in [Figure 7.2](#). These include the following parameters:

- significant wave height, H_s
- peak wave period, T_p
- mean wave direction, MWD
- swell and sea significant wave height, H_{sswell} and H_{ssea}
- maximum wave height, H_{max}
- swell and sea mean wave direction, MWD_{swell} and MWD_{sea}
- mean absolute wave periods, T_{m01} and T_{m02}
- swell and sea mean absolute wave periods, $T_{m02swell}$ and T_{m02sea}

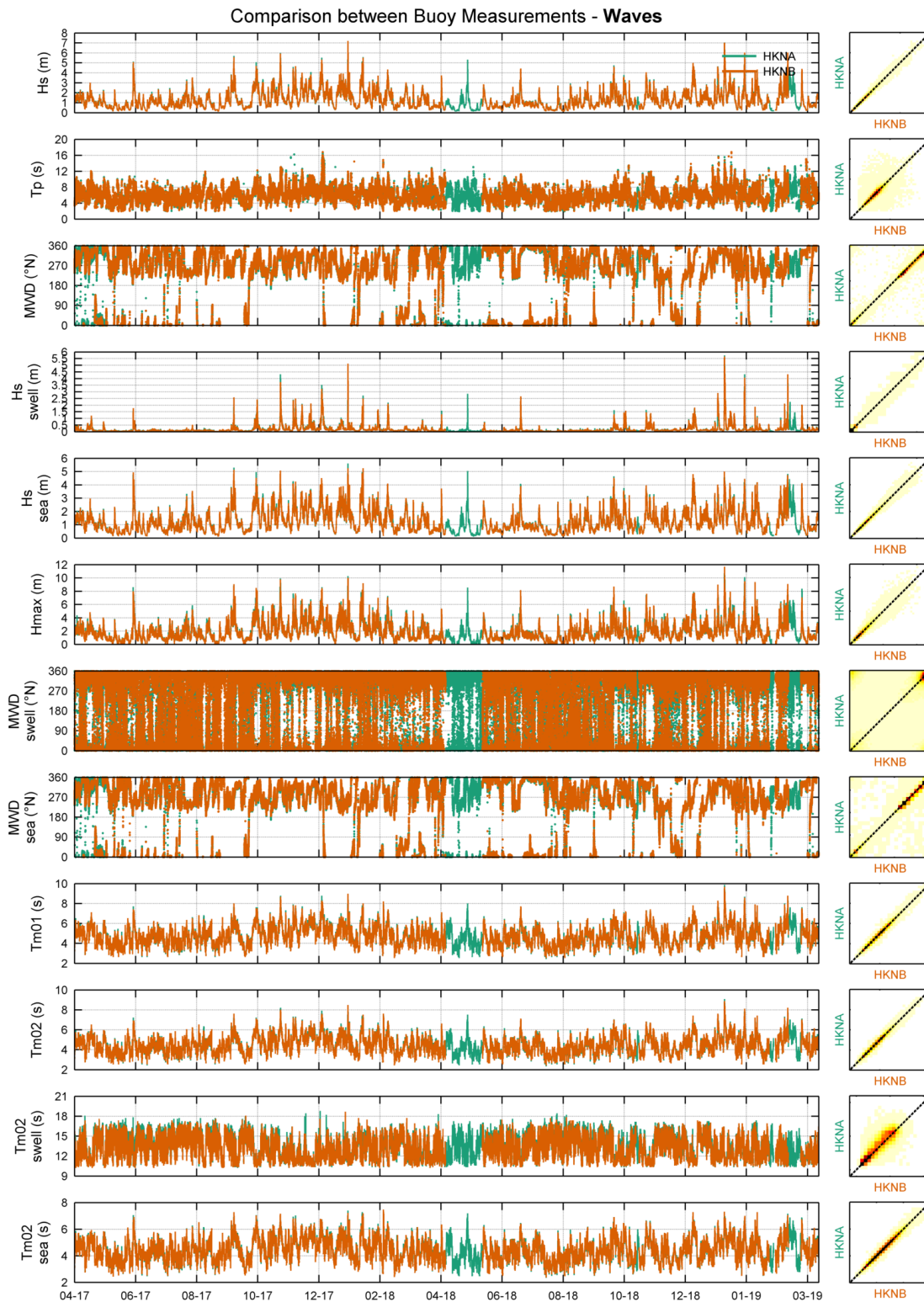


Figure 7.2: Wave parameters at each buoy.

The slope, bias, correlations and square correlations are calculated for all wave parameters measured at HKNA and HKNB to quantify their statistical differences (see [Table 7.1](#)). The agreement between the two buoys is excellent for all parameters except for the peak wave period and the mean wave period of swell which is good and the mean wave direction of swell which is poor. Discrepancies between T_p , $T_{m02swell}$ and MWD_{swell} are expected given

that these parameters depend more strongly on the sampling variability (randomness of the sea surface elevation) and discreteness of the wave spectra. Furthermore, as can be seen in [Figure 7.2](#), the mismatches in the mean wave direction of swell are in periods with almost no swell energy. These low levels of energy explain the variability in the resulting swell direction but also make it less important.

Table 7.1: Statistical comparison between HKNA and HKNB wave parameters.

Parameter	Unit	r^2 (-)	r (-)	Bias (unit)	Symmetrical Slope (-)	n (-)
hm0	m	0.99	0.99	-0.00	1.00	93755
tp	s	0.71	0.84	0.00	1.00	93755
mdir	°N	0.95	0.98	2.45	1.00	93755
hm0a	m	0.97	0.98	-0.01	0.99	93754
hm0b	m	0.99	0.99	-0.00	1.00	93755
hmax	m	0.93	0.96	-0.01	1.00	93755
mdira	°N	0.08	0.28	2.52	1.00	93755
mdirb	°N	0.95	0.97	2.47	1.00	93755
tm01	s	0.98	0.99	-0.01	1.00	93755
tm02	s	0.97	0.99	-0.01	1.00	93755
tm02a	s	0.76	0.87	-0.23	0.98	93755
tm02b	s	0.97	0.99	-0.00	1.00	93755

7.3 Validation of the HKN data

The Q1, IJmuiden, EPL and K13 wave observations were quality controlled in terms of outliers in significant wave height looking at deviation from the monthly mean and deviation from one timestamp to the next using as criteria 6 times the standard deviation of the monthly data and no outliers were found.

In order to further validate the HKNA data, the data was compared with the Q1, IJmuiden, EPL and K13 simultaneous observations. No directional comparisons are shown for Q1 because there are no wave direction observations available from the Q1 platform. [Figure 7.3](#), [Figure 7.4](#), [Figure 7.6](#) and [Figure 7.8](#) show comparisons between HKNA observations of H_s , T_p , mean wave period, $T_{m0.2}$, and (except for Q1) mean wave direction, MWD , and those at Q1, IJmuiden, EPL and K13, respectively. The correlation, root-mean-square error and bias statistics are printed in each of the figures. [Figure 7.5](#), [Figure 7.7](#) and [Figure 7.9](#) compare the significant wave height roses of the simultaneous observations. [Table 7.2](#), [Table 7.3](#) and [Table 7.4](#) show the error statistics between the HKNA and the fixed platform significant wave height and mean wave direction data per directional sector, i.e. when the HKNA mean wave direction at the considered level falls within the direction range given in the left column of the tables. Note that lower correlations in terms of mean wave direction are to be expected from this data binning. Furthermore, discrepancies are expected for given wave directions depending on the distance between the measuring locations, thus in particular for comparisons with data from EPL and K13. Discrepancies in terms of peak wave period at all locations are also expected given the discrete characteristics of the variable.

The following conclusions are taken from the assessment of these figures and tables:

- The comparisons between HKNA observations and those at Q1 are excellent in terms of significant wave height, swell wave height and mean wave period, whereas poor in terms of peak wave period.
- The comparisons between HKNA observations and those at IJmuiden are excellent in terms of significant wave height, swell wave height, mean wave period and mean wave direction, whereas poor in terms of peak wave period. The wave roses indicate that the

wave climate at HKNA is comparable to that at IJmuiden. Per directional sector the agreement is excellent in terms of significant wave height and poor to reasonable in terms of mean wave direction (cf. Table 7.2).

- The comparisons between HKNA observations and those at EPL are excellent in terms of significant wave height, good in terms of swell wave height and mean wave period, reasonable in terms of mean wave direction and poor in terms of peak wave period. The wave roses show a higher predominance of southwestern waves and a more northern alignment of northwestern waves at EPL than at HKNA (and IJmuiden). Per directional sector the agreements are reasonable to excellent in terms of significant wave height and poor in terms of mean wave direction (cf. Table 7.3).
- The comparisons between HKNA and K13 are excellent in terms of significant wave height, good in terms of swell wave height and mean wave period, and poor in terms of peak wave period and mean wave direction. The wave roses show that the southwestern (northwestern) waves have a more southern (northern) alignment at K13. Per directional sector the agreement is reasonable to excellent in terms of significant wave height and poor in terms of mean wave direction (cf. Table 7.4).

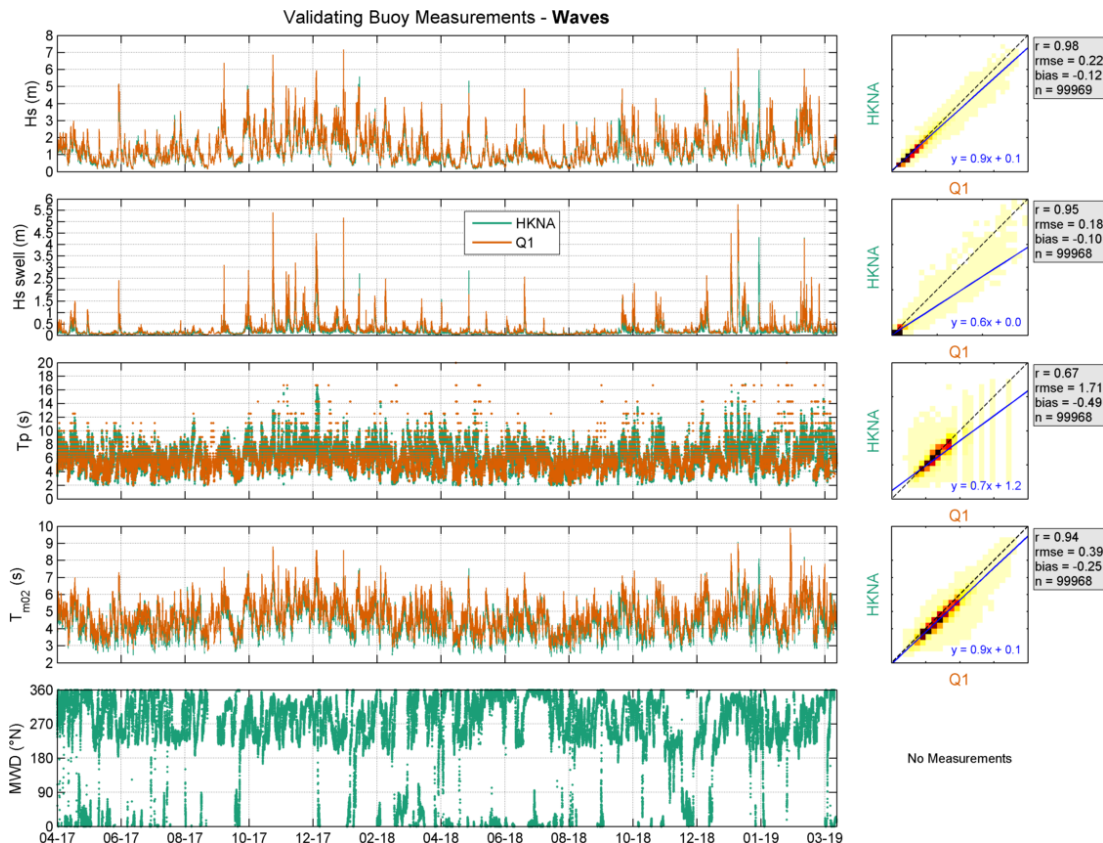


Figure 7.3: Validation of HKNA waves with Q1.

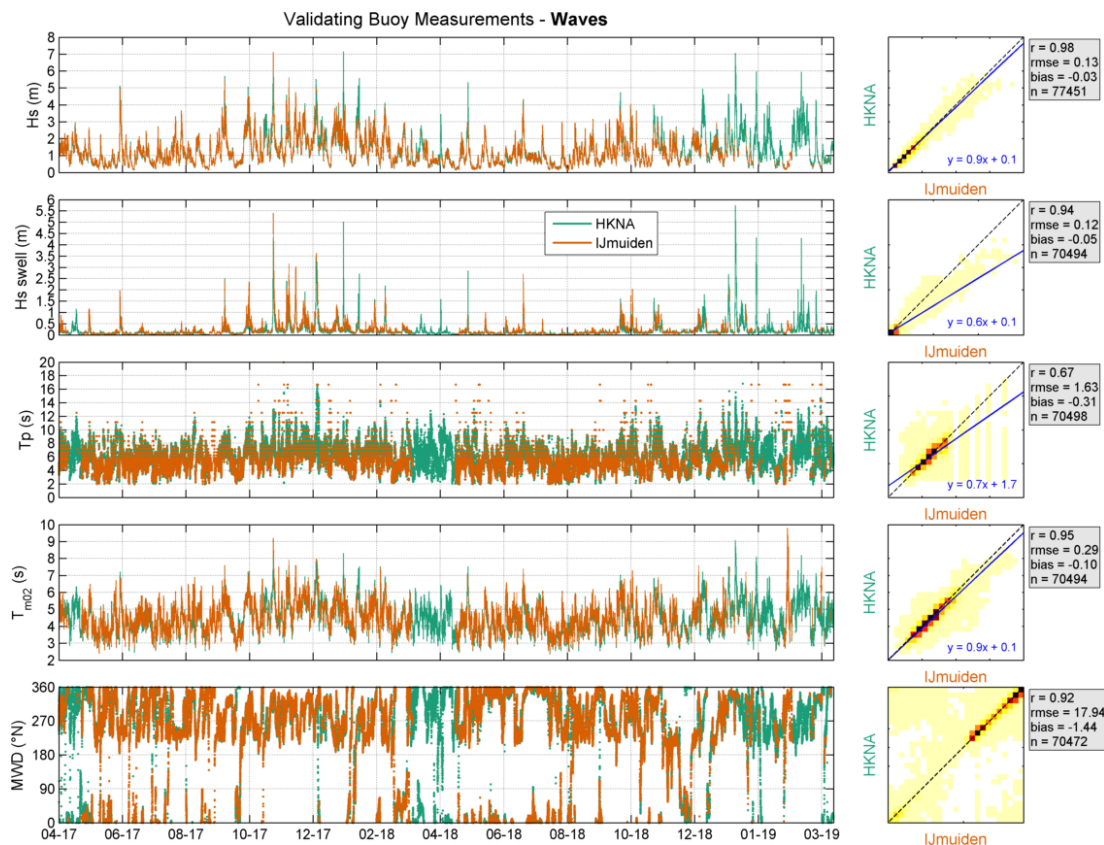


Figure 7.4: Validation of HKNA waves with IJmuiden.

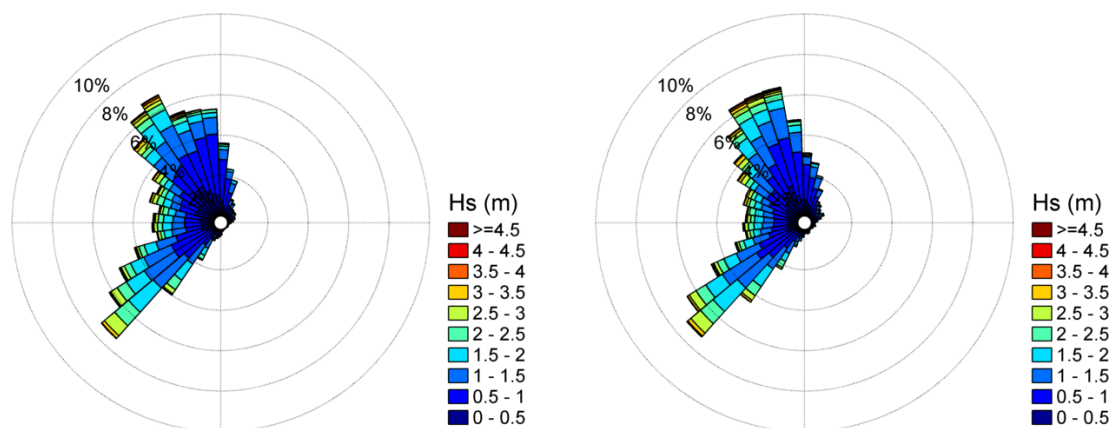


Figure 7.5: Roses of the simultaneously available HKNA (left) and IJmuiden (right) wave data.

Table 7.2: Direction statistical comparison between HKNA and IJmuiden.

Sector	n (-)	Significant wave height			Mean wave direction		
		r (-)	RMSE (m)	Bias (m)	r (-)	RMSE (°N)	Bias (°N)
337.5 °N : 22.5 °N	15615	0.98	0.13	-0.05	0.69	15.21	-2.51
22.5 °N : 67.5 °N	2497	0.98	0.13	-0.07	0.60	20.46	-4.75
67.5 °N : 112.5 °N	819	0.97	0.11	-0.06	0.43	25.69	1.39
112.5 °N : 157.5 °N	192	0.94	0.08	-0.04	0.34	37.40	13.46
157.5 °N : 202.5 °N	1164	0.97	0.11	-0.05	0.66	26.13	13.98
202.5 °N : 247.5 °N	18290	0.98	0.13	-0.02	0.75	11.04	1.63
247.5 °N : 292.5 °N	12337	0.99	0.12	0.00	0.69	22.62	-1.39
292.5 °N : 337.5 °N	19928	0.99	0.15	-0.04	0.61	19.98	-4.24

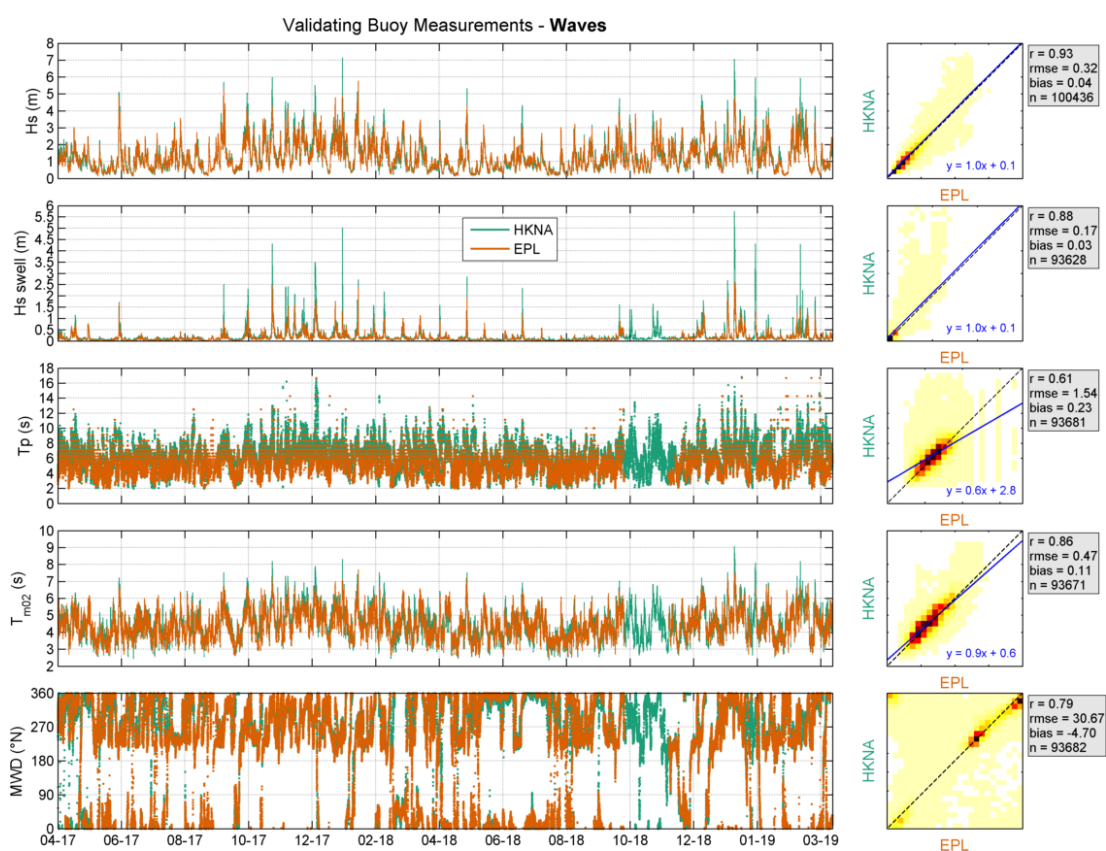


Figure 7.6: Validation of HKNA waves with EPL.

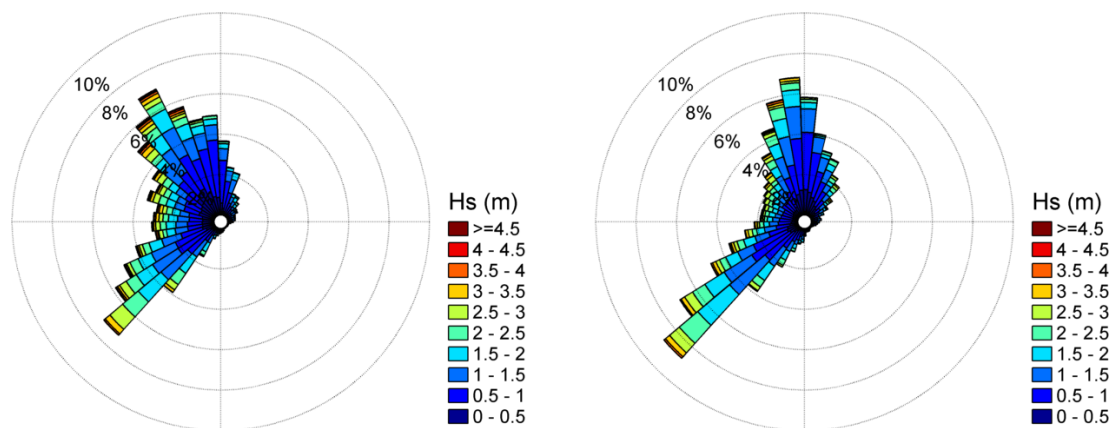


Figure 7.7: Roses of the simultaneously available HKNA (left) and EPL (right) wave data.

Table 7.3: Direction statistical comparison between HKNA and EPL.

Sector	n (-)	Significant wave height			Mean wave direction		
		r (-)	RMSE (m)	Bias (m)	r (-)	RMSE ($^{\circ}$ N)	Bias ($^{\circ}$ N)
337.5 $^{\circ}$ N : 22.5 $^{\circ}$ N	20310	0.92	0.25	-0.07	0.51	25.56	-11.15
22.5 $^{\circ}$ N : 67.5 $^{\circ}$ N	4408	0.93	0.40	-0.26	0.34	25.86	-2.78
67.5 $^{\circ}$ N : 112.5 $^{\circ}$ N	1376	0.92	0.29	-0.20	0.35	30.44	8.83
112.5 $^{\circ}$ N : 157.5 $^{\circ}$ N	301	0.78	0.20	-0.06	0.16	56.76	21.31
157.5 $^{\circ}$ N : 202.5 $^{\circ}$ N	1432	0.91	0.28	-0.15	0.49	39.55	13.56
202.5 $^{\circ}$ N : 247.5 $^{\circ}$ N	23264	0.93	0.28	0.03	0.52	18.15	2.17
247.5 $^{\circ}$ N : 292.5 $^{\circ}$ N	16655	0.95	0.34	0.15	0.46	38.42	2.92
292.5 $^{\circ}$ N : 337.5 $^{\circ}$ N	26402	0.95	0.36	0.14	0.47	36.67	-13.11

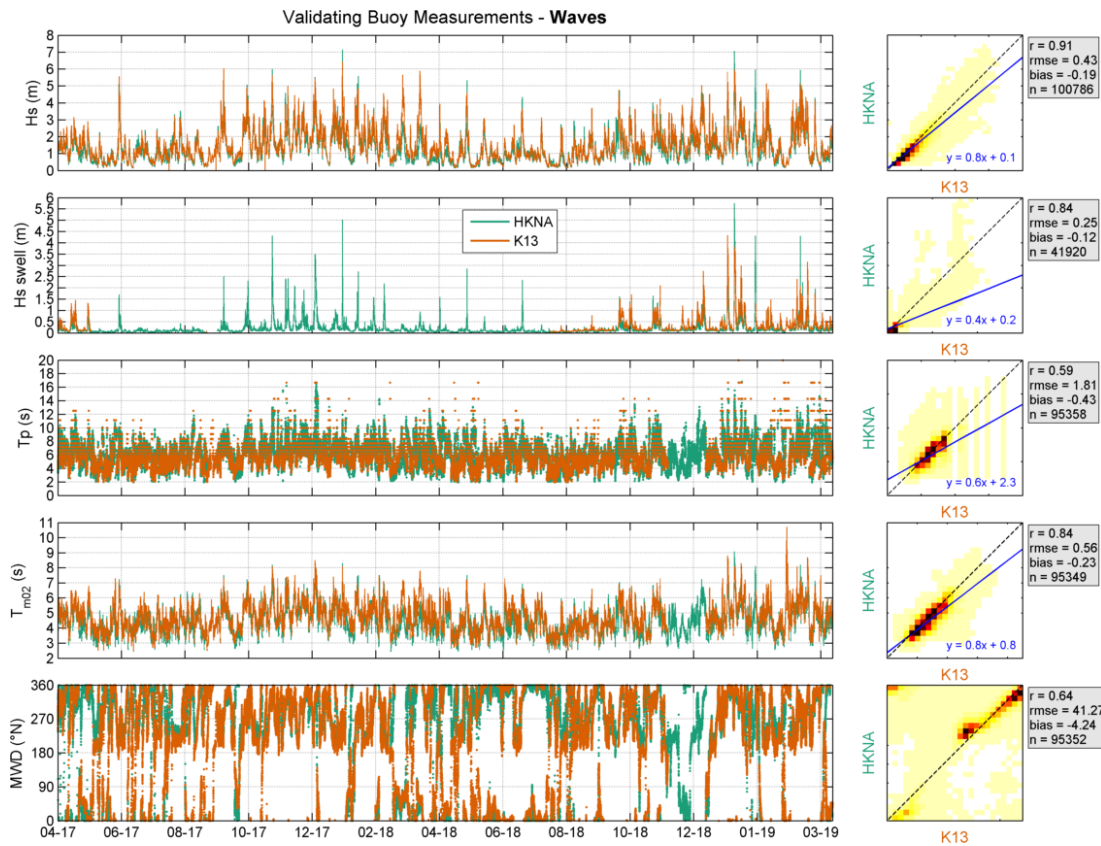


Figure 7.8: Validation of HKNA waves with K13.

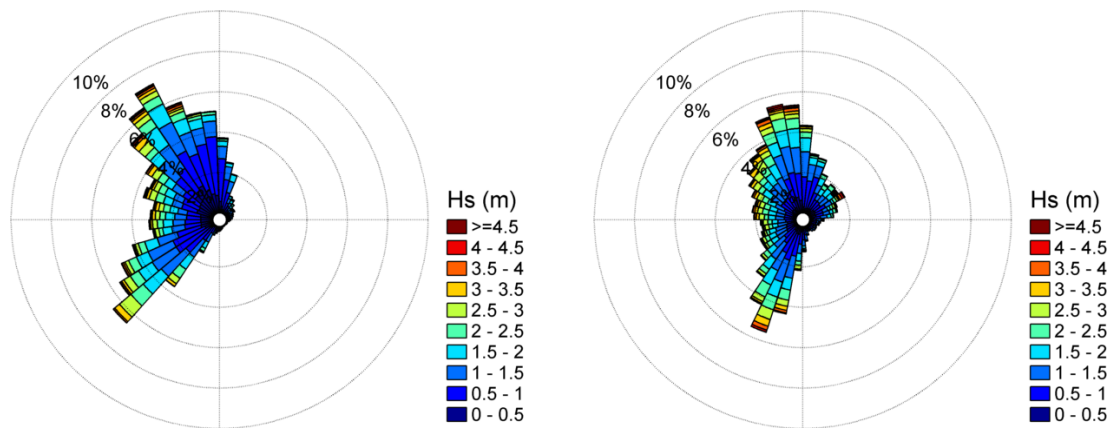


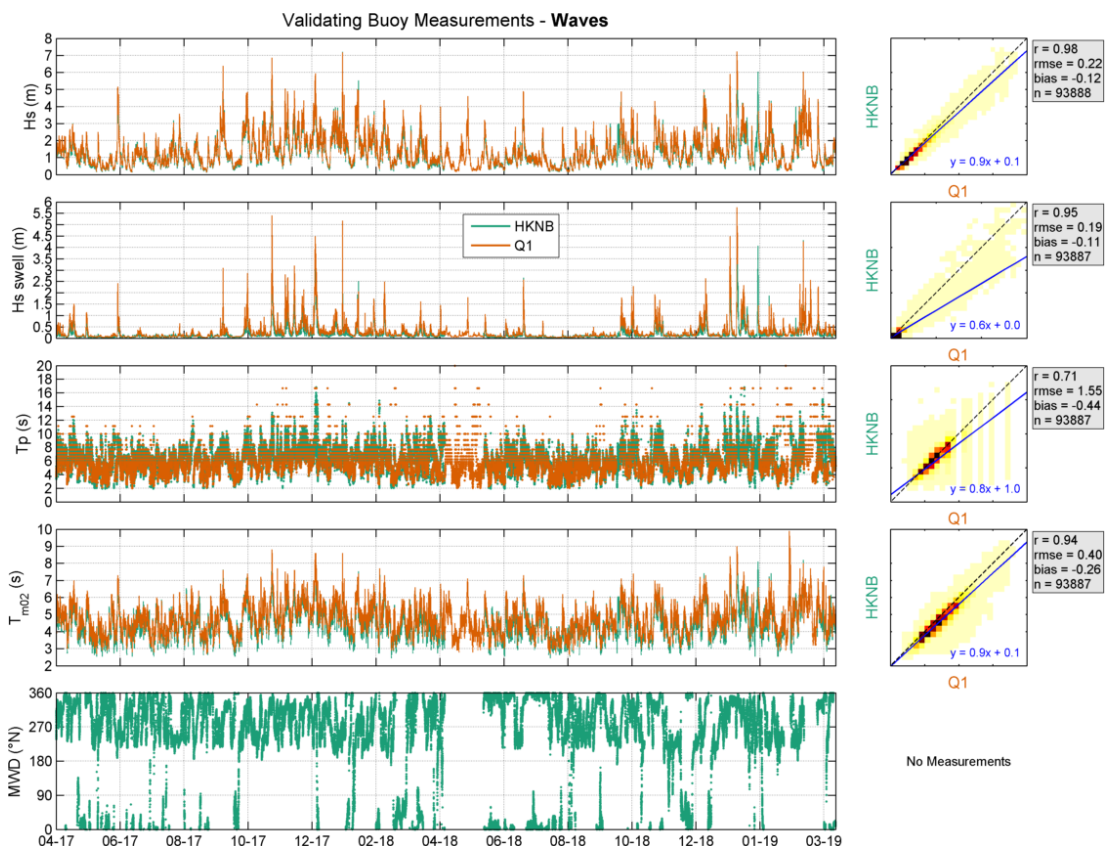
Figure 7.9: Roses of the simultaneously available HKNA (left) and K13 (right) wave data.

Table 7.4: Direction statistical comparison between HKNA and K13.

Sector	n (-)	Significant wave height			Mean wave direction		
		r (-)	RMSE (m)	Bias (m)	r (-)	RMSE ($^{\circ}$ N)	Bias ($^{\circ}$ N)
337.5 $^{\circ}$ N : 22.5 $^{\circ}$ N	21091	0.92	0.38	-0.24	0.51	37.36	-22.59
22.5 $^{\circ}$ N : 67.5 $^{\circ}$ N	3566	0.95	0.98	-0.75	0.32	36.40	-25.25
67.5 $^{\circ}$ N : 112.5 $^{\circ}$ N	1196	0.89	0.82	-0.70	0.20	30.36	-5.78
112.5 $^{\circ}$ N : 157.5 $^{\circ}$ N	318	0.70	0.54	-0.46	0.05	47.18	19.06
157.5 $^{\circ}$ N : 202.5 $^{\circ}$ N	1331	0.91	0.72	-0.55	0.42	41.51	25.60
202.5 $^{\circ}$ N : 247.5 $^{\circ}$ N	22496	0.88	0.43	-0.14	0.44	34.14	17.30
247.5 $^{\circ}$ N : 292.5 $^{\circ}$ N	17460	0.96	0.28	-0.07	0.41	48.37	6.47
292.5 $^{\circ}$ N : 337.5 $^{\circ}$ N	28396	0.96	0.31	-0.12	0.40	45.14	-13.47

The same comparisons just presented between the data from HKNA and the fixed stations are presented in the following for the HKNB data.

Figure 7.10, Figure 7.11, Figure 7.13 and Figure 7.15 show comparisons between HKNB observations of H_s , T_p , $T_{m0,2}$, and MWD and those at Q1, IJmuiden, EPL and K13, respectively. Figure 7.12, Figure 7.14 and Figure 7.16 compare the significant wave height roses of the simultaneous HKNB and IJmuiden, EPL and K13 observations (recall that there are no wave directions recorded at Q1). Table 7.5, Table 7.6 and Table 7.7 show the error statistics between the HKNB and the IJmuiden, EPL and K13 significant wave height and mean wave direction data per directional sector. The comparisons between the HKNB and the fixed station wave data are in line with those between the HKNA and the fixed station wave data.

**Figure 7.10:** Validation of HKNB waves with Q1.

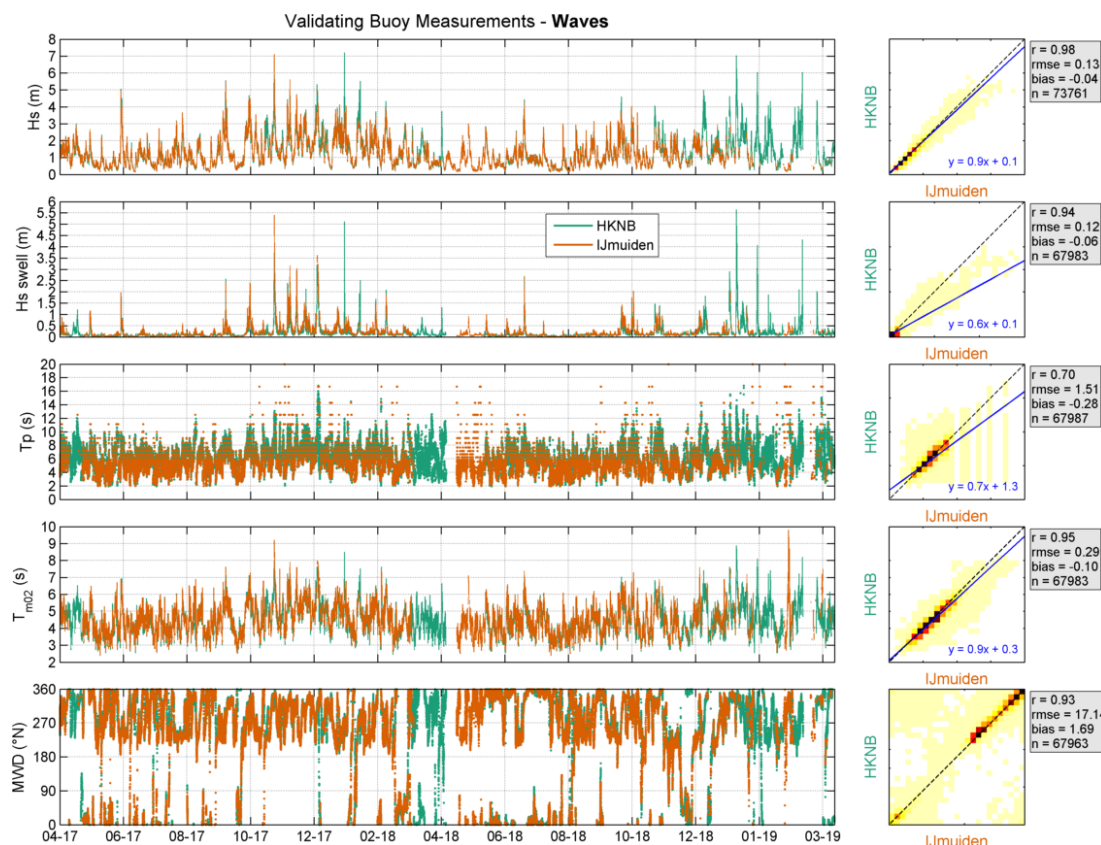


Figure 7.11: Validation of HKNB waves with IJmuiden.

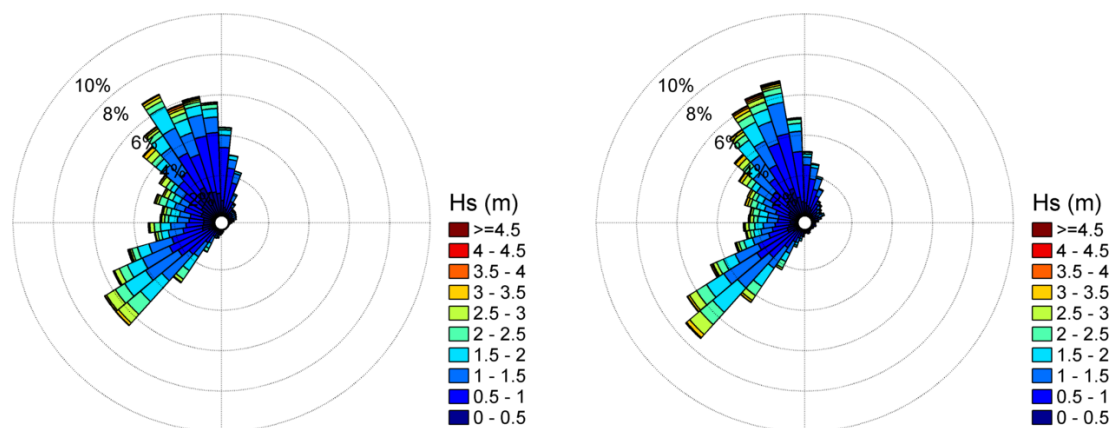
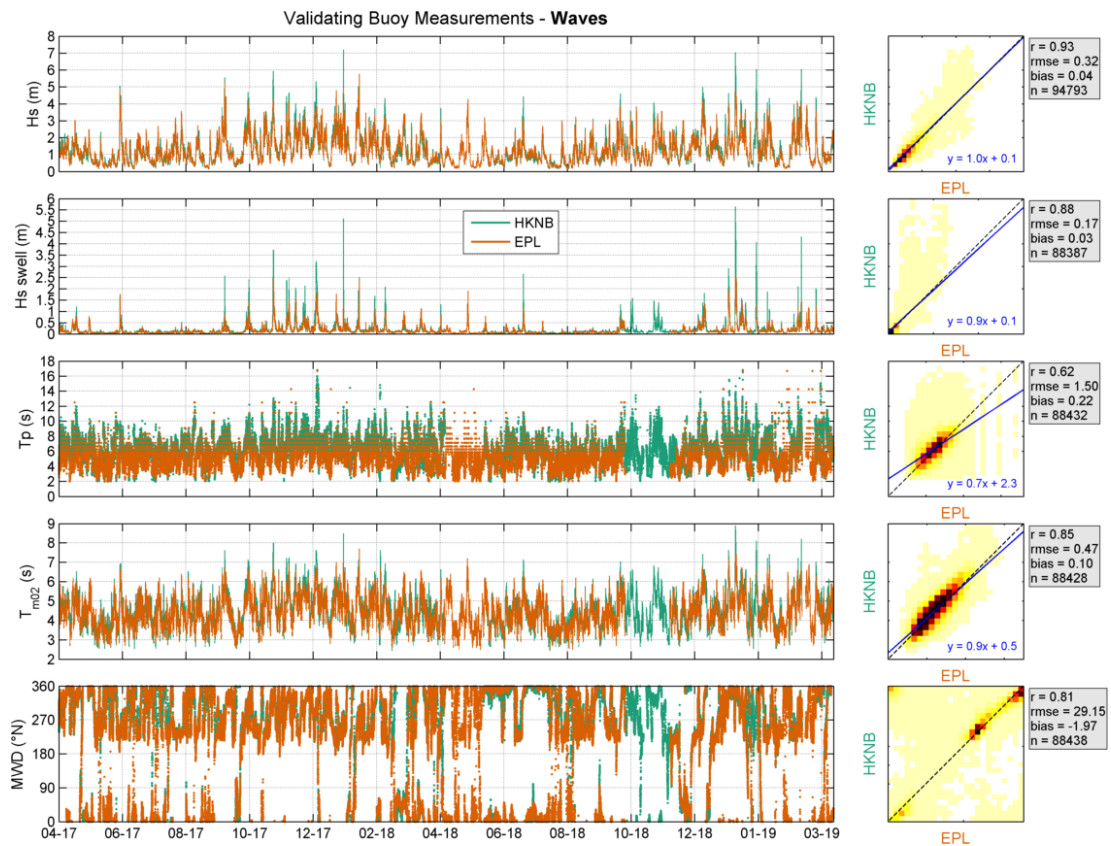


Figure 7.12: Roses of the simultaneously available HKNB (left) and IJmuiden (right) wave data.

Table 7.5: Direction statistical comparison between HKNB and IJmuiden.

Sector	n (-)	Significant wave height			Mean wave direction		
		r (-)	RMSE (m)	Bias (m)	r (-)	RMSE ($^{\circ}$ N)	Bias ($^{\circ}$ N)
337.5 $^{\circ}$ N : 22.5 $^{\circ}$ N	17204	0.98	0.14	-0.06	0.73	14.28	-0.25
22.5 $^{\circ}$ N : 67.5 $^{\circ}$ N	2561	0.98	0.13	-0.07	0.65	19.16	-4.56
67.5 $^{\circ}$ N : 112.5 $^{\circ}$ N	799	0.97	0.10	-0.06	0.43	20.39	0.47
112.5 $^{\circ}$ N : 157.5 $^{\circ}$ N	172	0.86	0.09	-0.05	0.42	35.32	13.18
157.5 $^{\circ}$ N : 202.5 $^{\circ}$ N	942	0.97	0.12	-0.05	0.63	28.53	18.25
202.5 $^{\circ}$ N : 247.5 $^{\circ}$ N	16726	0.98	0.14	-0.03	0.73	12.16	4.56
247.5 $^{\circ}$ N : 292.5 $^{\circ}$ N	11994	0.99	0.12	-0.00	0.70	21.27	3.51
292.5 $^{\circ}$ N : 337.5 $^{\circ}$ N	17917	0.99	0.14	-0.04	0.64	18.84	-0.41

**Figure 7.13:** Validation of HKNB waves with EPL.

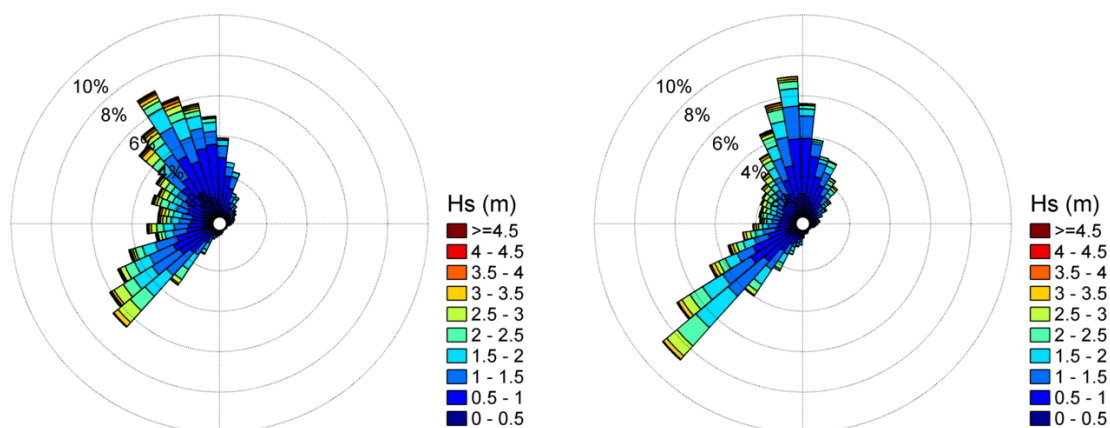


Figure 7.14: Roses of the simultaneously available HKNB (left) and EPL (right) wave data.

Table 7.6: Direction statistical comparison between HKNB and EPL.

Sector	n (-)	Significant wave height			Mean wave direction		
		r (-)	RMSE (m)	Bias (m)	r (-)	RMSE ($^{\circ}$ N)	Bias ($^{\circ}$ N)
337.5 $^{\circ}$ N : 22.5 $^{\circ}$ N	21070	0.92	0.27	-0.05	0.60	24.68	-10.23
22.5 $^{\circ}$ N : 67.5 $^{\circ}$ N	4309	0.94	0.40	-0.27	0.32	24.43	-2.83
67.5 $^{\circ}$ N : 112.5 $^{\circ}$ N	1288	0.92	0.28	-0.20	0.32	27.65	7.62
112.5 $^{\circ}$ N : 157.5 $^{\circ}$ N	273	0.77	0.19	-0.07	0.29	50.46	20.95
157.5 $^{\circ}$ N : 202.5 $^{\circ}$ N	1256	0.93	0.28	-0.16	0.47	42.32	16.93
202.5 $^{\circ}$ N : 247.5 $^{\circ}$ N	21189	0.93	0.29	0.03	0.51	17.63	4.22
247.5 $^{\circ}$ N : 292.5 $^{\circ}$ N	15468	0.95	0.34	0.14	0.47	35.40	7.95
292.5 $^{\circ}$ N : 337.5 $^{\circ}$ N	24038	0.95	0.36	0.15	0.50	35.41	-8.33

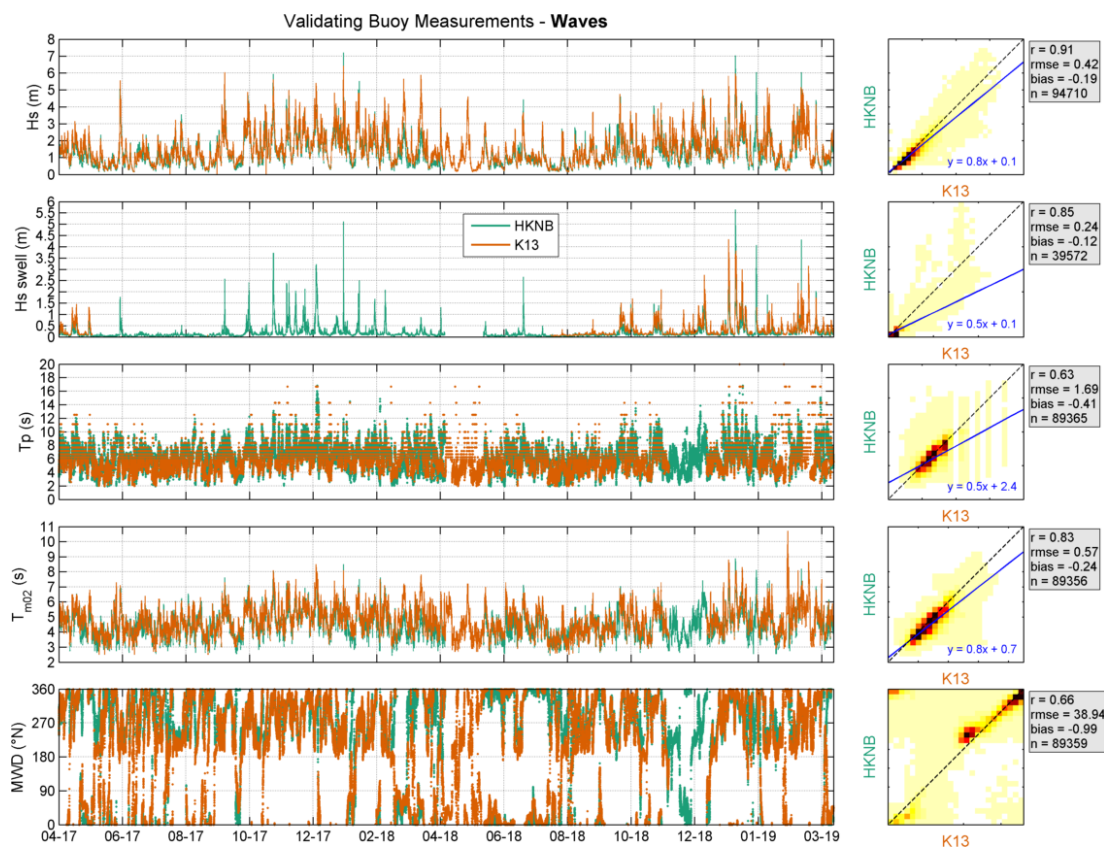


Figure 7.15: Validation of HKNB waves with K13.

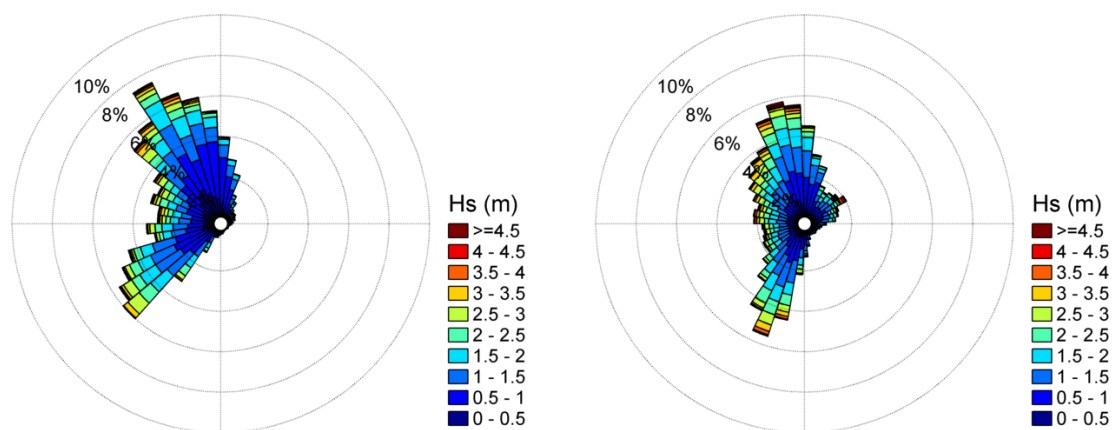


Figure 7.16: Roses of the simultaneously available HKNB (left) and K13 (right) wave data.

Table 7.7: Direction statistical comparison between HKNB and K13.

Sector	n (-)	Significant wave height			Mean wave direction		
		r (-)	RMSE (m)	Bias (m)	r (-)	RMSE ($^{\circ}$ N)	Bias ($^{\circ}$ N)
337.5 $^{\circ}$ N : 22.5 $^{\circ}$ N	21961	0.94	0.36	-0.22	0.57	35.51	-18.66
22.5 $^{\circ}$ N : 67.5 $^{\circ}$ N	3514	0.95	0.99	-0.75	0.35	35.41	-25.11
67.5 $^{\circ}$ N : 112.5 $^{\circ}$ N	1157	0.88	0.80	-0.69	0.24	28.14	-7.75
112.5 $^{\circ}$ N : 157.5 $^{\circ}$ N	298	0.70	0.53	-0.46	0.13	43.04	16.46
157.5 $^{\circ}$ N : 202.5 $^{\circ}$ N	1166	0.91	0.77	-0.59	0.34	42.85	28.54
202.5 $^{\circ}$ N : 247.5 $^{\circ}$ N	19970	0.88	0.44	-0.15	0.43	34.72	20.41
247.5 $^{\circ}$ N : 292.5 $^{\circ}$ N	16052	0.95	0.28	-0.08	0.46	44.91	10.82
292.5 $^{\circ}$ N : 337.5 $^{\circ}$ N	25741	0.96	0.30	-0.11	0.44	41.39	-8.05

7.4 Quality Statement

Based on a) the comparisons between the data from the buoys, which are excellent for all parameters, except as expected those depending strongly on the sampling variability (randomness of the sea surface elevation) and discreteness of the wave spectra (T_p , $T_{m02swell}$ and MWD_{swell}), and b) the validation of the data against the platform observations, in which mismatches can be explained by local effects, spatial variations and again discreteness of the wave spectra, it can be concluded that the accuracy of the Wavesense 3 is high. Furthermore, as can also be verified in the monthly validation reports, this is true over the whole campaign period.

7.5 Climate description

In this section we present some characteristics of the wave climate at HKN using only the validated HKNA data which have a data return above 97%. The availability of the HKNA data is higher than that of the HKNB data and there are no significant differences in the observations from both stations. [Figure 7.17](#) shows the significant wave height and peak wave period roses and [Figure 7.18](#) presents the percentages of joint significant wave height and mean wave period occurrences.

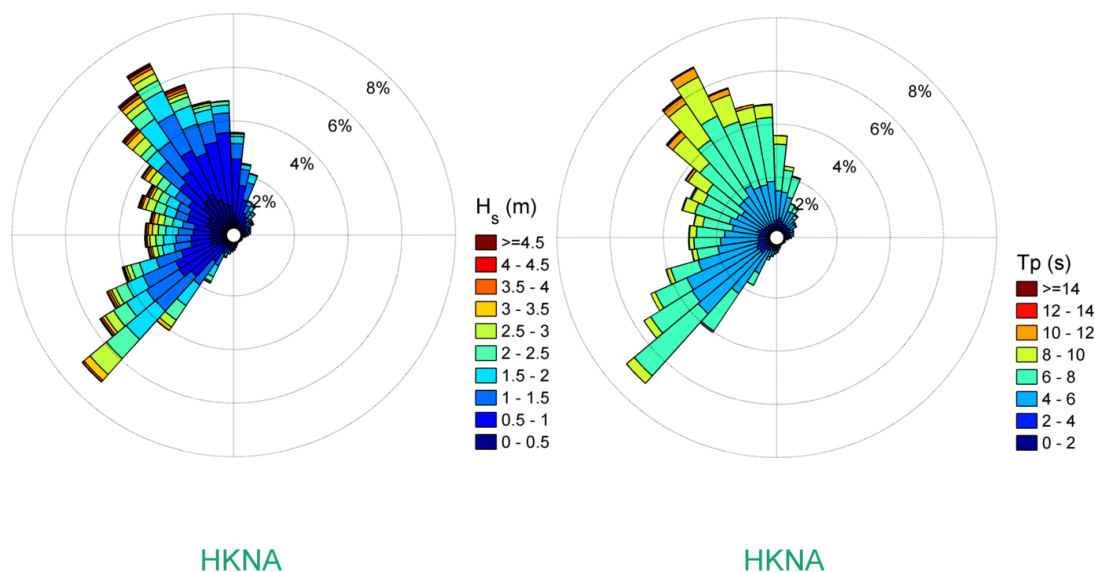


Figure 7.17: HKNA significant wave height and peak wave period roses.

H _s (m)	T _p (s)								
	0-2	2-4	4-6	6-8	8-10	10-12	12-14	>14	
>4.5				0.01	0.26	0.16	0.05	0.01	0.49
4.0-4.5				0.04	0.44	0.09	0.02	0.00	0.59
3.5-4.0				0.24	0.83	0.13	0.01	0.01	1.21
3.0-3.5			0.00	1.18	1.15	0.16	0.01	0.03	2.53
2.5-3.0			0.13	3.44	1.06	0.13	0.01	0.04	4.81
2.0-2.5			1.00	5.92	0.91	0.13	0.02	0.01	7.99
1.5-2.0		0.00	4.48	7.88	1.29	0.16	0.03	0.01	13.85
1.0-1.5		0.57	11.62	7.58	1.29	0.11	0.03	0.00	21.21
0.5-1.0		6.64	15.27	8.46	1.61	0.26	0.03		32.27
0.0-0.5	0.01	5.01	5.23	2.22	2.33	0.21	0.04	0.01	15.06
	0.01	12.23	37.73	36.95	11.17	1.55	0.24	0.12	100.00
	HKNA								Total

Figure 7.18: HKNA significant wave height and peak wave period joint occurrence table.

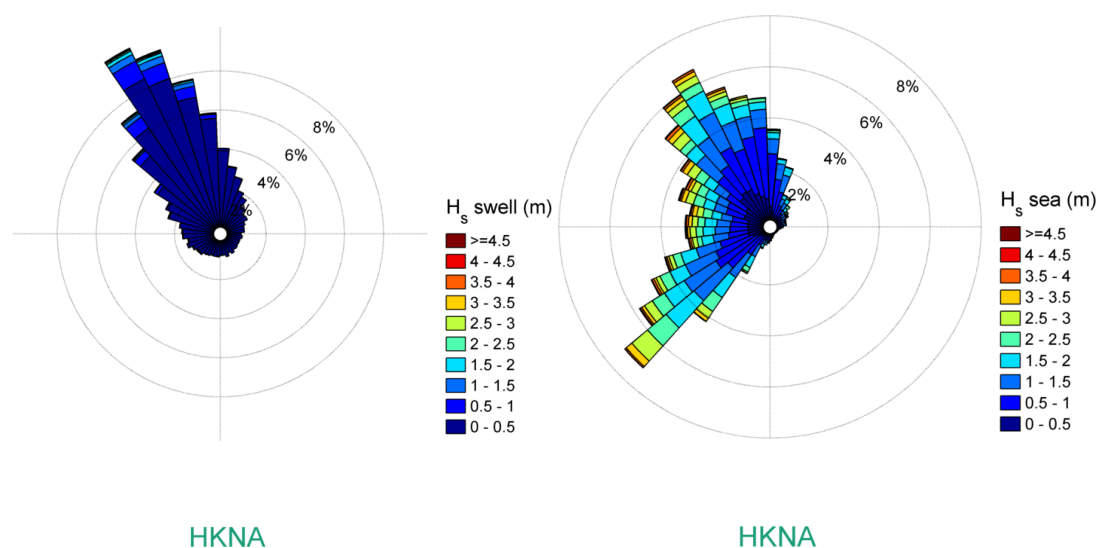


Figure 7.19: HKNA swell (left) and sea (right) significant wave height roses.

In order to give an idea of the energy distribution in the spectra at HKN, Figure 7.19 show the swell and sea roses and Figure 7.20 the distribution and rose of the ratio between the swell and the sea significant wave height. As can be seen in the figures the spectra is generally sea dominated and the swell component has a predominantly northwestern direction (recall that spectral energy up to 0.1Hz is classified as swell, cf. Table 3.1). To further illustrate the energy distribution in the spectra at HKN, Figure 7.21, Figure 7.22, Figure 7.23 show the 2d

wave spectra during the highest observation of the total, swell and sea significant wave height, respectively.

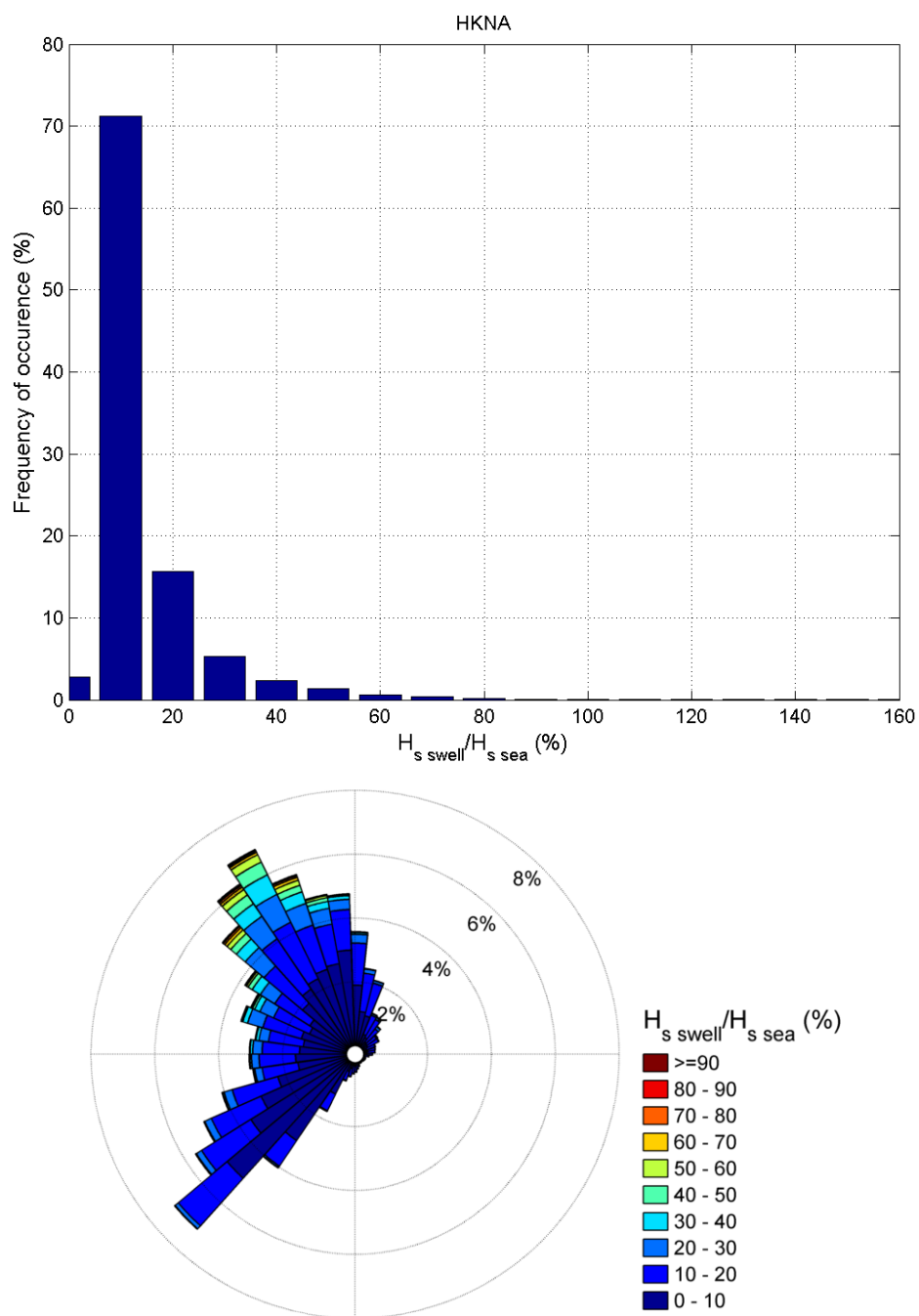


Figure 7.20: Distribution of $H_{s\text{ swell}}$ percentage of $H_{s\text{ sea}}$. Top panel: Frequency plot. Bottom panel: Rose of $H_{s\text{ swell}}/H_{s\text{ sea}}$ percentage versus the MWD.

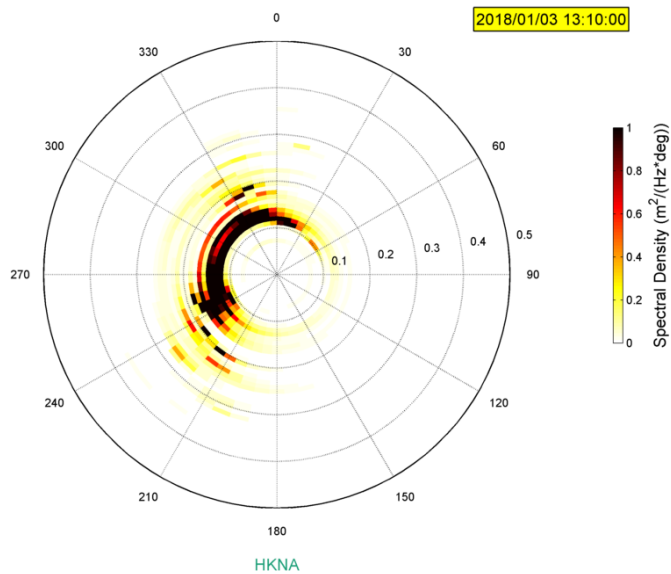


Figure 7.21: Directional wave spectrum of 03-Jan-2018 13:10:00, $H_s=7.15\text{m}$, $H_{sswell}=5.02\text{m}$, $H_{ssea}=5.10\text{m}$ and $MWD=286^\circ N$.

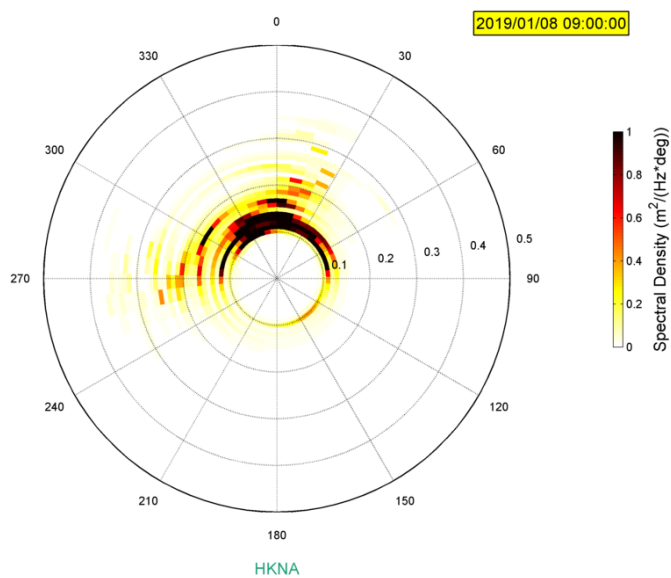


Figure 7.22: Directional wave spectrum of 08-Jan-2019 09:00:00, $H_s=7.03\text{m}$, $H_{sswell}=5.74\text{m}$, $H_{ssea}=4.08\text{m}$ and $MWD=337^\circ N$.

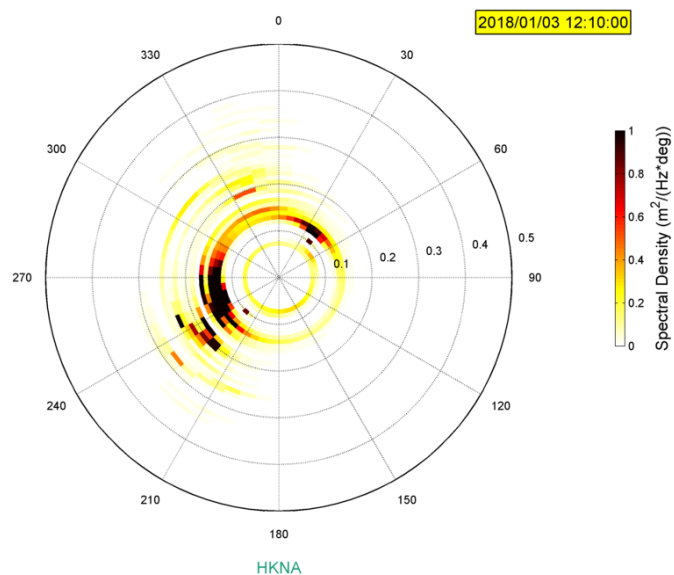


Figure 7.23: Directional wave spectrum of 03-Jan-2018 12:10:00, $H_s=6.88\text{m}$, $H_{sswell}=3.98\text{m}$, $H_{ssea}=5.61\text{m}$ and $MWD=255^\circ N$.

8 Temperature

8.1 Introduction

The measured air and water temperatures from both buoys are presented and analyzed within this chapter. The goal is to assess the reliability and accuracy of the retrieved data from both HKNA and HKNB. This is completed by first intercomparing the HKN data, followed by a statistical validation against the available data from fixed stations in the area.

8.2 Intercomparison of the HKN data

Note that there are four timeseries of water temperature measurements at HKN, those from the WLRs are bottom temperatures and those from the HKNA and HKNB buoys are surface temperatures.

Figure 8.1 shows the observed air and water temperature and their differences (which have been used in the analysis of the vertical wind speed profiles in Section 6.5). As noted, the availability of the HKNA data is higher (cf. Figure 5.1). The figure shows that the timeseries align. Both water and air temperatures show a clear yearly cycle with the water temperatures varying in this period between 3 and 25 °C and the air temperatures between 0 and 30 °C.

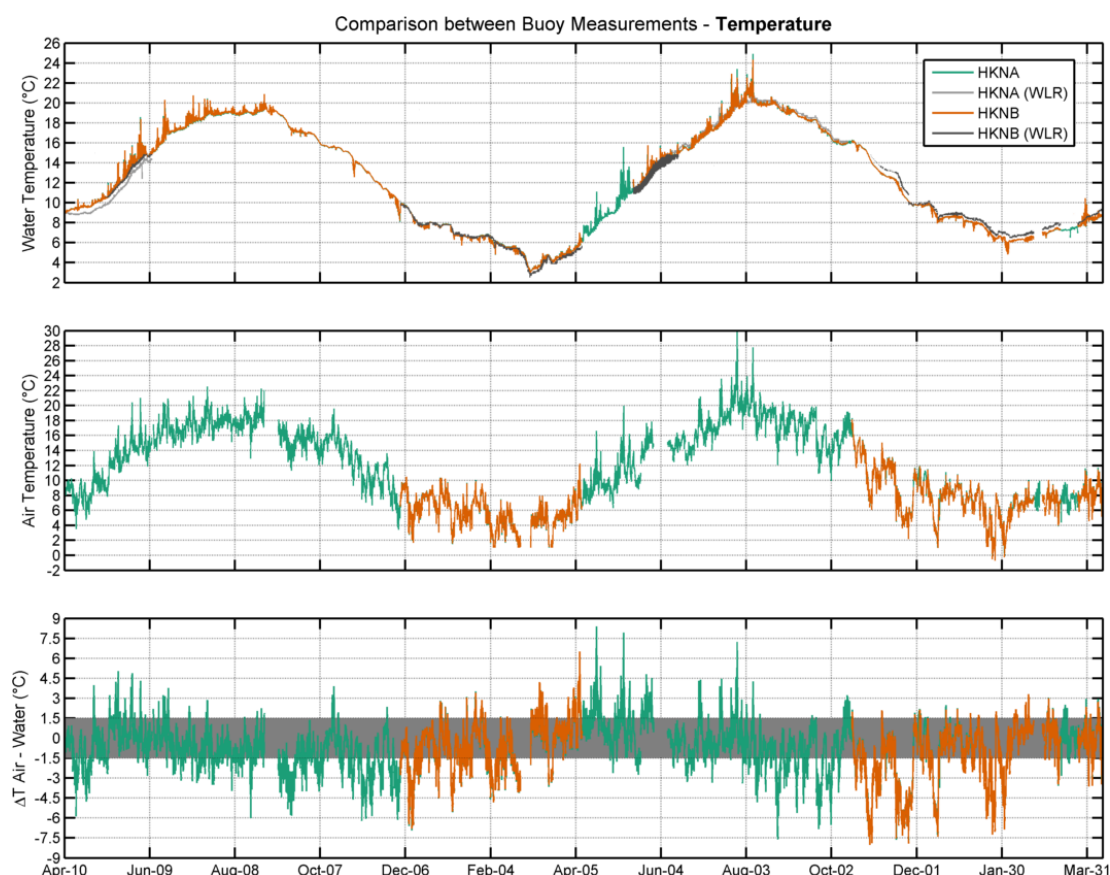


Figure 8.1: Temperature and temperature difference measured at HKN.

Figure 8.2 shows the intercomparisons of the measured air and surface water temperatures at both HKNA and HKNB. (Figure 8.2 contains no bottom water temperature data because

the overlapping period is too short for meaningful statistical comparisons). The figure shows, as could already be seen in Figure 8.1 that the agreements are all excellent.

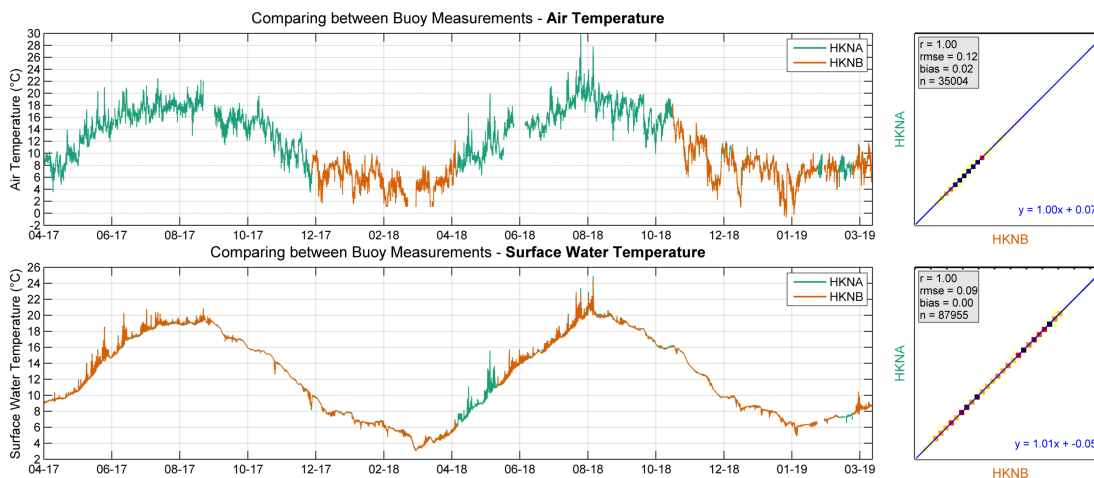


Figure 8.2: Timeseries (left) and scatter plot (right) comparisons between the measured at HKN air (top) and surface water (bottom) temperatures.

8.3 Validation of the HKN data

8.3.1 Water Temperature

A timeseries comparison between the observations from both buoys and sensors and the fixed stations is presented in Figure 8.3. The water temperature observations from the fixed stations are all surface temperatures. The figure shows that there are also some outliers in the fixed station temperature observations, these have not been removed because they are so few that they do not affect the statistics.

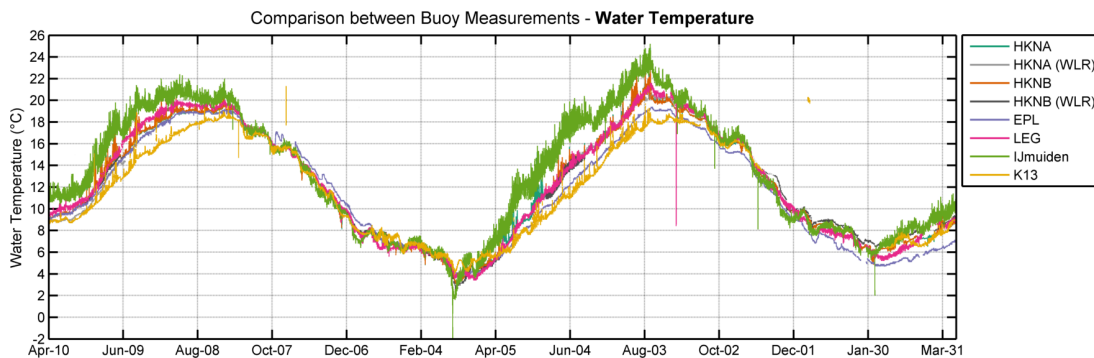


Figure 8.3: Water temperature measurements from all locations.

A direct comparison of the measured surface water temperature at HKNA and HKNB against the fixed stations is provided in Figure 8.4 and Figure 8.5, respectively. The agreements are in all cases excellent.

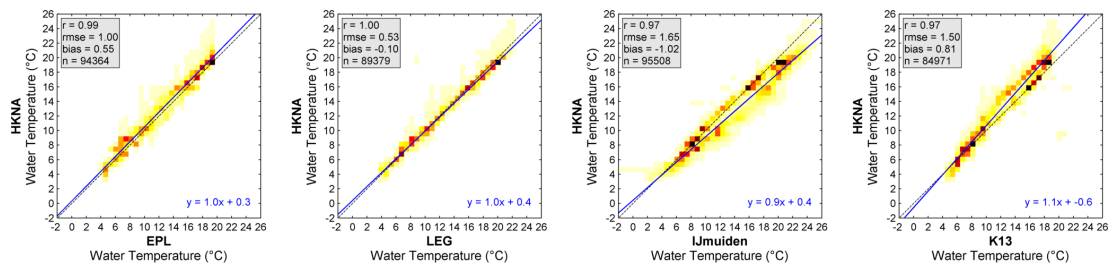


Figure 8.4: Surface water temperature comparison at HKNA.

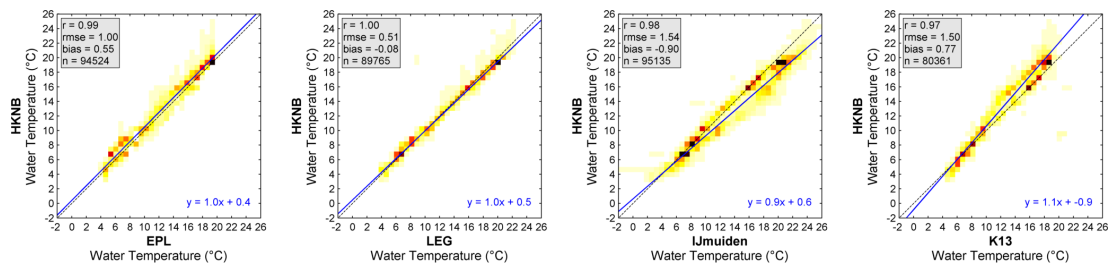


Figure 8.5: Surface water temperature comparison at HKNB.

8.3.2 Air Temperature

A timeseries comparison of the measured air temperature between the observations at HKNA and HKNB and the P11-b and Q1 fixed stations is shown in Figure 8.6. The respective scatter comparisons are provided in Figure 8.7 for HKNA and in Figure 8.8 for HKNB. As shown in the figures, the data align and the agreements are all excellent.

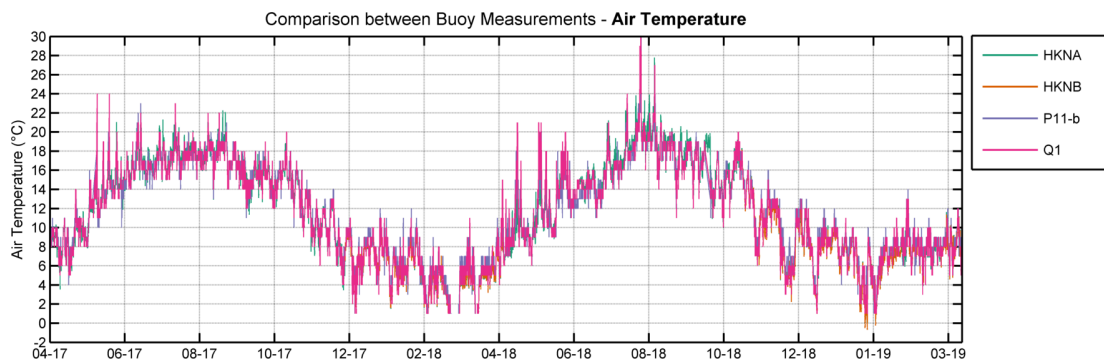


Figure 8.6: Air temperature measurements from all locations.

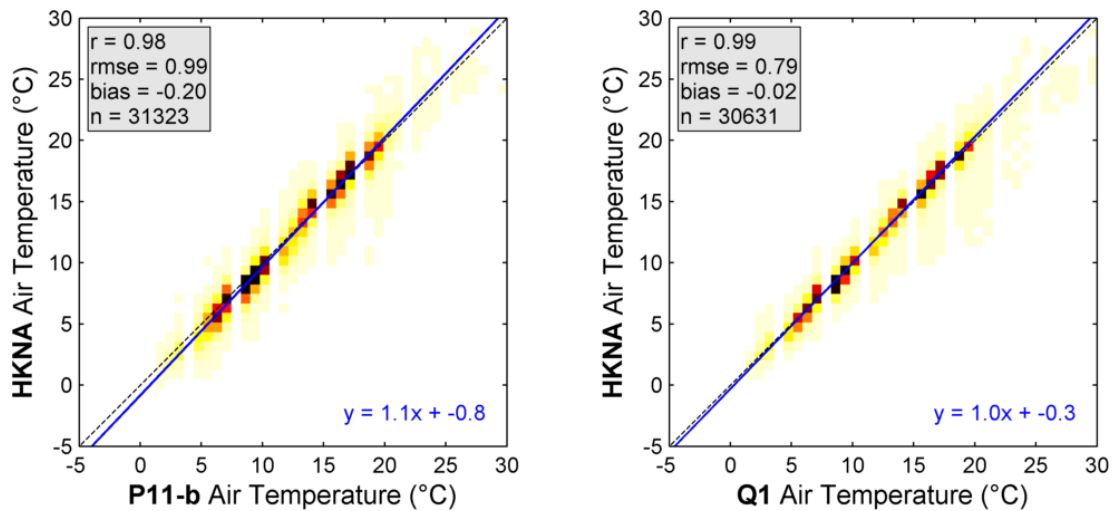


Figure 8.7: Air temperature comparison at HKNA.

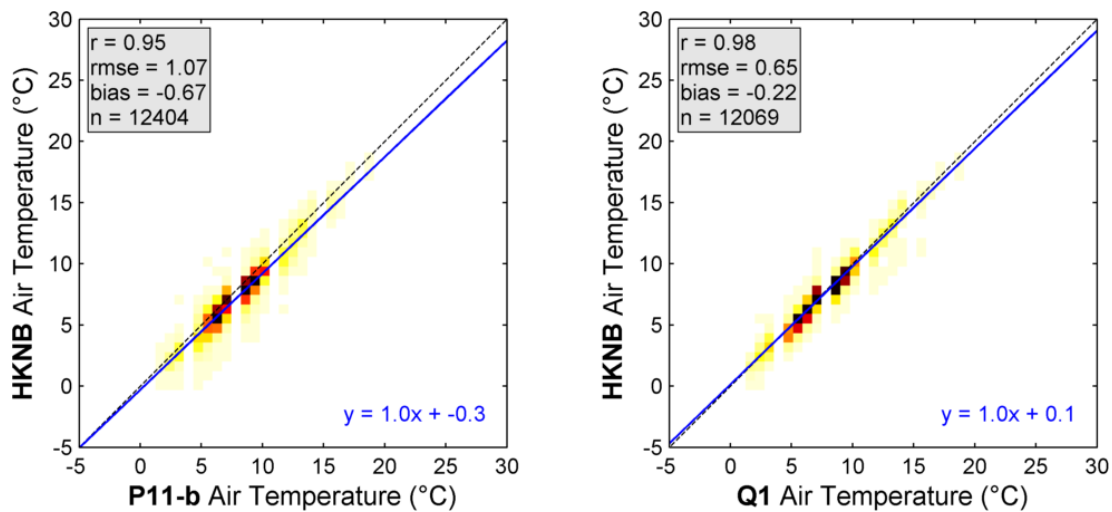


Figure 8.8: Air temperature comparison at HKNB.

8.4 Quality Statement

Based on the intercomparison of the buoy air and water surface temperature data and the validation of these data against those from the fixed stations, the buoy sensors are considered to be working properly and the data to be reliable. The bottom water temperature data could not be validated and should therefore be considered with care.

8.5 Climate description

Given its higher availability, the HKNA temperature observations are used for the climate description. As already noted when presenting [Figure 8.1](#), in HKN both the water and air temperatures follow a clear yearly cycle with the water temperatures varying in this period between 3 and 25 °C and the air temperatures between 0 and 30 °C and the differences between the air and water surface temperatures ranging between -8 and 8 °C. The distributions of the data are given in [Figure 8.1](#) and clearly show two modes for both the water and air temperature and that the differences between the air and water surface temperatures are mostly close to zero.

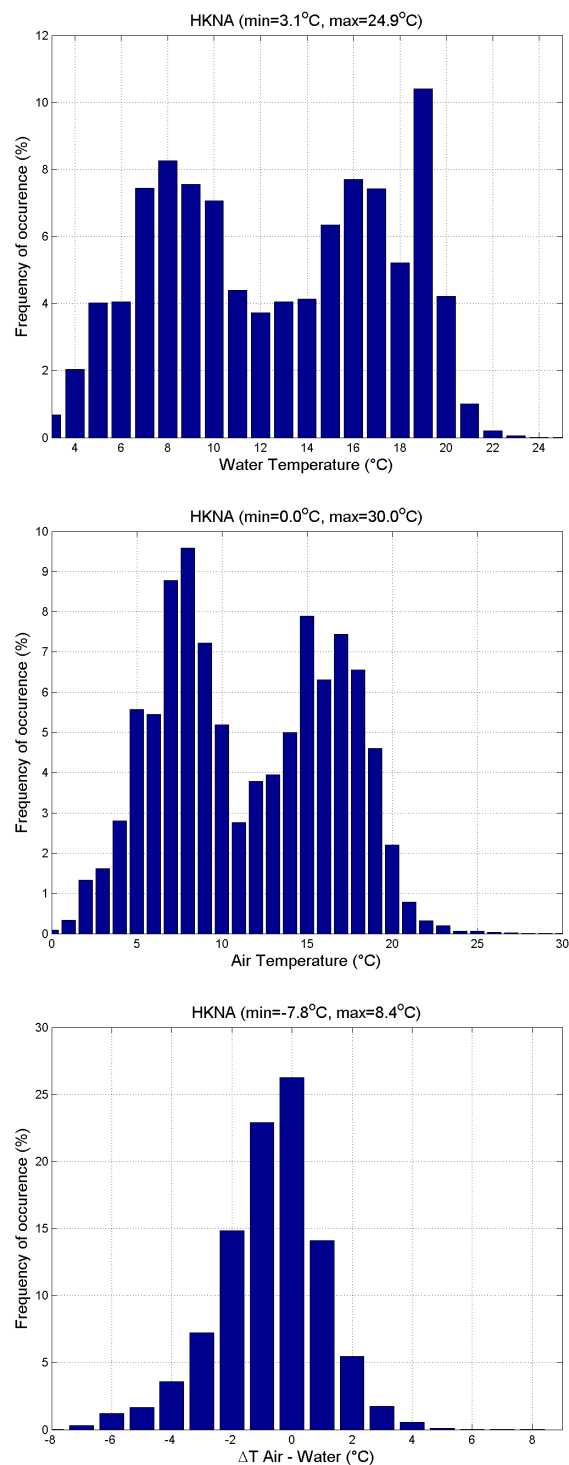


Figure 8.9: Distribution of temperature and temperature differences measured at HKNA.

9 Air Pressure

9.1 Introduction

The air pressure measurements from both buoys are presented and analyzed within this chapter. The goal is to assess the reliability and accuracy of the retrieved data from both HKNA and HKNB. This is done by comparing the timeseries and a statistical validation against the observations from the fixed stations in the area.

9.2 Validation of the HKN data

An overview of the available air pressure measurements (e.g. HKNA, HKNB, EPL, LEG, K13 and Q1) is shown in [Figure 9.1](#). All signals show near-identical variations in time, as expected, given their proximity with respect to macro-atmospheric forcings, and show a low pressure of less than 970 hPa in December 2017.

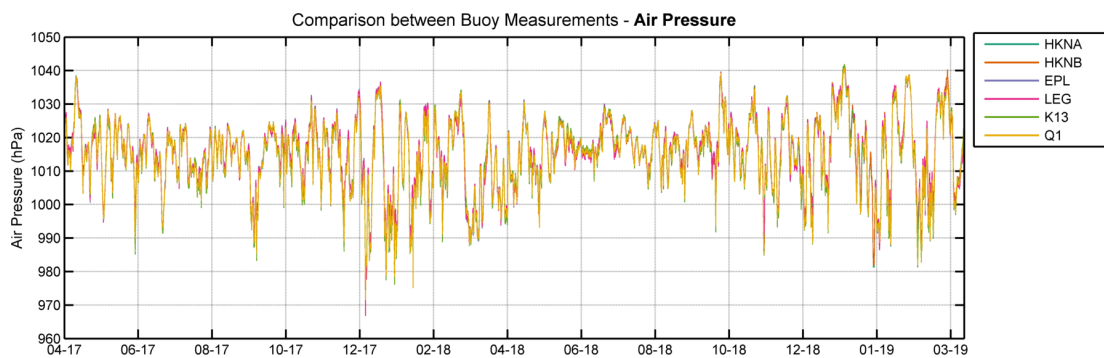


Figure 9.1: Air pressure measurements from all locations.

A direct comparison of the measured air pressure at HKNA and HKNB against the fixed stations is included in [Figure 9.2](#) and [Figure 9.3](#), respectively. The agreement between the HKNA and HKNB observations with those from all fixed locations is excellent.

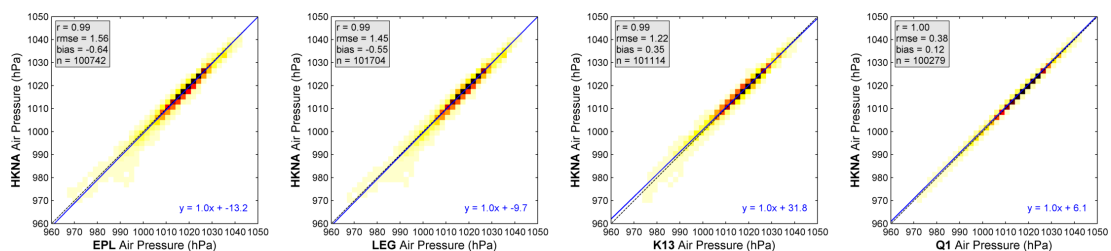


Figure 9.2: Air pressure comparison at HKNA.

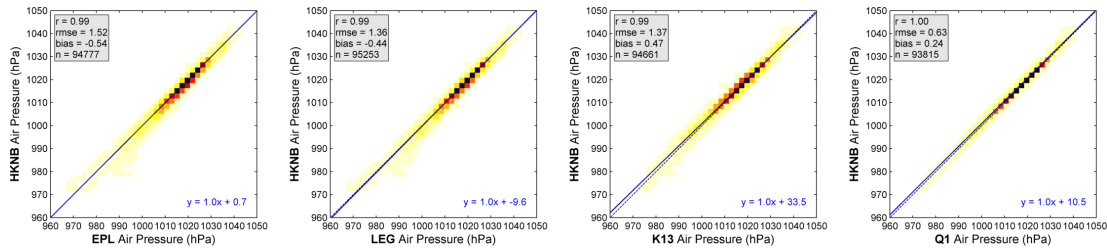


Figure 9.3: Air pressure comparison at HKNB.

9.3 Quality Statement

Based on the intercomparison of the buoy air pressure data and the validation of these data against those from the fixed stations, the buoy sensors are considered to be working properly and the data to be reliable.

9.4 Climate description

As shown above, the pressure gradients in HKN are in line with those observed elsewhere in the considered North Sea stations, with pressures varying between 970 and 1041 hPa in the considered two year period. Given its higher availability, the HKNA air pressure observations are used for the climate description. The distribution of the data is given in Figure 9.4.

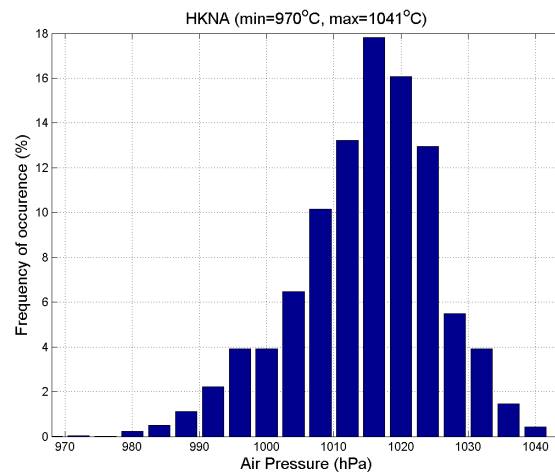


Figure 9.4: Distribution of air pressure measured at HKNA.

10 Water Level

10.1 Introduction

This chapter focuses on validating and analyzing processed water levels from the WLRs. The validation for water level requires additional work given the lack of data sources at the exact location of the HKN buoys. The previously described tidal wave propagation in the North Sea limits the ability to validate with nearby fixed platforms (i.e. distinct tidal amplitudes and phases). Thus, a previously set up hydrodynamic model by Deltares - running operationally - is used for validation.

10.2 Model description

The water levels (and later currents in [Chapter 11](#)) representative for the HKNA and HKNB locations are taken from the Dutch Rijkswaterstaat operational hydrodynamic model, known as the **D**utch **C**ontinental **S**helf **Z**uidelijke **N**oordzee model (DCSMv6-ZUNOV4) ([Zijl et al., 2013](#)), see [Figure 10.1](#).

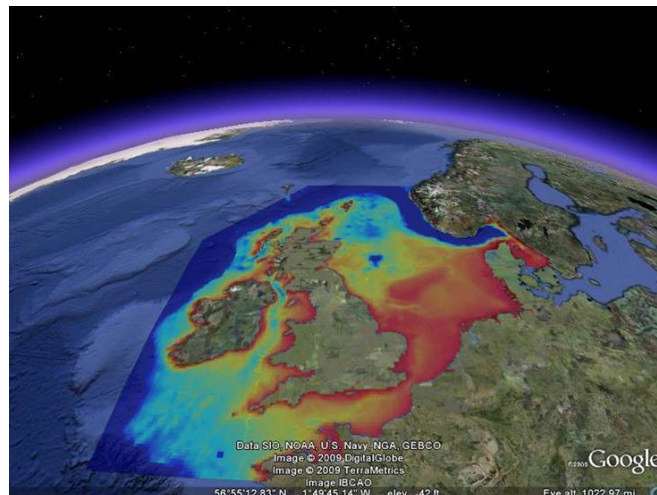


Figure 10.1: DCSMv6-ZUNOV4 model bathymetry (via Google Earth).

The DCSMv6-ZUNOV4 has a horizontal resolution of variable grid size up to approximately 200 m – 400 m in Dutch estuaries and in the Wadden Sea. It was set up by Deltares for the Dutch Government as an operational base model for - amongst others - storm surge warnings along the Dutch coast. The model is driven by boundary water levels and spatially varying pressure and wind fields. The water levels imposed at the open boundaries can be split into a tidal and non-tidal (surge) part. The tide is properly defined in the frequency domain (38 constituents), while surge is taken into account with an inverse barometer correction (IBC). The IBC varies in time and space (dependent on the local atmospheric pressure) and is added to the tidal water level variation along the open boundary. The model is of sufficient resolution to represent the water level variations and flow patterns around the Hollandse Kust (noord) project site. The underlying bathymetry of the model is based on the most detailed and accurate data available (i.e. in-house). Furthermore, the model benefits from real-time data assimilation in the form of steady-state Kalman filter. The DCSMv6-ZUNOV4 model is extensively validated against measurements around the entire North Sea and has been shown to deliver accurate output along the Dutch coastline ([Zijl et al., 2015](#)). Furthermore, in

all HKN data validation monthly reports the DCSMv6-ZUNOV4 have been validated against observations from the EPL, LEG, K13 and IJmuiden and in all months excellent correlations and bias close to zero have been shown.

10.3 Intercomparison of the HKN data

Figure 10.2 shows the intercomparison of the measured water levels at both HKNA and HKNB. The figures show that the data align. During the campaign an operational correction was used based on bathymetry. In the final dataset a bias between the observations and the model was determined and applied to the water level data.

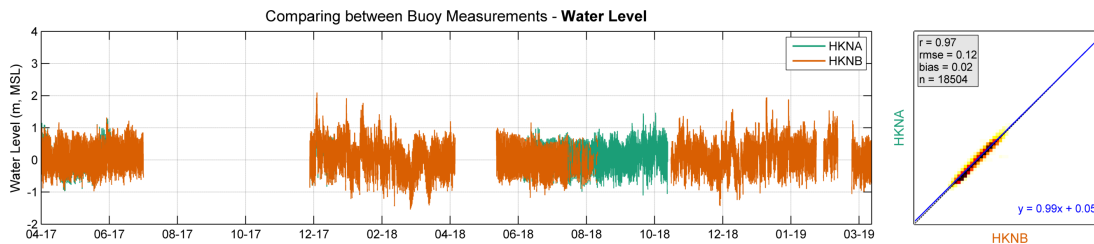


Figure 10.2: HKNA and HKNB water level.

10.4 Model Validation

Figure 10.3 shows the HKN data against the model data. The figure shows excellent agreements at both locations. Note that there are some outliers in the model data but these have not been removed since they do not affect the statistical comparisons.

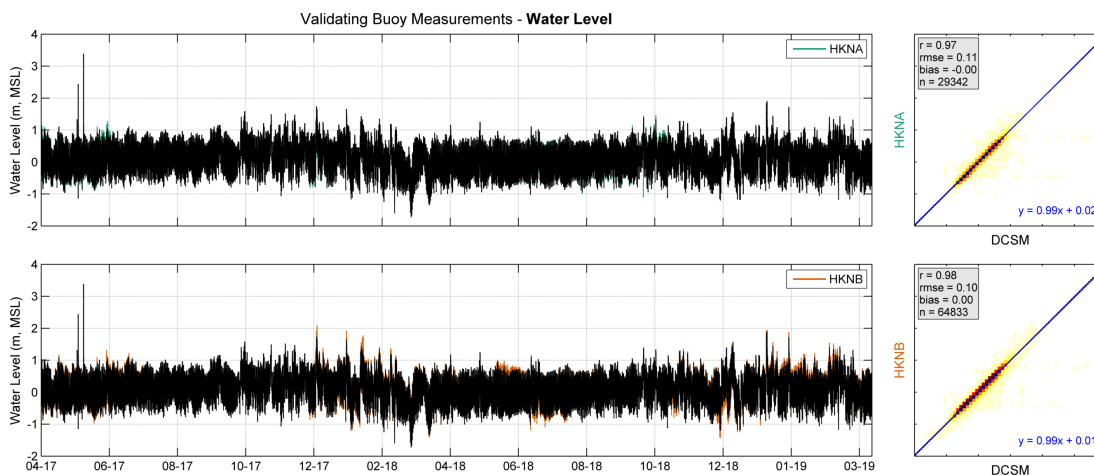


Figure 10.3: Validation of HKNA and HKNB water levels with DCSMv6-ZUNOV4 model output.

10.5 Quality Statement

Based on the intercomparison of the buoy processed water levels from the WLRs and the validation of these data against the model data, the inferred values are considered to be reliable in particular in terms of temporal variations. The accuracy of the absolute values depends on the validity of the applied bias corrections derived from the model data since the exact depth at which the WLRs were is not always known. Some care should therefore be taken when considering the data.

10.6 Climate description

Although due to the uncertainties on the depth at which the WLRs are located it is not possible to obtain accurate absolute water level observations from HKN, the validation of the data against the model data indicate that the water levels at HKN should be expected to vary between -2 and 2 m MSL.

11 Currents

11.1 Introduction

The measured current velocities from both buoys are presented and analyzed within this chapter. The goal is to assess the reliability and accuracy of the retrieved current data from both HKNA and HKNB. This is completed by first intercomparing the HKN data, followed by a statistical validation against the data from the DCSMv6-ZUNOV4 model.

There are current speed and direction observations at depths 4, 6, 8, 10, 12, 14, 16, 18 and 20 m available from HKNA and HKNB.¹

11.2 Intercomparison of the HKN data

To get a full overview of the data, [Figure 11.1](#) and [Figure 11.1](#) show the time evolution of vertical current profiles at HKNA and at HKNB, respectively. In order to further present the data, [Figure 11.3](#), [Figure 11.4](#) and [Figure 11.5](#) show the timeseries of the observed surface (4 m), 10 m and 20 m current speeds, respectively. [Figure 11.6](#) and [Figure 11.7](#) show the observed current speeds and directions, respectively, as a function of depth. The figures show a general alignment between the current speeds from both buoys.

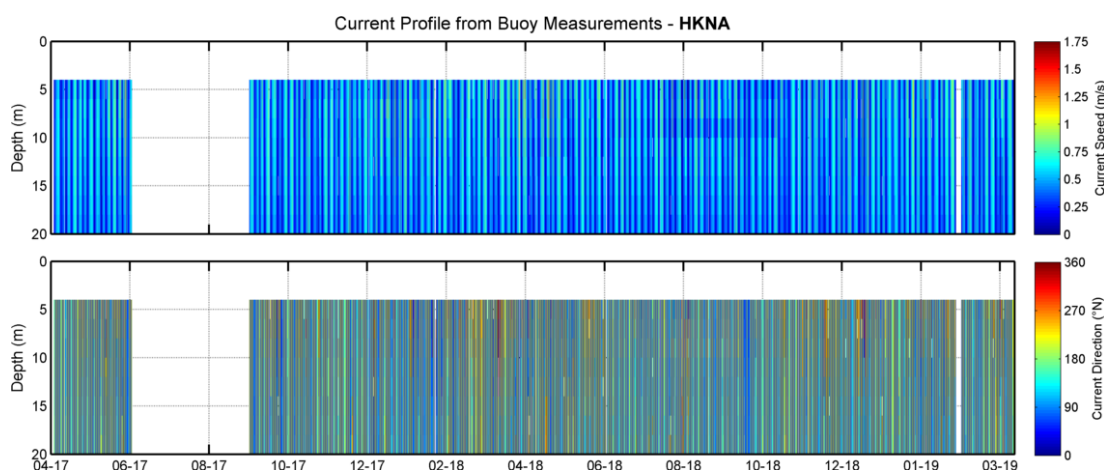


Figure 11.1: Time evolution of the vertical current speed (top panel) and direction (bottom panel) profiles at HKNA.

¹The current speed and direction are also measured at a depth of 22 m but not considered in this report because, due to the water level variations, data at this level are not always available or of lower quality (given that it is practically at the bottom).

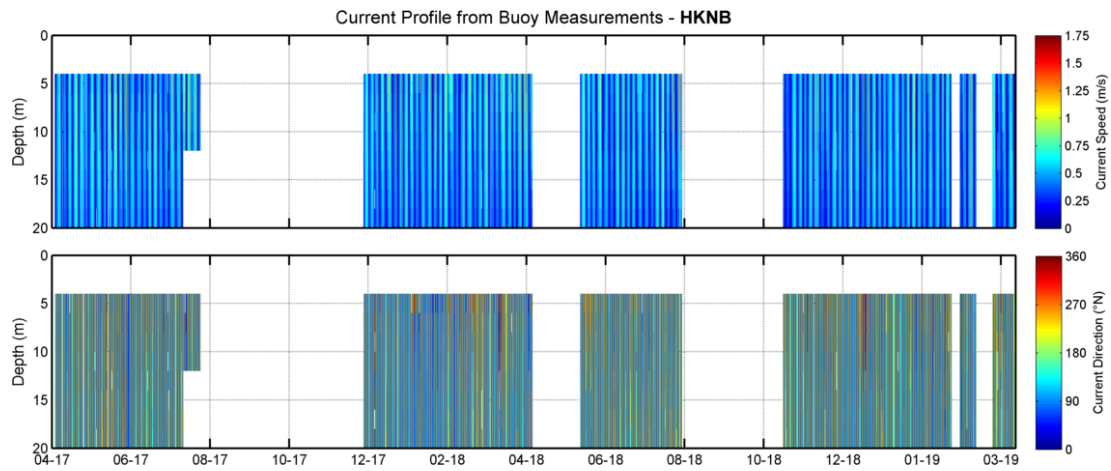


Figure 11.2: Time evolution of the vertical current speed (top panel) and direction (bottom panel) profiles at HKNB.

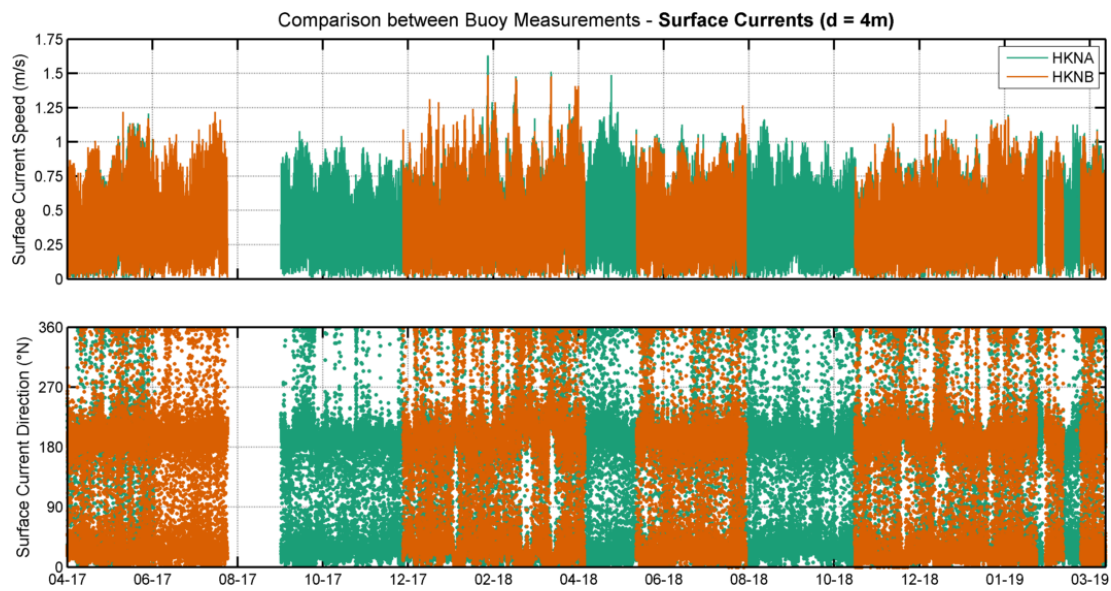


Figure 11.3: Timeseries of surface currents at each buoy. The oceanographic convention is used for the current directions, so all current directions are going to, clockwise from North.

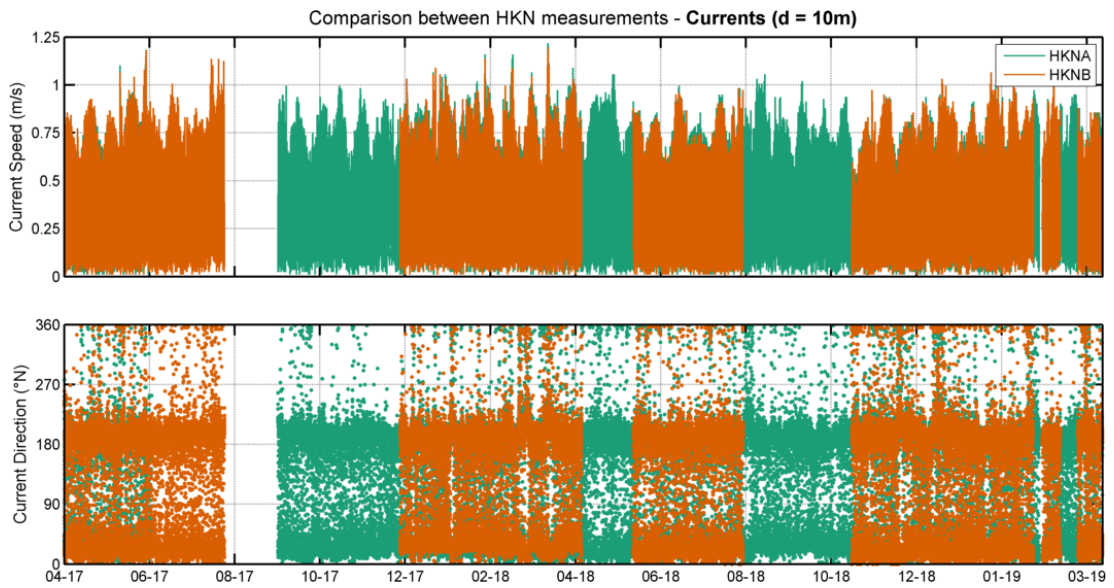


Figure 11.4: Timeseries of 10 m depth currents at each buoy. The oceanographic convention is used for the current directions, so all current directions are going to, clockwise from North.

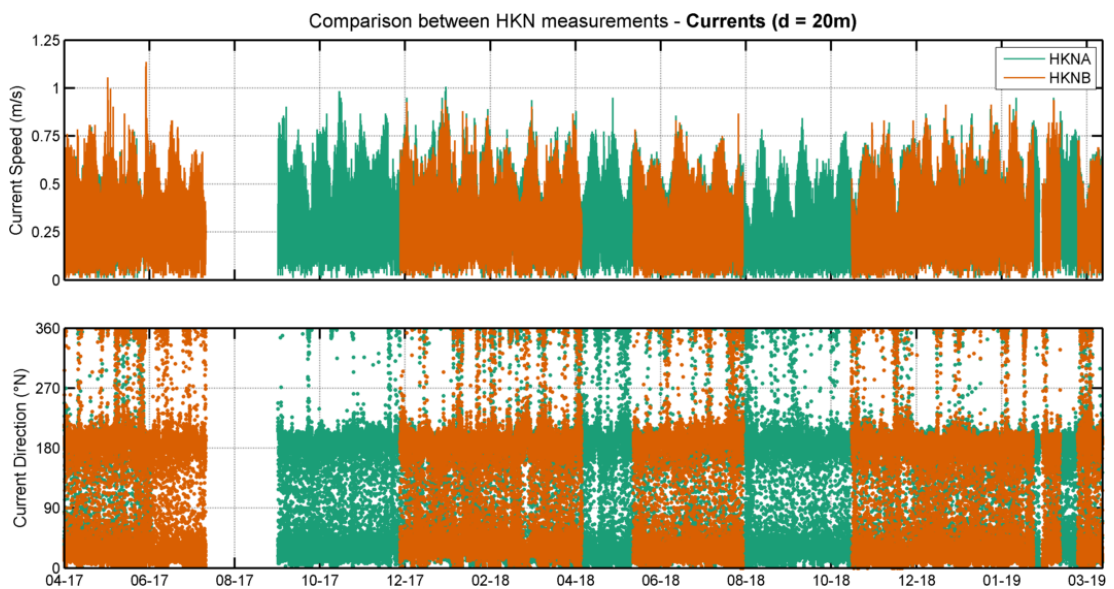


Figure 11.5: Timeseries of 20 m depth currents. The oceanographic convention is used for the current directions, so all current directions are going to, clockwise from North.

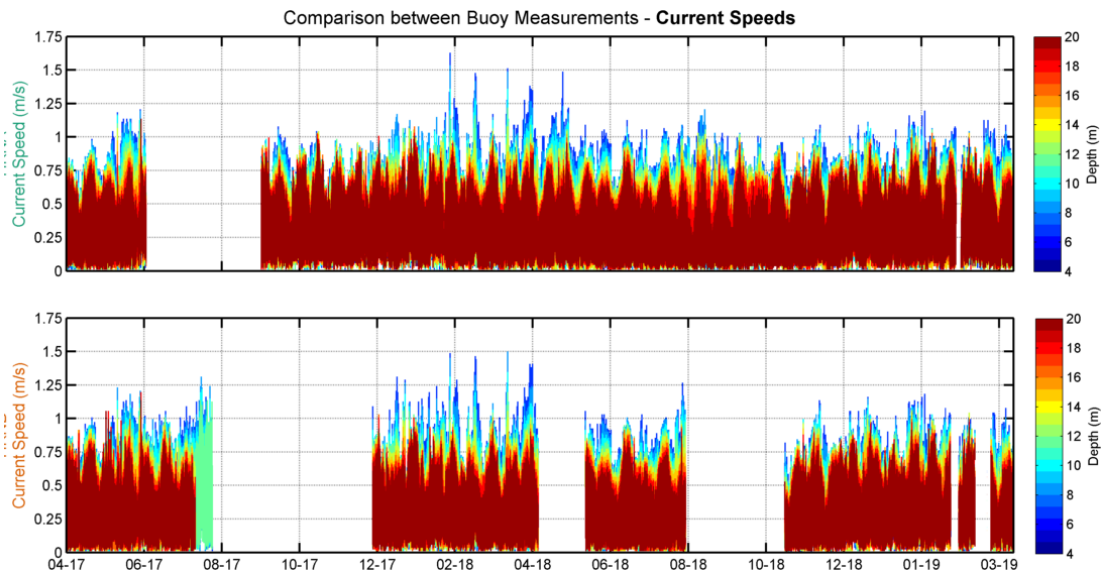


Figure 11.6: Timeseries of HKNA (top) and HKNB (bottom) current speeds (by depth) at each buoy.

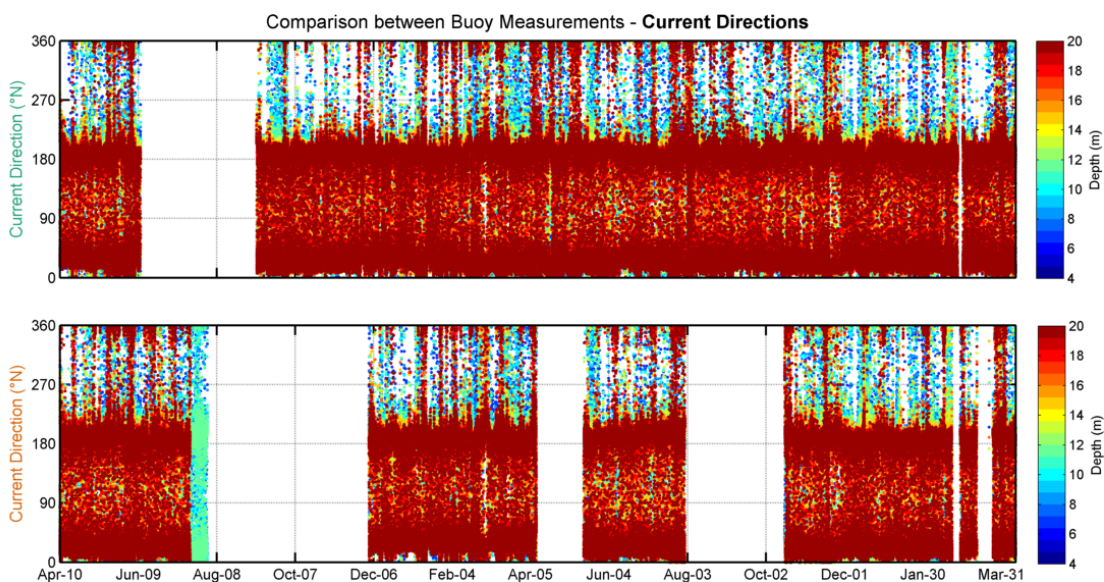


Figure 11.7: Timeseries of HKNA (top) and HKNB (bottom) current directions (by depth). The oceanographic convention is used for the current directions, so all current directions are going to clockwise from North.

In order to further quantify the differences between the two buoys, the slope, bias, correlations and square correlations between the HKNA and HKNB current speed observations at all depths and the bias, correlations and square correlations between the HKNA and HKNB current direction observations at all depths have been computed and are given in [Table 11.1](#). The correspondence in terms of current speed is excellent at all levels and in terms of current direction is good at all levels. The lower correlations in terms of current direction have in our opinion more to do with local effects and the nature and variability of the current direction signal than the accuracy of the instruments. Due to the rotating nature of the currents, especially when they rotate towards offshore (directions close to 350) the timing can be off. This occurs, however, during short time periods and mostly when the current speeds are low.

Table 11.1: Statistical comparison between LiDAR buoy current measurements with depth.

Depth (m)	Current Speed					Current Direction			
	r^2 (-)	r (-)	Bias (m/s)	Symm. Slope (-)	n (-)	r^2 (-)	r (-)	Bias (°N)	n (-)
4	0.90	0.95	-0.01	0.99	59937	0.65	0.80	-0.3	59937
6	0.92	0.96	-0.02	0.97	60017	0.71	0.85	-1.2	60017
8	0.93	0.96	-0.01	0.97	60044	0.70	0.84	-1.5	60044
10	0.93	0.97	-0.02	0.97	60089	0.66	0.81	-1.3	60089
12	0.95	0.97	-0.01	0.98	60107	0.67	0.82	-1.3	60107
14	0.94	0.97	-0.01	0.98	60140	0.67	0.82	-1.4	60140
16	0.93	0.97	-0.01	0.98	60080	0.69	0.83	-1.3	60080
18	0.92	0.96	-0.01	0.97	60069	0.70	0.83	-1.4	60069
20	0.90	0.95	-0.02	0.96	60076	0.69	0.83	-1.3	60076

11.3 Validation of the HKN data

A direct comparison of the depth-averaged current at HKNA and HKNB against the hydrodynamic model is included in [Figure 11.8](#) and [Figure 11.9](#), respectively. The comparisons are excellent in terms on current speed and poor in terms of current direction. These low correlations between the current directions have again in our opinion more to do with local effects and the nature and variability of the current direction signal than the accuracy of the data.

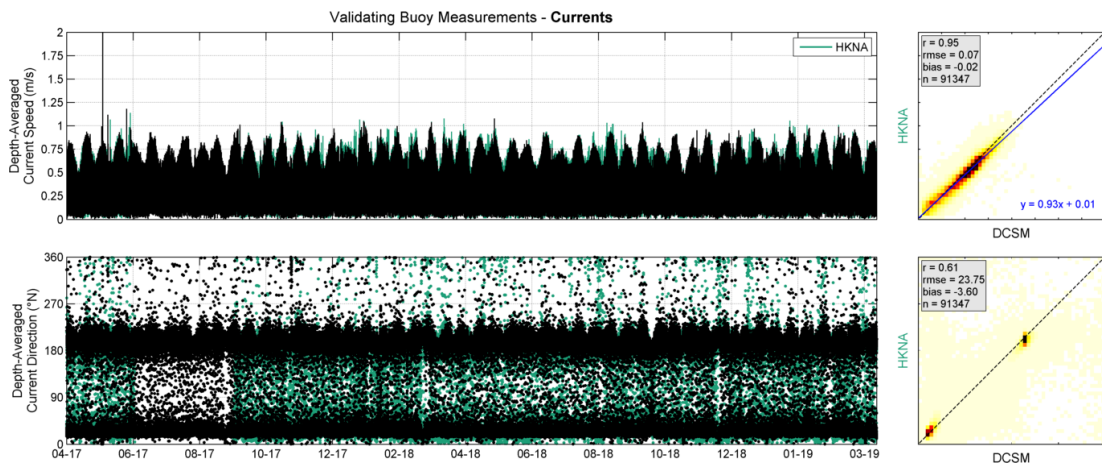


Figure 11.8: Depth-averaged current comparison at HKNA.

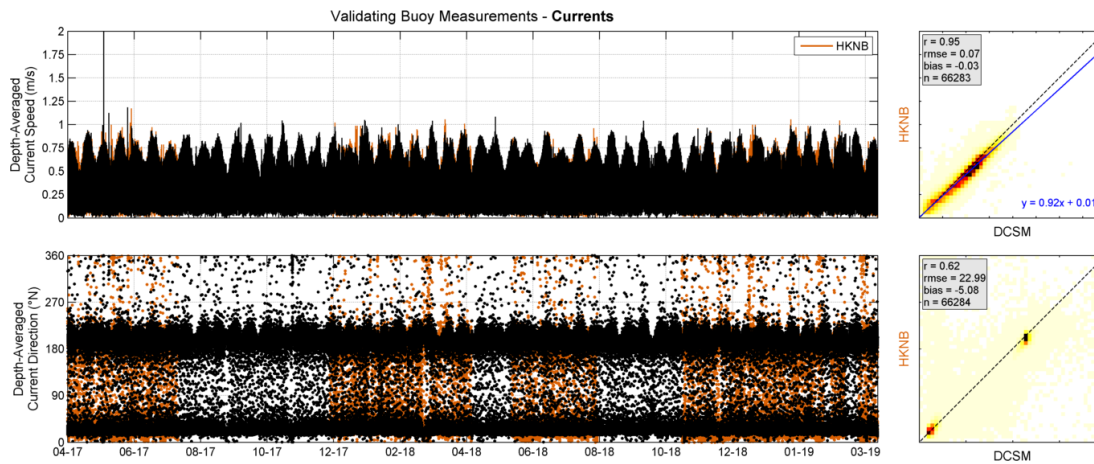


Figure 11.9: Depth-averaged current comparison at HKNB.

11.4 Quality Statement

Based on the comparisons between the data from the buoys and its validation against the model data, which all show excellent comparisons in terms of current speed and current direction mismatches that can be explained by local effects and the nature and variability of the current direction signal, it can be concluded that the accuracy of the current profiler is high. Furthermore, as can also be verified in the monthly validation reports, this is true over the whole campaign period.

11.5 Climate description

In this section we present some characteristics of the current velocity climate at HKN using the validated HKNA data which have a data return above 86%. The statistics from the HKNB data are not presented given that the main characteristics of these data are similar to those of the HKNA data and the HKNB data return (around 64%) is lower.

Figure 11.10 shows all observed HKNA vertical current profiles (grey lines) and the mean profile (red line). Due to the water level variations, the distance between the deepest measuring level and the bottom varies and this leads to a less reliable description of the profile close to the bed using the relative current velocity approach we have applied to compute the profile. Nevertheless, the shown mean profile appears realistic.

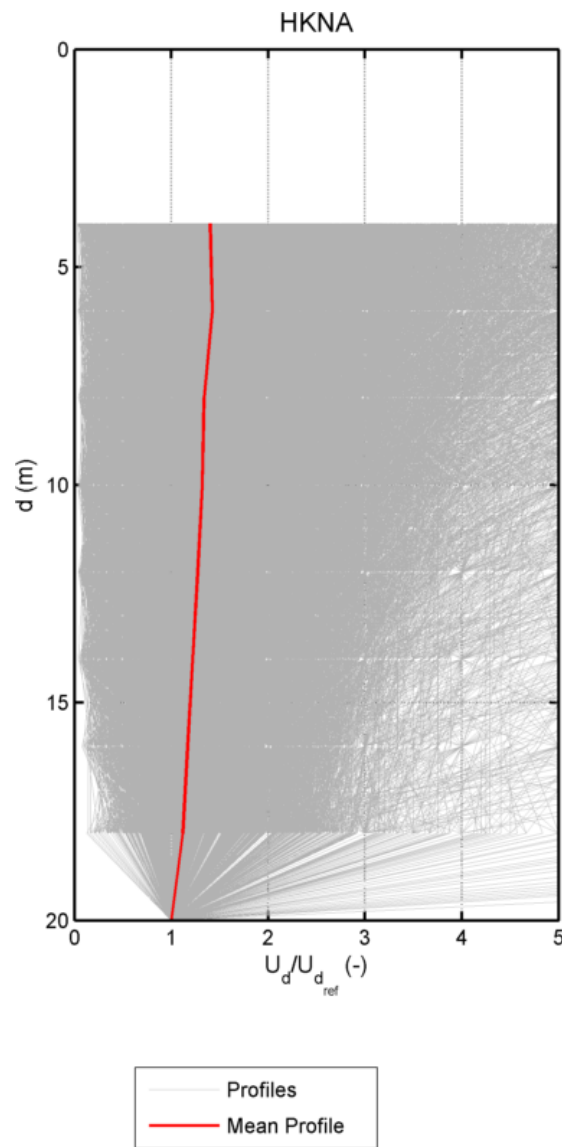


Figure 11.10: Normalized current speed vertical profiles.

Figure 11.11 shows the roses of the surface (4 m), 10 m and 20 m current speeds at HKNA.

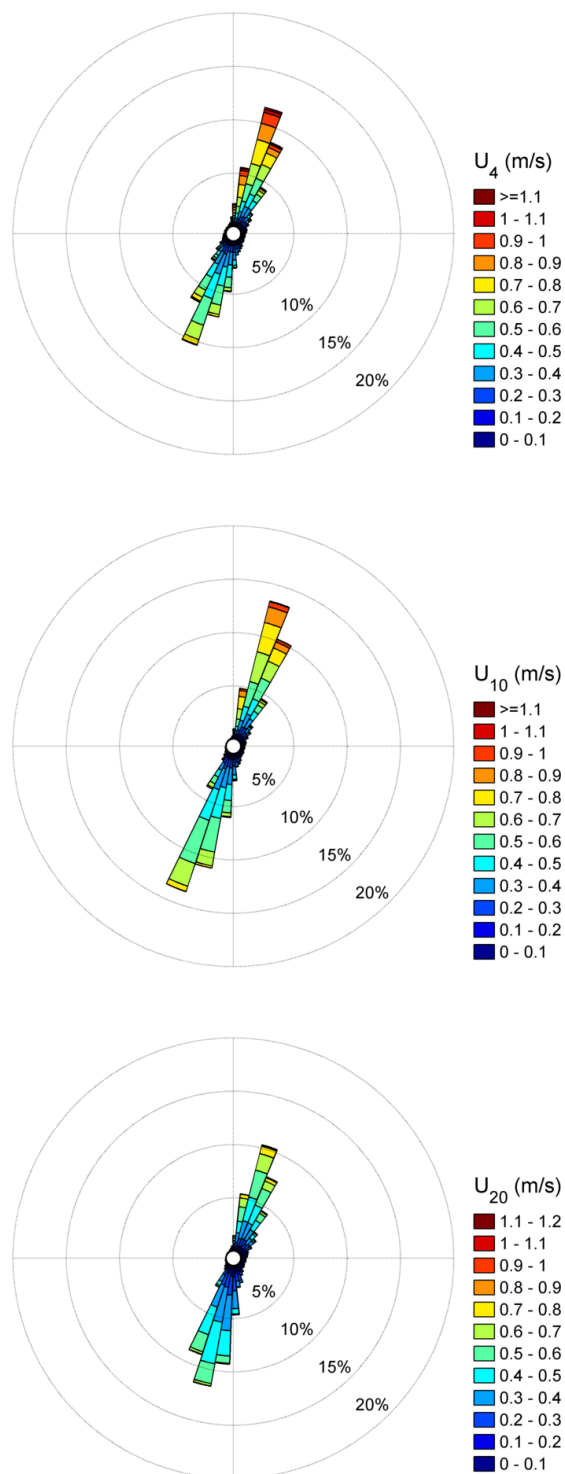


Figure 11.11: Roses of the surface (top), 10 m (middle) and 20 m (bottom) currents at HKNA. The current direction is the direction the piles point to away from the centre of the rose.

12 Final remarks

Two Carbon Trust pre-commercial Stage 2 classified *SEAWATCH Wind LiDAR Buoys*, HKNA and HKNB, and associated bottom mounted sensors were deployed by Fugro at the Hollandse Kust (noord) Wind Farm Zone on the 10th of April 2017 with the intention of measuring wind, waves, temperature, air pressure and currents for a period of one year. After the completion of one year of observations on the 9th of April 2018, another year was commissioned. The HKNA station was kept operational whilst the HKNB station was not kept operational during the transition of approximately 1 month. The second campaign year was completed on the 10th of April 2019. The buoys were kept operational to complete the in-situ validation of the HKNB buoy until June 2019.

In this report the full 24-month HKN field measurement campaign is described and the full two-year campaign data are validated and presented. During the measurement campaign, the available data (mostly satellite transmitted) were validated and made available on a monthly basis. The basis of this full campaign report and dataset is the data downloaded from each station over the course of the project. Consequently, the signal availability of the full two-year dataset differs from that of the monthly reported datasets.

The following conclusions ensue from the analysis and validation of the data.

- The availability of the wind data is acceptable to high, of the wave data is high from HKNA and good from HKNB, of the current data is at all levels acceptable from HKNA and limited from HKNB, of the air and water temperature is good and of the air pressure is high from HKNA, of the water level data from the WLR at HKNB is limited and only of the other WLR data is poor.
- The comparisons between the HKNA and HKNB wind velocities show at all levels and in terms of both wind speed and direction low biases and correlations and slopes close to 1. The agreement between the wind observations from HKN and from the reference stations is relatively high, especially when considering the differences in the location of the stations.
- The agreement between the wave data from the two buoys is excellent for all parameters except for the peak wave period and the mean wave period of swell which is good and the mean wave direction of swell which is poor. These poorer agreements are as expected, given that these parameters depend more strongly on the sampling variability (randomness of the sea surface elevation) and discreteness of the wave spectra. The agreement between the wave observations from HKN and from the reference stations is relatively high, especially when considering the distances between the stations.
- The validation of the temperature data shows that there is a general agreement between HKN temperature observations and those from the fixed stations.
- The validation of the air pressure data shows, as expected given their proximity in terms of macro-atmospheric forcings, an excellent agreement between the HKN observations and those from the fixed stations.
- The HKN inferred water levels had to be bias corrected given uncertainties in the depths at which the WLRs were located. The resulting processed water levels show a high agreement between stations and with the model data.
- The agreement between the current speed observations and model results is high. There are mismatches between the current directions, which are partly due to the nature and variability of the current direction signal.
- The overall results validate the assumption that the distance between the two stations is negligible and the datasets are interchangeable. Therefore, the station datasets can be combined into a single dataset with the highest possible availability. If the gaps in the data

collected at one of the stations are filled with the data collected at other station in order to compile a complete HKN dataset, the availabilities are then high for wind and waves, good for currents, high for pressure and water temperature, good for air temperature and limited for water level.

The overall conclusion of the validation is that the quality of the full campaign HKN dataset is high and the dataset, especially when keeping in mind validation comments above, trustworthy. This makes the dataset, which is rather comprehensive—including vertical wind and current profiles and directional wave spectra— a sound basis for site study analyses, for instance, for wind assessment studies, morphodynamics and metocean desk studies and in particular for the Hollandse Kust (noord) Wind Farm Zone.

References

- Deltares, 2017a. *Hollandse Kust (noord) Field Measurement Campaign Validation Report - April 2017*. Tech. rep., hkz_20170818_deltares_monthly_validation_report june 2017_f, (S. Caïres).
- Deltares, 2017b. *Hollandse Kust (noord) Field Measurement Campaign Validation Report - May 2017*. Tech. rep., hkz_20171211_deltares_monthly_validation_report may 2017_f, (S. Caïres).
- Deltares, 2018a. *Hollandse Kust (noord) Field Measurement Campaign Validation Report - April 2018*. Tech. rep., hkz_20180816_deltares_monthly_validation_report april 2018_f, (S. Caïres).
- Deltares, 2018b. *Hollandse Kust (noord) Field Measurement Campaign Validation Report - August 2017*. Tech. rep., hkz_20180313_deltares_monthly_validation_report august 2017_f, (S. Caïres).
- Deltares, 2018c. *Hollandse Kust (noord) Field Measurement Campaign Validation Report - August 2018*. Tech. rep., hkz_20181019_deltares_monthly_validation_report august 2018_f, (S. Caïres).
- Deltares, 2018d. *Hollandse Kust (noord) Field Measurement Campaign Validation Report - December 2017*. Tech. rep., hkz_20180514_deltares_monthly_validation_report december 2017_f, (S. Caïres).
- Deltares, 2018e. *Hollandse Kust (noord) Field Measurement Campaign Validation Report - February 2018*. Tech. rep., hkz_20180612_deltares_monthly_validation_report february 2018_f, (S. Caïres).
- Deltares, 2018f. *Hollandse Kust (noord) Field Measurement Campaign Validation Report - January 2018*. Tech. rep., hkz_20180606_deltares_monthly_validation_report january 2018_f, (S. Caïres).
- Deltares, 2018g. *Hollandse Kust (noord) Field Measurement Campaign Validation Report - July 2017*. Tech. rep., hkz_20180202_deltares_monthly_validation_report july 2017_f, (S. Caïres).
- Deltares, 2018h. *Hollandse Kust (noord) Field Measurement Campaign Validation Report - July 2018*. Tech. rep., hkz_20180927_deltares_monthly_validation_report july 2018_f, (S. Caïres).
- Deltares, 2018i. *Hollandse Kust (noord) Field Measurement Campaign Validation Report - June 2017*. Tech. rep., hkz_20180219_deltares_monthly_validation_report june 2017_f, (S. Caïres).
- Deltares, 2018j. *Hollandse Kust (noord) Field Measurement Campaign Validation Report - June 2018*. Tech. rep., hkz_20180917_deltares_monthly_validation_report june 2018_f, (S. Caïres).
- Deltares, 2018k. *Hollandse Kust (noord) Field Measurement Campaign Validation Report - March 2018*. Tech. rep., hkz_20180620_deltares_monthly_validation_report march 2018_f, (S. Caïres).
- Deltares, 2018l. *Hollandse Kust (noord) Field Measurement Campaign Validation Report - May 2018*. Tech. rep., hkz_20180824_deltares_monthly_validation_report may 2018_f, (S. Caïres).

- Deltares, 2018m. *Hollandse Kust (noord) Field Measurement Campaign Validation Report - November 2017*. Tech. rep., hkz_20180503_deltares_monthly_validation_report november 2017_f, (S. Caires).
- Deltares, 2018n. *Hollandse Kust (noord) Field Measurement Campaign Validation Report - October 2017*. Tech. rep., hkz_20180409_deltares_monthly_validation_report october 2017_f, (S. Caires).
- Deltares, 2018o. *Hollandse Kust (noord) Field Measurement Campaign Validation Report - October 2018*. Tech. rep., hkz_20181214_deltares_monthly_validation_report october 2018_f, (S. Caires).
- Deltares, 2018p. *Hollandse Kust (noord) Field Measurement Campaign Validation Report - September 2017*. Tech. rep., hkz_20180328_deltares_monthly_validation_report september 2017_f, (S. Caires).
- Deltares, 2018q. *Hollandse Kust (noord) Field Measurement Campaign Validation Report - September 2018*. Tech. rep., hkz_20181119_deltares_monthly_validation_report september 2018_f, (S. Caires).
- Deltares, 2019a. *Hollandse Kust (noord) Field Measurement Campaign Validation Report - December 2018*. Tech. rep., hkz_20190211_deltares_monthly_validation_report december 2018_f, (S. Caires).
- Deltares, 2019b. *Hollandse Kust (noord) Field Measurement Campaign Validation Report - February 2019*. Tech. rep., hkz_20190412_deltares_monthly_validation_report february 2019_f, (S. Caires).
- Deltares, 2019c. *Hollandse Kust (noord) Field Measurement Campaign Validation Report - January 2019*. Tech. rep., hkz_20190318_deltares_monthly_validation_report january 2019_f, (S. Caires).
- Deltares, 2019d. *Hollandse Kust (noord) Field Measurement Campaign Validation Report - March 1 2019 to April 10 2019*. Tech. rep., hkz_20190611_deltares_monthly_validation_report march 2019extended_f, (S. Caires).
- Deltares, 2019e. *Hollandse Kust (noord) Field Measurement Campaign Validation Report - November 2018*. Tech. rep., hkz_20190123_deltares_monthly_validation_report november 2018_f, (S. Caires).
- DNVGL, 2015a. *Assessment of the Fugro OCEANOR Seawatch Wind LiDAR Buoy Pre-Deployment Validation on Frøya, Norway*. Tech. Rep. GLGH-4257 13 10378-R-0004, Rev. A, issue date 2015-03-31, DNV GL.
- DNVGL, 2015b. *Assessment of the Fugro/Oceanor Seawatch Floating Lidar Verification at RWE Ijmuiden Met Mast*. Tech. Rep. GLGH-4257 13 10378-R-0003, Rev. B, issue date 2015-01-30, DNV GL.
- DNVGL, 2016a. *Floating Lidar Validation Analysis SEAWATCH Wind Lidar Buoy*. Tech. rep.,hkn_hkz_20170518_carbon trust_ws155 pre deployment validation_issue 7-12-2016_f, Natural Power.
- DNVGL, 2016b. *Frøya SEAWATCH WIND LIDAR BUOY WS 140 PRE-DEPLOYMENT VALIDATION - Assessment of the Fugro OCEANOR Seawatch Wind LiDAR Buoy WS 140 Pre-Deployment Validation on Frøya, Norway*. Tech. Rep.,HKZ_20161019_DNVGL_WS140 pre deployment validation_GLGH-4270 16 13920 258-R-0002-C_F GLGH-4270 16 13920-R-0002, Rev. C, DNV GL.

- DNVGL, 2016c. *Frøya SEAWATCH WIND LIDAR BUOY WS 156 PRE-DEPLOYMENT VALIDATION Assessment of the Fugro OCEANOR Seawatch Wind LiDAR Buoy WS 156 Pre-Deployment Validation on Frøya Norway*. Tech. Rep., HKN_HKZ_20160412_DNVGL_WS156 pre deployment validation_GLGH-4257 13 10378 266-R-0005-E_F GLGH-4257 13 10378-R-0005, Rev. E, DNV GL.
- DNVGL, 2016d. *Frøya SEAWATCH WIND LIDAR BUOY WS 158 PRE-DEPLOYMENT VALIDATION - Assessment of the Fugro OCEANOR Seawatch Wind LiDAR Buoy WS 158 Pre-Deployment Validation on Frøya Norway*. Tech. Rep., HKZ_20160704_DNVGL_WS158 pre deployment validation_GLGH-4270 16 13920 266-R-0001-D_F GLGH-4270 16 13920-R-0001, Rev. D, DNV GL.
- DNVGL, 2017. *Frøya SEAWATCH WIND LIDAR BUOY WS 149 POST-DEPLOYMENT VALIDATION - Assessment of the Fugro OCEANOR Seawatch Wind LiDAR Buoy WS 149 Post-Deployment Validation at Frøya Norway*. Tech. Rep., HKN_HKZ_BWFZ_20170707_DNVGL_WS149 post campaign validation GLGH-4270 17 14462 258-R-0001-D_F GLGH-4270 17 14462-R-0001, Rev. D, DNV GL.
- DNVGL, 2019a. *SEAWATCH WIND LIDAR BUOY WS158 OFFSHORE IN SITU VERIFICATION - Quality assessment of the Fugro Seawatch Wind LiDAR Buoy WS158*. Tech. Rep., 10148549-R-2-B_WS158vsWS156_FINAL 10148549-R-2, Rev. B, DNV GL.
- DNVGL, 2019b. *SEAWATCH WIND LIDAR BUOY WS158 OFFSHORE IN SITU VERIFICATION - Quality assessment of the Fugro Seawatch Wind LiDAR Buoy WS158*. Tech. Rep., 10148549-R-1-A_WS158vsWS156_20190614 10148549-R-1, Rev. A, DNV GL.
- Ecofys, 2016. *Uncertainty Assessment Fugro OCEANOR SEAWATCH Wind LiDAR Buoy at RWE Meteomast Ijmuiden 11.04.2014 - 27.10.2014*. Tech. rep., Ecofys.
- Fisher, N. I., 1993. *Statistical analysis of circular data*. Cambridge Univ. Press.
- Fisher, N. I. and A. J. Lee, 1983. "A correlation coefficient for circular data." *Biometrika* 70: 327–332.
- Fugro, 2017a. *Supply of Meteorological and Oceanographic data at Hollandse Kust (noord) Monthly Data Report: April 2017*. Tech. rep., hkn_20170818_fugro_monthly data report april 2017_f, (L. Lønseth and V. Neshaug).
- Fugro, 2017b. *Supply of Meteorological and Oceanographic data at Hollandse Kust (noord) Monthly Data Report: May 2017*. Tech. rep., hkn_20171219_fugro_monthly data report may 2017_f, (O. Storås and L. Lønseth).
- Fugro, 2018a. *Supply of Meteorological and Oceanographic data at Hollandse Kust (noord) Monthly Data Report: April 2018*. Tech. rep., hkn_20180824_fugro_monthly data report april 2018_f, (J.-P. Mathisen and V. Neshaug).
- Fugro, 2018b. *Supply of Meteorological and Oceanographic data at Hollandse Kust (noord) Monthly Data Report: August 2017*. Tech. rep., hkn_20180314_fugro_monthly data report august 2017_f, (L. Lønseth and V. Neshaug).
- Fugro, 2018c. *Supply of Meteorological and Oceanographic data at Hollandse Kust (noord) Monthly Data Report: August 2018*. Tech. rep., hkn_20181023_fugro_monthly data report august 2018_f, (I. Pathirana and V. Neshaug).
- Fugro, 2018d. *Supply of Meteorological and Oceanographic data at Hollandse Kust (noord) Monthly Data Report: December 2017*. Tech. rep., hkn_20180612_fugro_monthly data report december 2017_f, (P. Schjølberg and L. Lønseth).

- Fugro, 2018e. *Supply of Meteorological and Oceanographic data at Hollandse Kust (noord) Monthly Data Report: February 2018*. Tech. rep., hkn_20180612_fugro_monthly data report february 2018_f, (P. Schjølberg and L. Lønseth).
- Fugro, 2018f. *Supply of Meteorological and Oceanographic data at Hollandse Kust (noord) Monthly Data Report: January 2018*. Tech. rep., hkn_20180611_fugro_monthly data report january 2018_f, (J.-P. Mathisen and L. Lønseth).
- Fugro, 2018g. *Supply of Meteorological and Oceanographic data at Hollandse Kust (noord) Monthly Data Report: July 2017*. Tech. rep., hkn_20180226_fugro_monthly data report july 2017_f, (L. Lønseth and V. Neshaug).
- Fugro, 2018h. *Supply of Meteorological and Oceanographic data at Hollandse Kust (noord) Monthly Data Report: July 2018*. Tech. rep., hkn_20181001_fugro_monthly data report july 2018_f, (I. Pathirana and V. Neshaug).
- Fugro, 2018i. *Supply of Meteorological and Oceanographic data at Hollandse Kust (noord) Monthly Data Report: June 2017*. Tech. rep., hkn_20180221_fugro_monthly data report june 2017_f, (L. Lønseth and V. Neshaug).
- Fugro, 2018j. *Supply of Meteorological and Oceanographic data at Hollandse Kust (noord) Monthly Data Report: June 2018*. Tech. rep., hkn_20180920_fugro_monthly data report june 2018_f, (I. Pathirana and V. Neshaug).
- Fugro, 2018k. *Supply of Meteorological and Oceanographic data at Hollandse Kust (noord) Monthly Data Report: March 2018*. Tech. rep., hkn_20180621_fugro_monthly data report march 2018_f, (P. Schjølberg and L. Lønseth).
- Fugro, 2018l. *Supply of Meteorological and Oceanographic data at Hollandse Kust (noord) Monthly Data Report: May 2018*. Tech. rep., hkn_20180827_fugro_monthly data report may 2018_f, (J.-P. Mathisen and V. Neshaug).
- Fugro, 2018m. *Supply of Meteorological and Oceanographic data at Hollandse Kust (noord) Monthly Data Report: November 2017*. Tech. rep., hkn_20180509_fugro_monthly data report november 2017_f, (J.-P. Mathisen and L. Lønseth).
- Fugro, 2018n. *Supply of Meteorological and Oceanographic data at Hollandse Kust (noord) Monthly Data Report: October 2017*. Tech. rep., hkn_20180416_fugro_monthly data report october 2017_f, (P. Schjølberg and L. Lønseth).
- Fugro, 2018o. *Supply of Meteorological and Oceanographic data at Hollandse Kust (noord) Monthly Data Report: October 2018*. Tech. rep., hkn_20181221_fugro_monthly data report october 2018_f, (I. Pathirana and A. Berg).
- Fugro, 2018p. *Supply of Meteorological and Oceanographic data at Hollandse Kust (noord) Monthly Data Report: September 2017*. Tech. rep., hkn_20180404_fugro_monthly data report september 2017_f, (L. Lønseth and V. Neshaug).
- Fugro, 2018q. *Supply of Meteorological and Oceanographic data at Hollandse Kust (noord) Monthly Data Report: September 2018*. Tech. rep., hkn_20181123_fugro_monthly data report september 2018_f, (I. Pathirana and V. Neshaug).
- Fugro, 2019a. *Supply of Meteorological and Oceanographic data at Hollandse Kust (noord) Monthly Data Report: December 2018*. Tech. rep., hkn_20190218_fugro_monthly data report december 2018_f, (I. Pathirana and V. Neshaug).
- Fugro, 2019b. *Supply of Meteorological and Oceanographic data at Hollandse Kust (noord) Monthly Data Report: February 2019*. Tech. rep., hkn_20190416_fugro_monthly data report february 2019_f, (I. Pathirana and V. Neshaug).

- Fugro, 2019c. *Supply of Meteorological and Oceanographic data at Hollandse Kust (noord) Monthly Data Report: January 2019*. Tech. rep., hkn_20190326_fugro_monthly data report january 2019_f, (I. Pathirana and A. Berg).
- Fugro, 2019d. *Supply of Meteorological and Oceanographic data at Hollandse Kust (noord) Monthly Data Report: March 2019*. Tech. rep., hkn_20190613_fugro_monthly data report march 2019_f, (I. Pathirana and V. Neshaug).
- Fugro, 2019e. *Supply of Meteorological and Oceanographic data at Hollandse Kust (noord) Monthly Data Report: November 2018*. Tech. rep., hkn_20190123_fugro_monthly data report november 2018_f, (I. Pathirana and V. Neshaug).
- IEAwind, 2016. *IEA Wind Annex 32 Work Package 1.5, "State-of-the-Art Report: Recommended Practices for Floating Lidar Systems". Issue 1.0, 2 February 2016*. Tech. rep., IEAwind.
- IEA Wind, 2017. *"18. FLOATING LIDAR SYSTEMS", IEA Wind Expert group report on recommended practices*. Tech. Rep. 1st edition, <https://community.ieawind.org/HigherLogic/System/DownloadDocumentFile.ashx?DocumentFileKey=99ec44ff-4493-4bad-6510-d42d152ae963&forceDialog=0>, September 2017.
- IEC 61400-12-1, 2017. *Wind energy generation systems - Part 12-1: Power performance measurements of electricity producing wind turbines*. International standard, <https://webstore.iec.ch/publication/26603>, IEC.
- Kalverla, P. C., G.-J. Steeneveld, R. J. Ronda and A. A. Holtslag, 2017. "An observational climatology of anomalous wind events at offshore metemast IJmuiden (North Sea)." *Journal of Wind Engineering and Industrial Aerodynamics* 165: 86 - 99. DOI <https://doi.org/10.1016/j.jweia.2017.03.008>, ISSN 0167-6105.
- Natural Power, 2015. *Floating Lidar Validation analysis, Seawatch Wind Lidar Buoy*. Tech. Rep. ref. no. 1124607/D, Natural Power.
- OWA, 2013. *Carbon Trust Offshore Wind Accelerator roadmap for the commercial acceptance of floating LIDAR technology*. Tech. Rep. CTC819 Version 1.0, <https://www.carbontrust.com/media/422195/ctc819-owa-roadmap-commercial-acceptance-floating-lidar-technologies.pdf>, OWA.
- OWA, 2018. *Carbon Trust Offshore Wind Accelerator Roadmap for the Commercial Acceptance of Floating LIDAR Technology*. Tech. Rep. Version 2.0, OWA.
- Wieringa, J. and P. Rijkoort, 1983. *Windklimaat van Nederland (in Dutch)*. KNMI (staatsuitgeverij).
- ZephIR, 2013. *Z300 MODBUS interface, a user's guide, 19th Dec 2013, issue K*. Manual, (ZephIR LiDAR).
- Zijl, F., J. Sumihar and M. Verlaan, 2015. "Application of data assimilation for improved operational water level forecasting on the northwest European shelf and North Sea." *Ocean Dynamics* 65 (11).
- Zijl, F., M. Verlaan and H. Gerritsen, 2013. "Improved water-level forecasting for the Northwest European Shelf and North Sea through direct modelling of tide, surge and non-linear interaction." *Ocean Dynamics* 63 (7).